

Institut für Nutzpflanzenwissenschaften und Ressourcenschutz (INRES)

der

Rheinischen Friedrich-Wilhelms-Universität Bonn

**Functional characterization of the maize (*Zea mays* L.)
lateral rootless 1 gene**

Dissertation

zur Erlangung des Grades

Doktor der Agrarwissenschaften (Dr. agr.)

der Landwirtschaftlichen Fakultät

der Rheinischen Friedrich-Wilhelms-Universität Bonn

von

Marcel Baer

aus

Rheinbach

Bonn 2022

Referent: Prof. Dr. Frank Hochholdinger

Korreferent: Prof. Dr. Gabriel Schaaf

Tag der mündlichen Prüfung: 07.12.2022

Angefertigt mit Genehmigung der Landwirtschaftlichen Fakultät der Universität Bonn

CONTENT

Content	I
List of Figures.....	V
List of Tables	VII
List of Abbreviations	IIX
1.1 Zusammenfassung	X
1.2 Summary.....	XI
2 Introduction.....	1
2.1 Maize	1
2.2 The maize root system	2
2.3 Lateral roots	3
2.4 Maize root mutants with lateral root defects	4
2.5 The maize <i>lateral rootless 1 (lrl1)</i> mutant.....	4
2.6 DDB1-CUL4 ASSOCIATED FACTOR (DCAF).....	9
2.7 Protein-protein interaction analyses	11
2.7.1 Yeast two-hybrid (Y2H).....	12
2.7.2 Bimolecular fluorescence complementation (BiFC)	14
3 Objectives.....	16
4 Material and methods.....	17
4.1 Material.....	17
4.1.1 Plant material.....	17
4.1.2 Bacterial and yeast strains	17
4.1.3 Enzymes	18
4.1.4 Kits for molecular biology.....	18
4.1.5 Vectors.....	18
4.1.6 Software and internet tools for bioinformatics analyses	19
4.2 Methods	20

4.2.1	Growth conditions.....	20
4.2.2	Phenotypic analysis of the <i>lrt1</i> mutant in comparison to wild type....	20
4.2.3	Analysis of root gravitropic response of <i>lrt1</i>	21
4.2.4	Analysis of skotomorphogenesis in <i>lrt1</i>	21
4.2.5	Ethylene and ethylene inhibitor treatment of <i>lrt1</i>	21
4.2.6	Chemical treatments of <i>lrt1</i> with substances affecting peroxidase activity and ROS.....	22
4.2.7	Sequence analysis and phylogeny.....	22
4.2.8	Validation of the <i>lrt1</i> candidate gene by CRISPR-Cas9.....	23
4.2.9	Identification of DWD proteins in maize.....	24
4.2.10	Expression analysis	24
4.2.11	Yeast two hybrid experiments	25
4.2.12	Analysis of subcellular localization of LRT1 and DDB1 homologs using FRET co-localization	29
4.2.13	Analysis of Protein-protein interaction of LRT1 and DDB1 homologs using rBiFC.....	31
4.2.14	Analysis of Protein-protein interaction of LRT1 and DDB1L1 using FRET	31
5	Results	33
5.1	Phenotypic analysis of <i>lrt1</i>	33
5.2	Gravitropic response of <i>lrt1</i>	36
5.3	Skotomorphogenesis of <i>lrt1</i>	36
5.4	Effects of ethylene (ACC) on <i>lrt1</i>	37
5.5	Effect of chemical treatments altering the peroxidase activity and ROS in <i>lrt1</i>	39
5.6	Cloning of the <i>lrt1</i> gene	40
5.7	Validation of the <i>lrt1</i> candidate gene by CRISPR/Cas9	42
5.8	Phylogeny and sequence analysis of LRT1	43

5.9	Expression analysis.....	47
5.9.1	Root-type and tissue specific expression of <i>lrt1</i> and <i>lrt1-like</i>	47
5.9.2	Expression of <i>lrt1</i> and <i>lrt1-like</i> in the <i>lrt1</i> mutant.....	48
5.9.3	Expression of <i>lrt1</i> in the seminal- and lateral root defective mutant <i>rum1</i>	49
5.9.4	Expression of <i>lrt1</i> in the seminal- and crown root defective mutant <i>rtcs</i>	49
5.10	Subcellular localization of LRT1.....	50
5.11	Phylogeny and sequence analyses of DDB1 homologs in maize.....	52
5.12	Subcellular localization of DDB1L1 and DDB1L2.....	54
5.13	Analysis of the protein-protein interaction between LRT1 and DDB1 homologs.....	57
5.14	rBiFC and FRET analysis of interaction between LRT1 and DDB1 homologs.....	60
5.15	Identification of potential LRT1 interaction partners.....	64
6	Discussion	65
6.1	LRT1 affects different aspects of root development and reduces aboveground plant performance	65
6.2	Exogenous application of auxin and ethylene failed to recover the <i>lrt1</i> mutant	66
6.3	Changes in <i>lrt1</i> peroxidase activity and ROS do not directly affect the <i>lrt1</i> phenotype.....	67
6.4	The <i>lrt1</i> gene encodes a DCAF protein homolog.....	68
6.5	The <i>lrt1</i> gene is preferentially expressed in the primary root meristematic zone	70
6.6	Subcellular localization of LRT1 and the DDB1 homologs.....	71
6.7	Interaction between LRT1 and the DDB1 homologs DDB1L1 and DDB1L2.....	72

6.8	Future Protein-protein interaction analyses	74
7	Conclusions	76
8	References	77
9	Supplemental data.....	95
10	Acknowledgment.....	96

LIST OF FIGURES

- Figure 1** Model of maize genome evolution
- Figure 2** Architecture of the 14-day-old maize root system
- Figure 3** Maize primary root cross section during the initiation of a lateral root primordium
- Figure 4** Phenotype of the *lrt1* mutant in comparison to wild type plants
- Figure 5** Formation of a mature lateral root primordium in wild type maize and the *lrt1* mutant.
- Figure 6** Proposed model of LRT1 affecting different physiological and biosynthetic processes in maize root development
- Figure 7** The ubiquitin proteasome system and the CUL4 E3 ubiquitin ligase
- Figure 8** Protein-protein interaction analysis
- Figure 9** Analysis of the gravitropic response in the *lrt1* mutant
- Figure 10** Schematic representation of Fluorescence Resonance Energy Transfer (FRET)
- Figure 11** Phenotypic comparison between 10-day-old homozygous and heterozygous wild type seedlings and *lrt1* mutants
- Figure 12** Phenotypic comparison between mature wild type and *lrt1* plants
- Figure 13** Comparison of wild type and *lrt1* root systems grown in hydroponics
- Figure 14** Comparison of crown root development at the coleoptilar node between wild type and *lrt1*
- Figure 15** Quantification of crown root development between wild type and *lrt1*
- Figure 16** Gravitropic response in the *lrt1* mutant in comparison to wild type
- Figure 17** Skotomorphogenesis in the *lrt1* mutant in comparison to wild type
- Figure 18** Effect of ethylene (ACC) and silver nitrate in *lrt1* in comparison to wild type
- Figure 19** Phenotypic characterization of wild type and *lrt1* seedlings grown with peroxidase inhibitors and H₂O₂
- Figure 20** Differences in allele frequency between wild type and *lrt1* mutant pools in BSA seq

- Figure 21** Gene model of *lrt1*
- Figure 22** Validation of the *lrt1* gene by allelism tests
- Figure 23** Phylogenetic tree for LRT1 and homologous proteins from selected plant species
- Figure 24** Protein structure of *lrt1*
- Figure 25** Alignment of DWD motives of the LRT1 homologs in selected plant species
- Figure 26** Phylogenetic tree based on DWD motifs in *Zea mays*
- Figure 27** Expression of *lrt1* and *lrt1-like* in different root-types and tissues
- Figure 28** Correlation between *lrt1* and *lrt1-like* gene expression
- Figure 29** Expression of *lrt1* and *lrt1-like* in the primary root of *lrt1* mutants in comparison to heterozygous and homozygous wild type
- Figure 30** Expression of *lrt1* in *rum1* mutants
- Figure 31** Expression of *lrt1* in *rtcs* mutants
- Figure 32** Nuclear localization signals in LRT1
- Figure 33** Subcellular localization of LRT1
- Figure 34** Phylogenetic tree of DDB1 homologs in Arabidopsis
- Figure 35** Protein sequence models of DDB1 homologs
- Figure 36** Subcellular localization of DDB1-LIKE1
- Figure 37** Subcellular localization of DDB1-LIKE2
- Figure 38** BiFC assay of LRT1 and DDB1-LIKE1 in transient tobacco leaves
- Figure 39** BiFC assay of LRT1 and DDB1-LIKE2 in transient tobacco leaves
- Figure 40** FRET analysis of protein-protein interaction between LRT1 and DDB1-LIKE1

LIST OF TABLES

Table 1	List of bacterial and yeast strains used in this study
Table 2	Kits for molecular biology used in this study
Table 3	Vectors used in this study
Table 4	List of software and internet tools for bioinformatics analyses
Table 5	Co-transformed constructs for direct Y2H interaction analyses
Table 6	Reaction mixture used for Gateway BP reaction
Table 7	Reaction mixture used for Gateway LR reaction
Table 8	Identity/similarity matrix of DDB1 homologs
Table 9	Prediction of subcellular localization for DDB1 homologs
Table 10	β -Galactosidase assay of co-transformed DDB1L1, DDB1L2 and LRT1 constructs in yeast
Table 11	Growth of co-transformed constructs of DDB1-LIKE 1 and DDB1-LIKE2 with LRT1 in Yeast

Supplemental Table**Supplemental Table 1** Gene accessions related to *lrt1***Supplemental Table 2** Mutant alleles of *lrt1*

LIST OF ABBREVIATIONS

ACC	1-aminocyclopropane-1-carboxylic acid
AD	Gal4 activation domain
AM	Arbuscular mycorrhizal fungus
AP	Affinity purification
ARF	Auxin response factor
APX	Ascorbate peroxidase
AUX/IAA	AUXIN/INDOLE-3-ACETIC ACID
BD	Gal4 binding domain
BiFC	Bimolecular fluorescence complementation
BSA	Bulk segregant analysis
Co-IP	Co-immunoprecipitation
CUL 4	CULLIN 4
DCAF 1	DDB1 CUL4 ASSOCIATED FACTOR 1
DDB1	UV-DAMAGED DNA BINDING PROTEIN 1
DWD	DDB1 BINDING WD40
EMS	Ethyl methane sulfonate
FRET	Fluorescence resonance energy transfer
<i>hb3</i>	<i>homeobox-transcription factor 3</i>
HMGA	CHROMATIN-ASSOCIATED HIGH MOBILITY GROUP PROTEIN A
IAA	INDOLE-3-ACETIC ACID
LC-MS/MS	Liquid chromatography tandem-mass spectrometry
<i>lrt1</i>	<i>lateral rootless 1</i>
<i>lrt1-like</i>	<i>lateral rootless 1-like</i>
MS	Mass spectrometry
NHEJ	Non-homologous end joining

NLS	Nuclear localization signal
O/N	Over night
ONPG	Ortho-Nitrophenyl- β -D-galactopyranoside
POI	Protein of interest
PPI	Protein-protein interaction
PRX	Class III peroxidase
PXG	Pellet X-Gal
RT	Room temperature
<i>slr 1</i>	<i>short lateral roots 1</i>
<i>slr2</i>	<i>short lateral roots 2</i>
sgRNA	Single guide RNA
SNP	Single nucleotide polymorphism
SSR	Simple sequence repeats
rBiFC	Ratiometric bimolecular fluorescence complementation
RBX 1	RING-BOX1
<i>rum1</i>	<i>rootless with undetectable meristem 1</i>
WT	Wild type
Y2H	Yeast two-hybrid

1 ZUSAMMENFASSUNG/ SUMMARY

1.1 Zusammenfassung

Lateralwurzeln werden von allen Wurzeltypen gebildet und sind dadurch, dass sie die Wurzeloberfläche vergrößern, für eine ausreichende Wasser- und Nährstoffversorgung der Pflanze entscheidend. In Mais werden Lateralwurzeln an den Phloem-Polen in der Differenzierungszone von Perizykel- und Endodermiszellen in einem mehrstufigen Prozess gebildet.

Die Mutante *lateral rootless 1* wurde bei einem EMS Mutations-Screening identifiziert. Ihr fehlen während der frühen Entwicklung Lateralwurzeln an den embryonalen Primär- und Seminalwurzeln. Später bilden sich auch in diesen Wurzeln einige rudimentäre Lateralwurzeln. Sprossbürtige Wurzeln sind von dem Defekt nicht betroffen und bilden normale Lateralwurzeln. Bis zur Reife zeigt die *lrt1* Mutante eine verzögerte Entwicklung des Spross- und Wurzelsystems mit einer deutlichen Reduzierung der Spross- und Wurzeltrockenmasse im Vergleich zum Wildtyp.

Das *lrt1* Gen wurde durch eine Kombination von Kartierungs- und BSA-seq Experimenten auf dem langen Arm von Chromosom 10 kartiert. In der vorliegenden Arbeit konnte das *lrt1* Gen durch die erfolgreiche Erzeugung von zwei neuen, mit CRISPR/Cas9 erzeugten Mutantenallelen, bestätigt werden.

Phylogenetische Analysen ausgewählter Pflanzenarten zeigten, dass das *lrt1* Gen für ein DCAF-Protein-Homolog codiert, das eine Untereinheit des CUL4- basierten E3 Ubiquitin Ligase Komplexes ist. DCAF-Proteine sind Substratrezeptoren, die ihre Ubiquitylierung und damit ihren anschließenden Abbau im 26S-Proteasom ermöglichen.

Das Maisgenom besitzt 55 Gene mit einem bis drei DWD-Motiven, welche für DCAF Proteine charakteristisch sind. LRT1 wurde im Laufe der Evolution dupliziert und gehört zusammen mit seinem Paralog LRT1-LIKE zu einem monokotyledonen-spezifischen Ast der DCAF Proteine.

Mit Hilfe von Genexpressionsanalysen konnte in der vorliegenden Arbeit gezeigt werden, dass *lrt1* bevorzugt in der meristematischen Zone von Wurzeln exprimiert wird und dass die paralogen Gene *lrt1* und *lrt1-like* wahrscheinlich in unterschiedlichen molekularen Signalwegen auftreten.

Ein FRET-Co-Lokalisierungsexperiment zeigte, wie für ein DCAF-Protein erwartet, eine nukleare Lokalisierung von LRT1.

Zusammenfassend konnte gezeigt werden, dass das in der vorliegenden Studie klonierte *lrt1*-Gen für ein Protein codiert, das homolog zur DCAF-Untereinheit des CUL4-Komplexes ist und sich als wichtiger Regulator der Lateralwurzelerwicklung bei Mais erwiesen hat.

1.2 Summary

All root types form lateral roots. They are critical for efficient water and nutrient uptake by increasing the absorbing surface of the root system. In the maize differentiation zone, pericycle and endodermis cells adjacent to the phloem poles contribute to the formation of lateral roots in a multi-step process.

The lateral rootless mutant *lrt1* was initially identified in an EMS mutation screening. It lacks lateral roots on the embryonic primary and seminal roots during early development. During later development these root types are able to build some rudimentary lateral roots. Shoot borne roots are not affected by this defect and are able to build normal lateral roots. Up to maturity, the *lrt1* mutant shows a delayed development of the shoot and root system with a clear reduction in shoot and root dry mass in comparison to wild type plants.

The *lrt1* gene was mapped to the long arm of chromosome 10 by a combination of mapping and BSA-seq experiments. In the present study, the *lrt1* gene was validated by the generation of two novel mutant alleles by genome editing via CRISPR/Cas9.

Phylogenetic analyses in selected plant species showed that the *lrt1* gene encodes a DCAF protein homolog, which is a subunit of the CUL4-based E3 ubiquitin ligase complex (CRL4). DCAF proteins are substrate receptors, which enable their ubiquitylation and thus their subsequent degradation in the 26S proteasome.

The maize genome contains 55 genes with one to three DWD-motifs, which are characteristic for DCAF proteins. LRT1 has been duplicated during evolution and maps together with its paralog LRT1-LIKE to a monocot-specific clade of DCAF proteins.

Gene expression analysis showed, that *lrt1* is preferentially expressed in the root meristematic zone and that the paralogous genes *lrt1* and *lrt1-like* likely act in independent molecular pathways.

A FRET co-localization experiment demonstrated the nuclear localization of LRT1, as expected for a DCAF protein.

In summary, the cloned *lrt1* gene encodes a protein homologous to the DCAF subunit of the CRL4 complex and was validated to be an important regulator of lateral root development in maize.

2 INTRODUCTION

2.1 Maize

Three crop plants, rice (*Oryza sativa*), wheat (*Triticum aestivum*) and maize (*Zea mays*) provide ~60% of the human food energy intake (FAO, 2020, www.fao.org). With 1,162 billion tons of grain yield in 2020, maize is the world's most prolific crop plant, followed by wheat (761 million tons) and rice (757 million tons) (<http://www.fao.org/faostat/>). Beside its importance in human nutrition, maize also considerably contributes to animal nutrition and is an energy crop for the production of biogas and its conversion into electricity (Deutsches Maiskomitee e.V. (DKM), www.maiskomitee.de).

Maize is a monocotyledonous model plant for genetic studies (HAKE and ROSS-IBARRA, 2015, STRABLE and SCANLON, 2009), since controlled crosses and self-pollinations are easy to perform as female (pistillate) and male (staminate) flowers are situated on separate parts of the plant.

Caused by a genome duplication which occurred between five and 12 million years ago, a tetraploid ancestor of maize arose by the hybridization of two diploid progenitors (Figure 1). Comparisons of the duplicated regions of the genome of modern maize with orthologous regions of the unduplicated genomes of rice (*Oryza sativa*) and sorghum (*Sorghum bicolor*) showed that many of the duplicated genes were fractionated during the evolutionary history, leading to modern diploid maize (HABERER *et al.*, 2005; SCHNABLE *et al.*, 2011). In modern maize, 3,000 to 5,000 pairs of paralogs are retained and can be divided into two distinct subgenomes (Figure 1) based on the synteny to the unduplicated sorghum genome (*Sorghum bicolor*) (SCHNABLE *et al.*, 2011).

Consequently, modern maize genes can be divided into two groups. For the first group, pairs of duplicated genes are existing, that are shared by both subgenomes or only single-copy genes are present in only one of the two subgenomes. The second group contains genes that cannot be assigned to any subgenome. This class of genes is characterized by a lack of syntenic orthologs in the genomes of other grass species. Most of these non-syntenic genes emerged by single-gene duplication mechanisms, most likely after the last genome duplication of maize (WOODHOUSE *et al.*, 2010). The modern diploid maize genome is organized in 10 chromosomes and has a medium sized genome of 2.4 Gb (B73, JIAO *et al.*, 2017; SCHNABLE *et al.*, 2009) in comparison to rice (0.4 Gb) and wheat (16 Gb) and encodes 41,577 protein coding genes (B73 RefGen_v5).

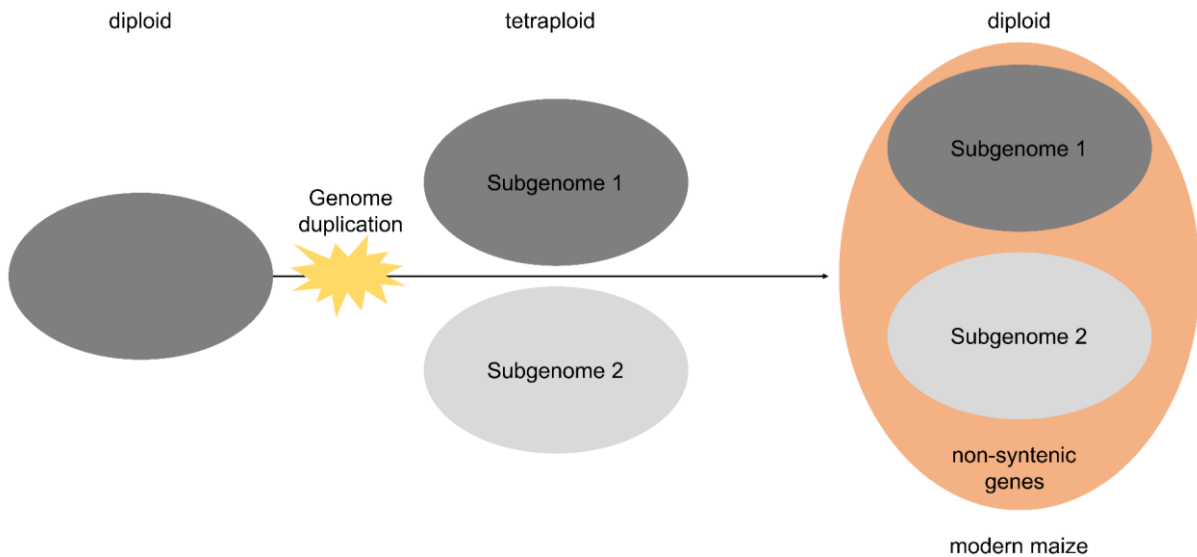


Figure 1 Model of maize genome evolution according to SCHNABLE and LYONS (2011) and SCHNABLE *et al.*, (2011). A genome duplication by the hybridization of two diploid progenitors occurred between five and 12 million years ago.

2.2 The maize root system

Maize has a complex root system, which is important for its productivity. It is composed of embryonic roots, which are formed during embryogenesis and postembryonic roots which are initiated after germination. A single primary root and a variable number of seminal roots are part of the embryonic root system (Figure 2). Postembryonic shoot-borne roots can be divided into crown roots which are formed at consecutive underground nodes and brace roots which are formed at consecutive aboveground nodes (HOCHHOLDINGER *et al.*, 2004 a).

Lateral roots emerge from all embryonic and postembryonic root types and belong to the post-embryonic root system. Whereas the embryonic roots are important for the seedling during early development, the post-embryonic root system represents the major part of the root system of adult plants (HOCHHOLDINGER *et al.*, 2004 a). Lateral roots are instrumental for water and nutrient uptake since they significantly increase the absorbing surface of the maize root system (HOCHHOLDINGER *et al.*, 2004 b, HOCHHOLDINGER *et al.*, 2018; YU *et al.*, 2016). In addition, root hairs, which are tubular extensions of epidermal cells, also increase the absorbing surface of the root (MARZEC *et al.*, 2015). Compared to other root types, lateral roots display the highest developmental variability to unfavorable environmental conditions (YU *et al.*, 2019).

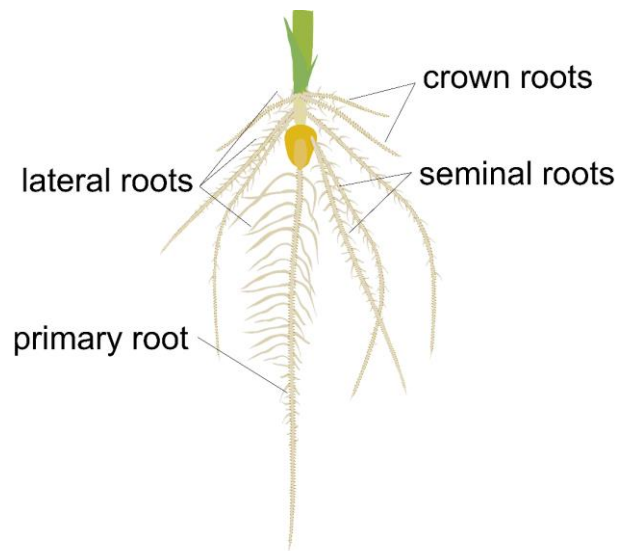


Figure 2 Architecture of the 14-day-old maize root system.

2.3 Lateral roots

In maize, lateral roots are initiated from pericycle and endodermal cells opposite of phloem poles in the differentiation zone in a multistep process. After anticlinal cell divisions of phloem pole pericycle cells and subsequent periclinal divisions of these cells, endodermal cells start dividing anticlinically. Both anticlinal and periclinal divisions give rise to the lateral root primordium (Figure 3). Endodermal cells give rise to the epidermis and columella of the newly formed lateral roots, all other cell types are formed by pericycle cells (BELL and MCCULLY, 1970; JANSEN *et al.*, 2012).

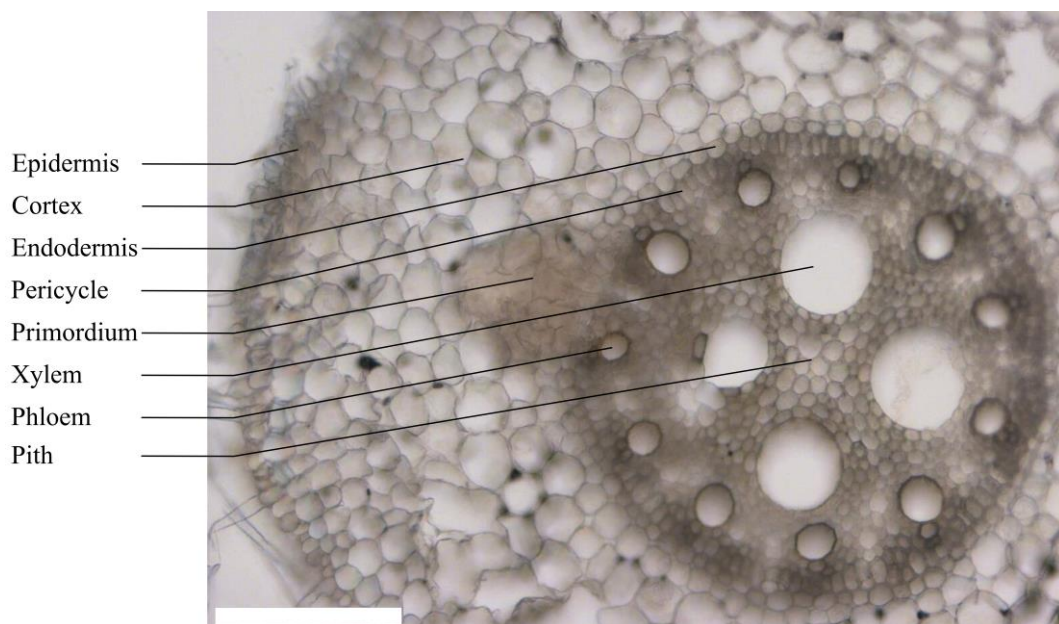


Figure 3 Maize primary root cross section during the initiation of a lateral root primordium: Scale bar = 150 μm .

2.4 Maize root mutants with lateral root defects

Genotypes with lateral root defects show a strong reduction in nutrient uptake and biomass production since lateral roots represent the most important part for nutrient and water uptake among all root types (ROGERS and BENFEY, 2015; YU *et al.*, 2016).

A number of lateral root defective mutants have been identified in maize and rice (reviewed in: YU *et al.*, 2016). In maize, so far four mutants have been identified that are confined to lateral root defects in embryonic primary and seminal roots while lateral root formation on post-embryonic roots is not affected. By contrast, lateral root defects in rice mostly also affect the shoot-borne root system (YU *et al.*, 2016).

The mutants *short lateral roots 1* and *2* (*slr1* and *slr2*) have a normal lateral root initiation, displayed by lateral root primordia which are not different from wild type but both mutants show a reduced lateral root elongation which lead to a reduced lateral root length (HOCHHOLDINGER *et al.*, 2001).

The maize *rootless with undetectable meristem 1* (*rum1*) mutant does not initiate embryonic seminal roots and is defective in lateral root initiation in the primary root. Lateral root formation in the shoot-born root system is not affected in this mutant (WOLL *et al.*, 2005). The *rum1* gene encodes an Aux/IAA protein, which controls downstream auxin response genes by their interaction with ARF25 and ARF34 proteins (VON BEHRENS *et al.*, 2011).

2.5 The maize *lateral rootless 1* (*lrt1*) mutant

The *lateral rootless 1* (*lrt1*) mutant was identified within a segregating F₂-generation of an EMS (ethyl methane sulfonate) mutagenized population of the inbred line B73 (HOCHHOLDINGER and FEIX, 1998). Based on phenotypic analyses of segregating populations it was confirmed that the genetic mutation is monogenic and recessive. The *lrt1* mutant does not form any lateral roots during its early postembryonic development (Figure 4A). In initial studies no lateral root primordia were observed in 4-day old mutants (HOCHHOLDINGER AND FEIX, 1998), although some rudimentary primordia structures were observed infrequently, which did not lead to an outgrowth of lateral roots. Later, HUSAKOVA *et al.* (2013) observed bulges of lateral root primordia on 6-day-old *lrt1* primary roots grown in hydroponics and 8-day-old *lrt1* primary roots grown in moist paper. It was also demonstrated, that lateral root primordia were initiated at comparable numbers in *lrt1* mutants compared to wild type plants, whereas a high reduction in the emergence of lateral root primordia was observed (51% reduction for non-aerated hydroponics and 69% for aerated hydroponics). These differences in lateral root primordia

formation were most likely caused by differences in the cultivation conditions and the age of the sampled roots (HUSAKOVA *et al.*, 2013). In *lrt1*, lateral root emergence was observed significantly further apart from the root tips.

Lrt1 plants are also smaller than wild type plants and retarded in growth (Figure 4B).

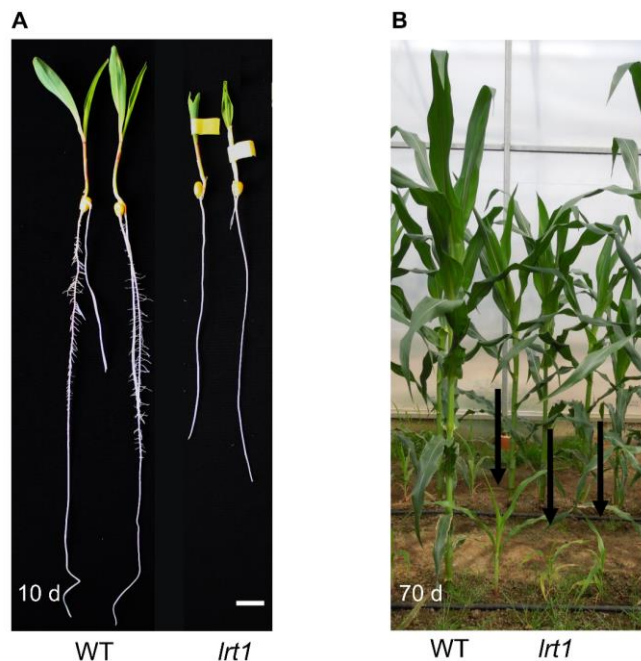


Figure 4 Phenotype of the *lrt1* mutant in comparison to wild type plants. **A:** Picture of 10-day-old seedlings grown in the paper roll system. **B:** Picture of 70-day-old plants grown in the greenhouse (*lrt1* plants highlighted by arrows). WT: wild type.

The lateral root primordia of the *lrt1* mutant showed clear defects throughout development. During the early stages, the lateral root primordia were wider and not confined, which leads to an abnormal high number of dividing pericycle cells with a disordered spatial arrangement (Figure 5). During later stages, cells of the surface layers of the lateral root primordia are more expanded and highly vacuolated, which leads to a loss of the typical structure of the lateral root primordia. Furthermore, lignification of cell walls especially on the base of older lateral root primordia was observed, but also lignification of primary root pericycle cells between protoxylem poles, the initiation side of lateral roots. Lateral root emergence is hindered in *lrt1* because the tissues above the lateral root primordia do not separate normally. Lateral roots, which are able to grow out of the primary root stop their growth shortly after emergence and exhibit a defective structure of the apical meristem, where cell lineages of initials are not visible. In some cases, *lrt1* also forms longer lateral roots with thicker and randomly curved tips and an unusual structure and swelling of the epidermal layers (HUSAKOVA *et al.*, 2013).

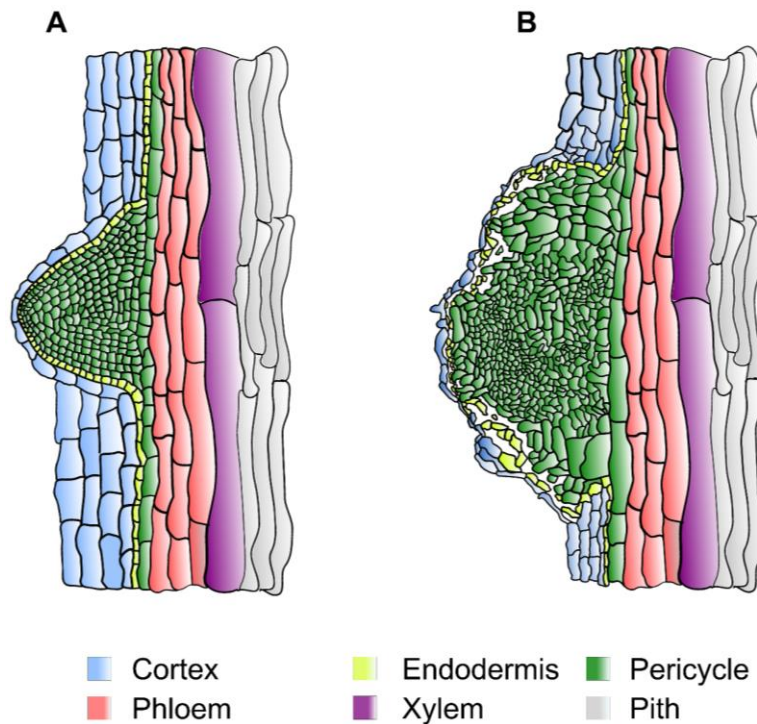


Figure 5 Formation of a mature lateral root primordium in wild type maize (A) and the *lrt1* mutant (B).

Beside the defects in lateral root development, the arrangement of cortical cells is altered because of irregularities in cell division. They are most obvious in the outermost layers of the hypodermis and overlaying epidermis, especially in subapical and older parts of the primary root (HUSAKOVA *et al.*, 2013).

Furthermore, *lrt1* seedlings grown in the dark display significantly reduced mesocotyl elongation. (HOCHHOLDINGER and FEIX, 1998).

A comparison of *lrt1* and wild type primary root proteomes of 9-day-old seedlings demonstrated that 10% of proteins primarily accumulated in *lrt1* primary roots (HOCHHOLDINGER *et al.*, 2004 b). These proteins probably respond to direct or indirect signals from the lateral roots in wild type plants and are therefore likely regulated by lateral roots. Particularly the repression of specific genes in the primary root by direct or indirect signals from the lateral roots is interrupted in the lateral rootless mutant *lrt1* which led to the observed accumulation of proteins whose transcription and translation is normally suppressed in wild type plants (HOCHHOLDINGER *et al.*, 2004 b; HOCHHOLDINGER *et al.*, 2018). Especially proteins related to lignin metabolism were among those proteins, which were identified to accumulate in *lrt1* primary roots. The Casparian strip of the endodermis is composed of primary cell wall components including lignin and act as a barrier to the apoplastic transport of water and solutes (HOSE *et al.*, 2001). The alteration of the chemical composition of the Casparian strip could be

a potential target for signals that originate in the lateral roots to modulate the proteome of the primary root in order to alter the capacity for the uptake of water and nutrients (HOCHHOLDINGER *et al.*, 2004 a, HOSE *et al.*, 2001).

In the primary root of the *lrt1* mutant, a higher peroxidase activity was detected (HUSAKOVA *et al.*, 2013). Also a L-ascorbate peroxidase (APX), which transforms H_2O_2 into H_2O and dehydroascorbate (DHA; SHARMA and DUBEY, 2004) was identified to preferentially accumulate in the *lrt1* primary root (HOCHHOLDINGER *et al.*, 2004). Furthermore, a higher expression of different class III peroxidases (PRXs) was identified in the primary root of *lrt1* compared to arbuscular mycorrhizal fungi (AMF) treated *lrt1* plants, in which the mutant phenotype was recovered (YU, 2022).

Peroxidases catalyzes the oxidoreduction between hydrogen peroxide and diverse reductants as phenolic compounds, lignin precursors, auxin, or secondary metabolites (HIRAGA *et al.*, 2001; PASSARDI *et al.*, 2004).

PRXs exists in large gene families with 73 genes in Arabidopsis (WELINDER *et al.*, 2002) and 138 genes in rice (PASSARDI *et al.*, 2004). They are involved in many physiological processes like in the modification of cell wall structures such as suberin polymerization (ARRIETA-BAEZ and STARK, 2006) and lignification, auxin catabolism, wound healing and pathogen defense (HIRAGA *et al.*, 2001). PRXs are also involved in modulating the balance between cell proliferation and differentiation by changing the O_2^- : H_2O_2 ratio in the root (Figure 6).

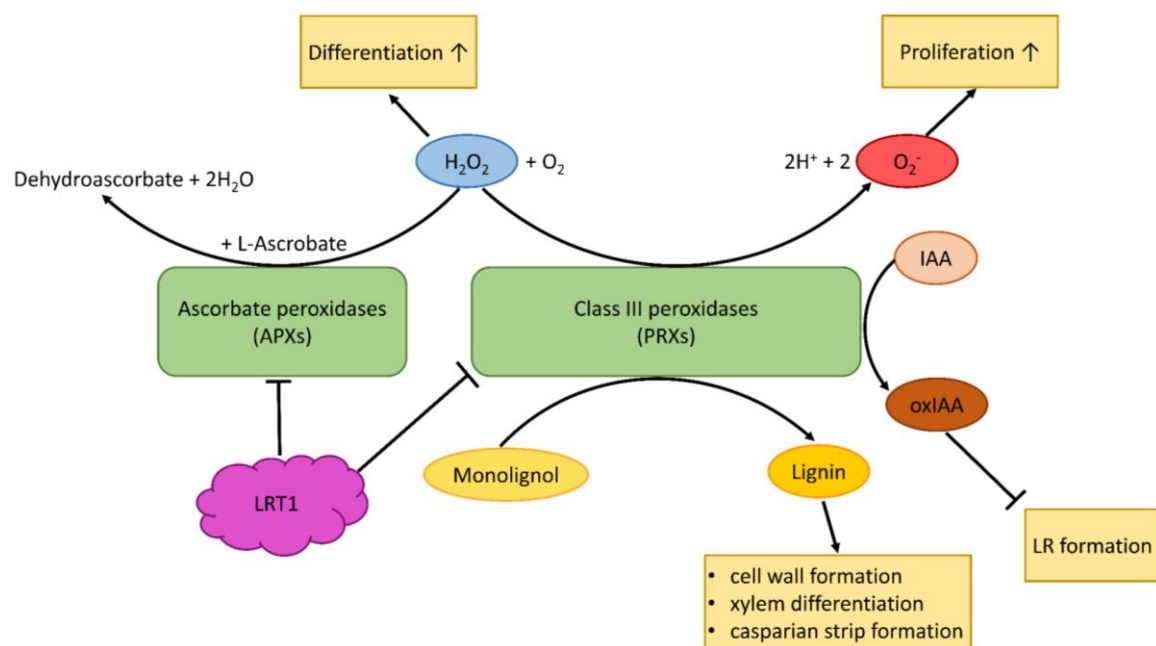


Figure 6 Proposed model of LRT1 affecting different physiological and biosynthetic processes in maize root development mediated by an inhibition of ascorbate peroxidases (APX) and Class III peroxidases (PRXs).

Under normal conditions superoxide (O_2^-) accumulates in the meristem whereas hydrogen peroxide (H_2O_2) accumulates in the elongation zone of the root. Upregulation of PRXs lead to a higher O_2^- content expanding the proliferation zone whereas an inhibition of PRXs lead to an increased H_2O_2 level, expanding the differentiation zone (Figure 6; TSUKAGOSHI *et al.*, 2010; ELJEBBAWI *et al.*, 2021).

Auxin is able to induce accumulation of H_2O_2 , leading to the initiation of lateral root formation MA *et al.* (2013). PRXs are able to degrade IAA (Figure 6). Thereby, overexpression of PRXs lead to a reduction of auxin, leading to a decreased auxin pool (COSIO *et al.*, 2009). Decreased auxin levels in turn inhibit lateral root formation (MORIWAKI *et al.*, 2011). On the other hand, inhibition of PRXs lead to an increased auxin pool (COSIO and DUNAND, 2009).

Peroxidases could also be involved in the regulation of cell wall loosening to enable the emergence of lateral root primordia through overlaying cells in the primary root (MASE and TSUKAGOSHI, 2021). In *lrt1* primary roots, separation of cell walls beside emerging lateral roots, normally enabling their emergence, is defective and the development of the *lrt1* lateral root primordia was often associated with ectopic lignification (HUSAKOVA *et al.*, 2013).

The previously described changes in peroxidase activity and thereby changes in ROS potentially changes the proportion between proliferation and differentiation in the *lrt1* mutant. By changes in peroxidase activity (APX and PRXs) further processes like lignification and endogenous auxin degradation could also be affected. Probable effects of the upregulated peroxidase activity in the *lrt1* mutant by a potential direct, or more likely indirect, involvement of LRT1 is summarized in Figure 6.

Most of the cloned genes associated with lateral root development in maize and rice are involved in auxin-related processes (YU *et al.*, 2016). In the *lrt1* mutant, the defective phenotype was not reversed by exogenous application of auxin (HOCHHOLDINGER AND FEIX, 1998) and a disturbance of the PIN1 efflux transporter localization was not observed. This led to the conclusion that auxin signaling is likely not directly affected in *lrt1* (SCHLICHT *et al.*, 2006).

Application of the symbiotic arbuscular mycorrhizal fungus (AM) *Glomus mosseae* to growing *lrt1* plants resulted in a full recovery of aboveground growth in comparison to wild type plants (PASZKOWSKI AND BOLLER, 2002). Furthermore, *Glomus mosseae* inoculation led to an induction of highly branched lateral root bushes on late crown and brace roots in *lrt1* plants. Thus, the recovery of the *lrt1* growth retardation might be explained by an increased nutrient absorption mediated by fungal hyphae as well as by the formation of the described lateral root bushes (PASZKOWSKI and BOLLER, 2002).

Similar to the recovery of *lrt1* plants by symbiosis with AM, the cultivation of *lrt1* plants under high-phosphate conditions lead to a complementation of the growth retardation (PASZKOWSKI and BOLLER, 2002). This is in line with the fact, that AM hyphae are able to penetrate into smaller soil pores and thereby mobilize adsorbed phosphate, which is otherwise not accessible to the plant (SMITH AND READ, 1997, PASKOWSKI AND BOLLER, 2002).

Moreover, it was demonstrated that the *lrt1* mutant is able to acquire more nitrogen than the seminal- and lateral rootless mutant *rum1* in nitrogen-poor soil, indicating that *lrt1* has an alternative way to maximize nitrogen acquisition (YU *et al.*, 2021).

Furthermore, the *lrt1* mutant is able to synthesize and excrete a higher amount of the flavones apigenin and luteolin to the rhizosphere in comparison to wild type plants (YU *et al.*, 2021).

Finally, it was demonstrated that the mutant *lrt1* is able to increase nitrogen uptake, biomass and lateral root formation under nitrogen deficient conditions in connection with soil-derived *Oxalobacteraceae* isolates of the genus *Massilia*. This was also the case when *lrt1* mutants were transplanted to soil harboring flavone-enriched rhizosphere microbiota (YU *et al.*, 2021). These properties seem to be auxin independent. Instead, they are rather mediated by a LRT1 molecular component that regulate plant development and which has an influence on the interaction of the root with microorganisms under low nitrogen conditions.

2.6 DDB1-CUL4 ASSOCIATED FACTOR (DCAF)

Gene expression is a highly regulated multistep process including transcription, translation and protein stability (BUCCITELLI and SELBACH, 2020). Beside the intracellular protein degradation by proteolysis in the lysosome, protein degradation by the ubiquitin-proteasome system is an important and universal posttranslational modification, which is a highly regulated process of many short-lived proteins in eukaryotic cells (CIECHANOVER *et al.*, 1984, AHN *et al.*, 2011). Proteasomal degradation includes the modification of protein substrates with multiple copies of ubiquitin chains followed by proteolysis of the ubiquitin-tagged proteins by the 26S proteasome (HERSHKO *et al.*, 1998).

In *Arabidopsis* 3,178 ubiquitinated proteins were identified, which are involved in many biological functions such as auxin, brassinosteroid, abscisic acid and jasmonic acid signalling pathways, defense and immune response and root development like lateral root morphogenesis and root hair elongation (SONG *et al.*, 2021). Furthermore, 40 transcription factor families with ubiquitylated proteins such as Aux/IAA, bHLH and NAC identified ubiquitin as a key regulator of transcription factor stability (SONG *et al.*, 2021). In the *Arabidopsis* genome more

than 1300 loci encoding for core components of the Ubiquitin/ 26S pathway were identified which correspond to ~5% of the proteome, pointing out how important and universally represented these processes are (VIERSTRA, 2003).

The CUL4-based E3 ligases represent a large subfamily of CULLIN-RING E3 ubiquitin ligases and consist of three core subunits: CULLIN4 (CUL4), a RING finger protein RING-BOX1 (RBX1) and UV-DAMAGED DNA BINDING PROTEIN1 (DDB1) (LEE and ZHOU, 2007) and are one of the key regulators in numerous processes of plant development and physiology (BIEDERMANN and HELLMANN, 2011).

The ubiquitination is mediated by a well ordered series of enzymatic reactions (Figure 7A). E1 activates ubiquitin in an ATP-dependent manner, creating a covalent thiolester-linked E1-ubiquitin complex with a second ubiquitin bound at the adenylation active site. The thiolester-linked ubiquitin is transferred to a reactive cysteine on an E2 conjugating enzyme by transesterification. Finally, ubiquitin-loaded E2s are released from E1s for substrate attachment by E3s.

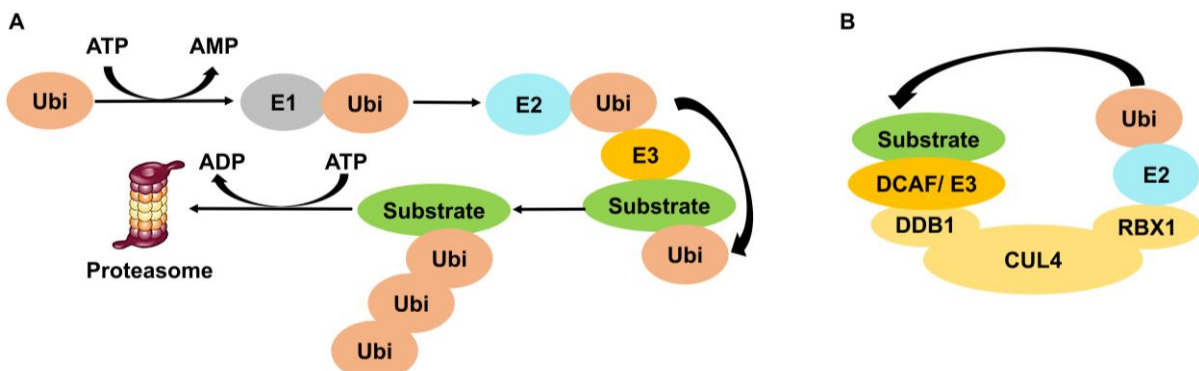


Figure 7 A: The ubiquitin proteasome system (modified according to PAGAN *et al.*, 2013) and **B:** the CUL4 E3 ubiquitin ligase. Ubi: ubiquitin, E1: ubiquitin activating enzyme, E2: ubiquitin conjugating enzyme, E3: E3 ligase, CUL4: CULLIN4, RBX: RING-BOX1, DDB1: UV-DAMAGED DNA BINDING PROTEIN, DCAF: DDB1 CUL4-ASSOCIATED FACTOR.

While the core subunits of this complex (Figure 7B, light yellow subunits) are highly conserved, the DDB1 protein in CUL4-based E3 ligases is able to interact with a high number of diverse DDB1 CUL4 ASSOCIATED FACTORS (DCAF, Figure 7B). Substrate specificity is mainly achieved by the DCAF proteins, which are required for binding of targets and optimal transfer of Ubiquitin from E2 enzyme to the substrate. The most conserved feature of DDB1 binding proteins is the presence of ~seven WD40 domains of which at least one ends in an aspartate-arginine motif (WDxR). In Arabidopsis so far 119 and in rice 151 DCAF proteins were identified (BIEDERMANN and HELLMANN, 2010). Furthermore, a conserved amino acid

sequence of 16 to 17 amino acids called the DDB1 BINDING WD40 (DWD)-box was observed to mediate the interaction of DCAF proteins with DDB1 (LEE *et al.*, 2008). Nevertheless, so far only a small proportion of DCAF proteins have been tested for their binding capability to DDB1 whereby the importance of those proteins is still unclear (CHOI *et al.*, 2014).

2.7 Protein-protein interaction analyses

The function and activity of proteins is mainly influenced by the interaction with other proteins. Protein biosynthesis, transport and degradation as well as gene regulation rely on protein-protein interaction (XING *et al.*, 2016). On average, plants have about 32,000 protein coding genes (MICHAEL, 2014). Maize has 41,577 protein coding genes (B73 RefGen_v5). Between 75,000 and 150,000 interaction pairs are estimated for plant proteomes of 30,000-40,000 proteins, based on extrapolation of the yeast interactome (MORSY *et al.*, 2008; RAMÍREZ-SÁNCHEZ *et al.*, 2016).

Overall, two main types of protein-protein interactions (PPIs) can be differentiated. Constitutive protein-protein interactions are very stable and primarily from subunits of permanent complexes which fulfill main functions in the cell. On the other hand, regulative PPIs exist in specific cellular or developmental segments or in response to environmental signals (STRUK *et al.*, 2018). These regulative protein-protein interactions are part of biochemical cascades and often transient since these proteins continuously associate and dissociate from each other (NOOREN and THORNTON, 2003). Protein-modifying enzymes such as proteases belong to this type, which shortly interact with their substrates (FERRO and TRABALZINI, 2013). Furthermore, protein-protein interactions can be divided in obligate and non-obligate based on their stability and can be transient or permanent based on their half-life. Furthermore, they can possess a homo- or heterooligomeric structure based on their composition (RAO *et al.*, 2013).

Analyzing protein-protein interactions is especially important to understand biological processes on the molecular level (PAWSON and NASH, 2003). To identify these interactions, different methods are available which include biochemical, molecular biological, genetic as well as physical methods (PHIZICKY and FIELDS, 1995). *In vivo* as well as *in vitro* methods are available whereby *in vivo* techniques have the benefit that potential protein-protein interactions can be accessed in the native location (XING *et al.*, 2016). Moreover, large scale methods that create databases for proteome wide physical connections between protein pairs are available (DE LAS RIVAS and FONTANILLO, 2010). Beside experimental methods, it is also possible to do computational identification of protein-protein interactions. Computationally predicted protein-

protein interaction data are also available for plant proteomes including Arabidopsis, soybean, rice and maize (DING and KIHARA, 2019; XING *et al.*, 2016; ZHU *et al.*, 2016; MUSUNGU *et al.*, 2015).

In plant science Yeast two-hybrid (Y2H), Fluorescence resonance energy transfer (FRET), bimolecular fluorescence complementation (BiFC) and split-luciferase complementation are mainly used to analyze protein-protein interactions (XING *et al.*, 2016). Furthermore, high-throughput scans of protein microarrays are performed in plants (POPESCU *et al.*, 2007). Even if it is not possible to analyze dynamic protein-protein interactions with *in vitro* protein microarrays, they enable a fast detection of weak and transient protein-protein interactions (FUENTES *et al.*, 2007).

Affinity purification coupled with mass spectrometry (AP-MS) is also used in plants and allows for a fast, selective and sensitive detection of protein-protein interactions under near-physiological conditions (VAN LEENE *et al.*, 2015). Basically, the protein of interest is fused to an affinity tag, which allows the purification together with its interaction partners. At the end the isolated protein complex is analyzed by liquid chromatography tandem-mass spectrometry (LC-MS/MS) (FUKAO, 2012).

In the following section, I will focus on the molecular biological Yeast-two-hybrid (Y2H) screening and the biochemical bimolecular fluorescent complementation assay (BiFC) which were both used in this study.

2.7.1 Yeast two-hybrid (Y2H)

The basic principle of the yeast two-hybrid method is based on the Gal4 transcription activator protein which contains a DNA binding and an activation domain. Those two separate and independent Gal4 domains, which are not able to function alone, can be fused to proteins whose interaction should be examined. Thereby one protein, which is called bait, is fused to the DNA binding domain and the second protein, which is called prey, is fused to the activation domain. If both proteins interact, they are able to bring the activation domain into close proximity of the binding domain, causing a functional Gal4 transcription activator domain, which leads to the expression of downstream reporter genes (Figure 8A, FIELDS and SONG, 1989; YOUNG, 1998).

The Y2H method can be used either to directly verify the interaction of two proteins of interest or to screen complete prey plasmid cDNA libraries. This allows to identify proteins that are able to interact with the bait protein of interest, which is a main advantage of this method (STYNEN *et al.*, 2012). The cDNA libraries can be constructed from certain plant tissues or

organs which allows the evaluation of physiologically or developmentally important interactions (XING *et al.*, 2016).

Furthermore, large scale interaction networks in plants like *Arabidopsis* (DEFOLTER *et al.*, 2005; DREZE *et al.*, 2011; VERNOUX *et al.*, 2011 and Trigg *et al.*, 2017), barley (SCHOONHEIM *et al.*, 2007), wheat (TRADIF *et al.*, 2007) and rice (DING *et al.*, 2009) were created using Y2H.

Y2H is able to detect weak and transient protein-protein interaction since once the interaction took place, transcriptional activation of the reporter genes amplifies the signal and increases the sensitivity of the method.

A major limitation of the classical Y2H method is the requirement of the nuclear localization of the interaction partners, which theoretically can be avoided by relocation to the nucleus using truncated versions of the proteins of interest, which in turn leads often to proteins which are not functional (XING *et al.*, 2016). However, the mating-based split-ubiquitin system (mbSUS) was invented to also analyze interactions of membrane proteins (MILLER *et al.*, 2005).

To be able to study interactions between components of a multi-subunit complex, the yeast three-hybrid (Y3H) method was developed which includes a third protein as bridge to connect two not directly interacting proteins (MARUTA *et al.*, 2016).

Using multiplexed Cre reporter-mediated Y2H coupled with next-generation sequencing enables high-throughput and large-scale interactome mapping (STRUK *et al.*, 2018).

Y2H can also be applied for a (semi-)quantitative evaluation of interaction by using the enzymatic β -galactosidase-encoding reporter LacZ which labels yeast cells with a colorimetric substrate, such as 5-bromo-4-chloro-3-indolyl- β -D-galactopyranoside (X-Gal) or o-Nitrophenyl- β -D-galactopyranoside (ONPG) (MÖCKLI and AUERBACH, 2004).

Since reporter gene activation needs between two and three days in Y2H experiments, it cannot detect fast changes in the interaction affinity which are often caused by environmental factors (STRUK *et al.*, 2018).

The heterologous expression of a plant protein in other organisms like yeast can affect their subcellular localization. Translation by low translation efficiency due to suboptimal codon usage (GREFEN, 2014) or posttranslational modifications like protein folding can also be changed by a heterologous expression. Thus, it might be impossible to detect a protein-protein interaction from the host organism (XING *et al.*, 2016). To avoid this problem, the protoplast two-hybrid (P2H) has been invented where the GAL4-based Y2H principle is used for a transient

transformation of *Arabidopsis* protoplasts and the interaction visualization by using the β -glucuronidase (GUS) reporter (EHLERT *et al.*, 2006). Also using other homologous expression systems like BiFC is an option to analyze protein-protein interactions in plants and therefore become increasingly popular also because of the underlying simple protocols (KUDLA and BOCK, 2016).

2.7.2 Bimolecular fluorescence complementation (BiFC)

The bimolecular fluorescence complementation (BiFC) method is based on the observation, that it is possible to split a fluorophore like GFP or YFP into a N- and a C-terminal fragment, which are not fluorescent respectively. Mediated by the interaction of two proteins, the fused fluorophore fragments are able to refold, mature and fluoresce (Figure 8B, GHOSH *et al.*, 2000).

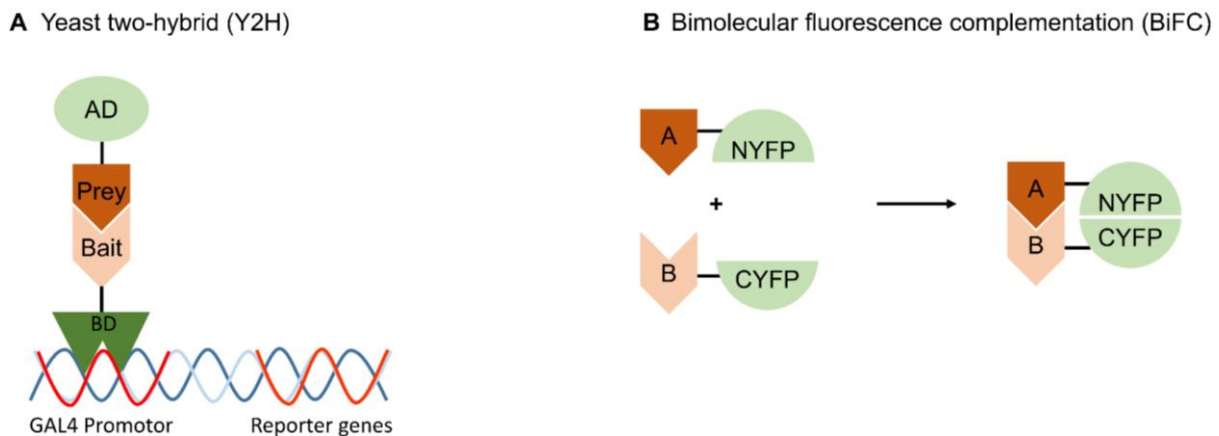


Figure 8 Protein-protein interaction analysis via yeast two-hybrid (Y2H, **A**) and bimolecular fluorescence complementation (**B**). AD: Gal4 activation domain; BD: Gal4 DNA-Binding domain; A+B: Proteins of interest tested for interaction.

BiFC as well as Y2H are dependent on the simultaneous expression of two fusion proteins in the same cell. As a consequence, these co-transformations causes several problems like different copy numbers, variations in the expression level which can cause alteration or a complete loss of interacting partners. Furthermore, without having internal controls a quantitative interpretation of results is challenging (GREFEN and BLATT, 2018).

To avoid these problems, GREFEN and BLATT (2018) invented a 2in1 ratiometric BiFC approach (rBiFC) which allows the simultaneous expression of two different genes by the introduction of multiple expression cassettes within one vector backbone. In this system the expression cassettes of the genes of interest are flanked by the N- and C- terminal halves of YFP respectively. In addition, a monomeric red fluorescent protein (mRFP) is integrated in the vector which allows ratiometric analysis (GREFEN and BLATT 2018).

Since only spatial proximity is required and not direct interaction of the proteins fused to the fluorophore halves, fluorophore complementation can occur as the result of short distance of the two fluorophore halves to each other (KERPPOLA, 2006).

Apart from that, BiFC is also a very useful tool to examine multiple alternative protein complexes (HU and KERPPOLA, 2003; WAADT *et al.*, 2008) as well as ternary protein complexes by a developed dual-color trimolecular fluorescence complementation assay (TriFC; OFFENBORN *et al.*, 2015). This technique combines protein fragments of mCerry and mVenus, in which a scaffold protein is bilaterally fused to C-terminal fragments of both fluorescent proteins and combined with potential interacting proteins fused to an N-terminal fluorescent protein fragment (OFFENBORN *et al.*, 2015).

3 OBJECTIVES

The overall aim of this thesis was the validation of the *lrt1* candidate gene and its functional characterization as a DCAF homolog to understand the function and molecular interaction of LRT1 during lateral root formation of maize. The following hypotheses were tested:

- (1) The *lrt1* gene is causal for the lateral rootless phenotype in the *lrt1* mutant
- (2) The *lrt1* gene encodes a DCAF homolog.
- (3) The LRT1 protein and its paralog LRT1-LIKE display the typical sequence motifs of DCAF proteins and are phylogenetically related to other members of the gene family.
- (4) The *lrt1* gene influences peroxidase activity associated with changes in ROS and thereby changing the proportion between proliferation and differentiation in the root.
- (5) The *lrt1* and *lrt1-like* genes are expressed in a root-type and tissue-specific, development-dependent and cell type-specific manner in maize roots.
- (6) The LRT1 protein is localized in the nucleus.
- (7) The LRT1 protein interact with DDB1 in CULLIN4-based E3 ligase (CRL4) complexes.
- (8) LRT1 is a substrate receptor of a CULLIN4-based E3 ligase (CRL4) complex and thus interacts with yet unknown protein substrates.

4 MATERIAL AND METHODS

4.1 Material

4.1.1 Plant material

In the present study different root types (primary, seminal, lateral and crown roots) and root tissues (meristematic zone, elongation zone, cortex and stele) of the maize inbred line B73 and the mutants *lrt1* and *rum1* were used for gDNA and RNA isolation. Isolated gDNA was used for genotyping and sequencing, RNA was used for cDNA synthesis as basis for sequencing, expression analysis and cloning procedures. All samples which originated from *lrt1* and *rum1* mutants were verified by genotyping prior to use.

4.1.2 Bacterial and yeast strains

Table 1 List of bacterial and yeast strains used in this study

Organism	Genotype	Reporter gene	Marker gene	Reference
<i>E. coli</i> DH5 α	F ⁻ , lacZ Δ M15, Δ lacZU169 <i>recA1</i> , <i>endA1</i> , <i>hsdRMS</i> , <i>phoA</i> <i>supE</i> , <i>thi-1</i> , <i>gyrA96</i> , <i>relA</i>	LacZ	<i>thi-1</i>	Thermo Fisher Scientific, Waltham, USA
<i>S. cerevisiae</i> Y187	MAT α , <i>ura3-52</i> , <i>his3-200</i> , <i>ade2-101</i> , <i>trp1-901</i> , <i>leu2-3</i> , 112, <i>gal4Δ</i> , <i>gal80Δ</i> , <i>met-</i> , URA3 : : GAL1UAS– Gal1TATA–LacZ MEL1	MEL1, LacZ	<i>trp1</i> , <i>leu2</i>	HARPER <i>et al.</i> , 1993
<i>S. cerevisiae</i> Yeast Gold	MAT α , <i>trp1-901</i> , <i>leu2-3</i> , <i>ura3-52</i> , <i>his3-200</i> , <i>gal4Δ</i> , <i>gal80Δ</i> , LYS2 : : GAL1UAS– Gal1TATA–His3, MEL1, GAL2UAS–Gal2TATA–Ade2 URA3 : : MEL1UAS– Mel1TATA <i>AUR1-C</i>	AbAr, HIS3, ADE2, MEL1	<i>trp1</i> , <i>leu2</i>	NGUYEN, ClonTech, Mountain View, CA, USA
<i>S. cerevisiae</i> PJ694A	MAT α , <i>trp1-901</i> , <i>leu2-3</i> , <i>ura3-52</i> , <i>his3-200</i> , <i>gal4Δ</i> , <i>gal80Δ</i> , LYS2 : : GAL1-HIS3, GAL2-ADE2, <i>met2::GAL7-</i> <i>lacZ</i>	ADE2, HIS3, LacZ	<i>trp1</i> , <i>leu2</i>	JAMES <i>et al.</i> , 1996
<i>A. tumefaciens</i> AGL-1				LAZO, <i>et al.</i> , 1991
<i>A. tumefaciens</i> C58C1				ASHBY <i>et al.</i> , 1988

4.1.3 Enzymes

All enzymes which were used in the present study and which are listed below originated from Thermo Fisher Scientific (Waltham, MA, USA).

FastAP Thermosensitiv Alkaline Phosphatase

FastDigest Restriction enzymes

Gateway™ BP Clonase™ II Enzyme mix

Gateway™ LR Clonase™ II Enzyme mix

Phusion High-Fidelity DNA Polymerase

T4 DNA Ligase

4.1.4 Kits for molecular biology

Table 2 Kits for molecular biology used in this study

Kit	Manufacturer
CloneJET PCR Cloning Kit	Thermo Fisher Scientific, Waltham, USA
Make Your Own “Mate & Plate™” Library	ClonTech, Mountain View, CA, USA
Matchmarker® Gold Yeast Two-Hybrid System	ClonTech, Mountain View, CA, USA
Monarch® DNA Gel Extraction Kit	NEB Ipswich, USA
Monarch® Plasmid Miniprep Kit	NEB Ipswich, USA
PerfeCTa SYBR Green SuperMix	Quantabio, Beverly, USA
qScriptcDNA SuperMix	Quantabio, Beverly, USA
RevertAid First Strand cDNA Synthese Kit	Thermo Fisher Scientific, Waltham, USA
RNeasy Plant Mini Kit	QUIAGEN, Hilden, Deutschland

4.1.5 Vectors

Table 3 Vectors used in this study

Name	Resistance	Experiment	Source
pJET1.2/blunt	Amp	Cloning of <i>lrt1</i> , <i>lrt1-like</i> , <i>ddb1-like1</i> , <i>ddb1-like 2</i>	Thermo Fisher Scientific, Waltham, USA
pDONR™ 221 P1-P4	Kan	Cloning for BiFC and FRET	Thermo Fisher Scientific, Waltham, USA

Table 3 continued

Name	Resistance	Experiment	Source
pDONR™ 221 P3-P2	Kan	Cloning for BiFC and FRET	Thermo Fisher Scientific, Waltham, USA
pFRETvr-2in1-CC	Spec	Subcellular localization	HECKER <i>et al.</i> (2015)
pBiFCt-2in1-NN	Spec	Interaction LRT1 with DDB1L1 and DDB1L2	GRAFEN and BLATT (2012)
pBiFCt-2in1-NN	Spec	Interaction LRT1 with DDB1L1 and DDB1L2	GRAFEN and BLATT (2012)
pBiFCt-2in1-NN	Spec	Interaction LRT1 with DDB1L1 and DDB1L2	GRAFEN and BLATT (2012)
pBiFCt-2in1-NN	Spec	Interaction LRT1 with DDB1L1 and DDB1L2	GRAFEN and BLATT (2012)
pBiFCt-2in1-NN	Spec	Interaction LRT1 with DDB1L1 and DDB1L2	GRAFEN and BLATT (2012)
pGADT7	Amp	Y2H	Takara, Kusatsu, Japan
pGADT7-Rec	Amp	Y2H	Takara, Kusatsu, Japan
pGADT7-T	Amp	Y2H	Takara, Kusatsu, Japan
pGBKT7	Kan	Y2H	Takara, Kusatsu, Japan
pGBKT7-53	Kan	Y2H	Takara, Kusatsu, Japan
PGBKT7-Lam	Kan	Y2H	Takara, Kusatsu, Japan

4.1.6 Software and internet tools for bioinformatics analyses

Table 4 List of Software and internet tools for bioinformatics analyses used in this study

Resource	Reference
BioEdit Sequence Alignment Editor	http://www.mbio.ncsu.edu/bioedit/bioedit.html
Bowtie2	LANGMEAD and SALZBERG, 2012
Chromas	http://technelysium.com.au/wp/chromas/
FigTree v1.43	http://tree.bio.ed.ac.uk/software/figtree/
Ident and Sim	STOTHARD, 2000
ICE	https://ice.synthego.com/#/
ImageJ	SCHNEIDER <i>et al.</i> , 2012
Localizer	SPERSCHNEIDER <i>et al.</i> , 2017

Table 4 continued

Resource	Reference
Maize Genetics and Genomics Database	http://www.maizegdb.org
Mega X	KUMAR <i>et al.</i> , 2018
MrBayes	RONQUIST and HUELSENBECK, 2003
National Center for Biotechnology Information	http://www.ncbi.nlm.nih.gov
Phytozome 12	https://phytozome-next.jgi.doe.gov
PredictProtein	http://www.predictprotein.org
Primer 3	http://bioinfo.ut.ee/primer3-0.4/
RStudio	https://www.R-project.org/
Serial Cloner	http://serialbasics.free.fr/serial_cloner.html
UniProt	https://www.uniprot.org/
ZEN 3.4	Zeiss, Jena, Germany

4.2 Methods

4.2.1 Growth conditions

Unless otherwise stated in the respective methods part, all seedlings were germinated in germination paper rolls (Anchor paper, Minnesota, USA) located in 5 l buckets filled with ~2 l of distilled water and incubated in a growth cabinet (Conviron Germany GmbH, Berlin, Germany) with a photoperiod of 16 h light (2700 lux) at 28 °C and 8 h dark at 18 °C.

4.2.2 Phenotypic analysis of the *lrt1* mutant in comparison to wild type

For phenotypic analysis of shoot length, primary root length over time and seminal root number in total 68 homozygous wild type, 97 heterozygous wild type and 54 mutants were analyzed. Plants were grown in a hydroponic system for 10 days in distilled water without nutrient supplementation.

Crown root phenotyping to compare *lrt1* and wild type plants was performed 23 and 30 days after germination in order to examine the possibility of crown root formation in the *lrt1* mutant.

4.2.3 Analysis of root gravitropic response of *lrt1*

Segregating *lrt1* seedlings were grown in rhizoboxes (Figure 9A and B) for 10 days before rotation by 90°. For analysis, the root angle of every primary root tip was measured in relation to the horizontal 3 h, 6 h, 12 h, 24 h, 48 h and 72 h after rotation whereby the angle right after rotation was set to 0. Measurement of root tip angles was performed with the software ImageJ (SCHNEIDER *et al.*, 2012). Significance was analyzed and grouped in R using the Tukey's test.

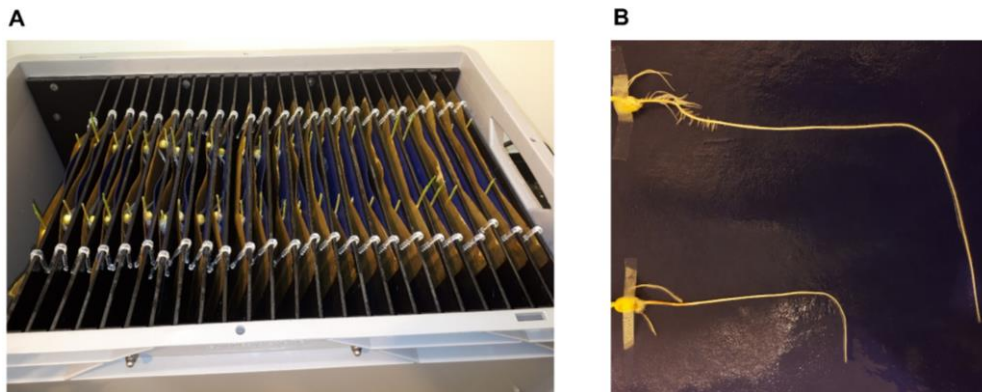


Figure 9 Analysis of gravitropic response in *lrt1*. **A:** Rhizobox containing 25 slides with two maize kernels each. **B:** Rhizobox slide with two maize kernels fixed with tape on blue and uncovered germination paper.

4.2.4 Analysis of skotomorphogenesis in *lrt1*

For the analysis of skotomorphogenesis, 10 homozygous *lrt1* plants and 10 wild type plants were germinated in the paper roll system as previously described (4.2.1) in dark and control conditions. In dark conditions, the seedlings were grown without light for 7 days at 26 °C. In control conditions, the seedlings were grown in a day/night cycle with 16 h light and 8 h dark, both at 26 °C. Seven days after germination, mesocotyl and coleoptile length of all plants for both treatments were measured. Significance was analyzed and grouped in R using the Tukey's test.

4.2.5 Ethylene and ethylene inhibitor treatment of *lrt1*

The effect of exogenous ethylene and ethylene inhibitor supplementation on the *lrt1* mutant was analyzed using the ethylene precursor 1-aminocyclopropane-1-carboxylate (ACC) in concentrations of 1 μ M, 5 μ M, 10 μ M and 1 mM silver nitrate (AgNO_3), which inhibits ethylene receptors, in concentrations of 100 μ M, 500 μ M and 1 mM. The experiment was performed in the paper roll system (4.2.1) in 1 l cylinders completely covered with aluminum foil to prevent roots from light stress. Seeds from a family which is segregating for the *lrt1* mutant were used, phenotyped and genotyped 14 days after germination and treatment.

4.2.6 Chemical treatments of *lrt1* with substances affecting peroxidase activity and ROS

The effect of different chemicals affecting the peroxidase activity and ROS was analyzed in the *lrt1* mutant in comparison to wild type seedlings. Therefore, the effect of exogenous application of the peroxidase inhibitors potassium cyanide (KCN) and salicylhydroxamic acid (SHAM), as well as the peroxidase activity modulator umbelliferone and the reactive oxygen species hydrogen peroxide (H₂O₂) in concentrations of 10 μM, 100 μM and 1mM was analyzed. The experiment was performed in the paper roll system (4.2.1) in 1 l cylinders completely covered with aluminum foil to prevent root from light stress. Seeds from a family which is segregating for the *lrt1* mutant were used, phenotyped and genotyped 14 days after germination and treatment.

4.2.7 Sequence analysis and phylogeny

The annotation of the *lrt1* gene differed between version 3 and version 4 of the maize genome sequence. While in version 3 the *lrt1* gene was annotated as two genes (GRMZM2G348735 and GRMZM2G1108699), these sequences and a sequencing gap between them was merged into one accession (Zm00001d026691) from version 4 on (Supplemental Table 1). To confirm the predicted exon-intron structure of *lrt1*, oligonucleotide primer pairs covering the complete region of the predicted *lrt1* gene were designed to amplify overlapping fragments of ~1 kb, using cDNA or gDNA as a template. Subsequently, an exon-intron gene model was constructed based on amplicons sequenced by Sanger sequencing and aligned using BioEdit (HALL, 1999). The obtained gene model corresponded to the suggested gene model in version 4 (Zm00001d026691) and version 5 (Zm00001eb434410) of the B73 reference genome.

The predicted protein sequence of *lrt1* was used to perform a blastp search against the selected plant species *Arabidopsis thaliana*, *Brachypodium distachyon*, *Chlamydomonas reinhardtii*, *Cucumis sativus*, *Camellia sinensis*, *Oropetium thomaeum*, *Oryza sativa*, *Physcomitrella patens*, *Populus trichocarpa*, *Setaria italica*, *Setaria viridis*, *Solanum lycopersicum*, *Sorghum bicolor*, *Theobroma cacao* and *Zea mays* in the Phytozome 12 plant genomics portal (<https://phytozome.jgi.doe.gov/pz/portal.html>). All homologous protein sequences representing the longest transcript per gene were downloaded and aligned using the MUSCLE algorithm in MEGA 10 (KUMAR *et al.*, 2018). The Phylogenetic tree was generated by MrBayes (RONQUIST and HUELSENBECK, 2003) using the mixed model algorithm with four chains and 1 M generations. Subsequently, the phylogenetic tree was built using FigTree software (<http://tree.bio.ed.ac.uk/software/figtree/>).

4.2.8 Validation of the *lrt1* candidate gene by CRISPR-Cas9

The Golden Gate entry clone pGG-A-ZmUBILp-B was constructed by PCR amplification using pEN-L4-UBIL-R1 (KARIMI *et al.*, 2007) as a template and the oligonucleotide primers 5′-TTTTGGTCTCAACCTGTGCAGCGTGACCCGGTCGTGC-3′ and 5′-TTTTGGTCTC-AGTTTGCAGAAGTAACACCAAACAAC-3′. The resulting PCR product was cloned into a *Bsa*I-digested GreenGate pGGA000 entry vector (LAMPROPOULOS *et al.*, 2013). The Cas9 GatewayTM entry clone pEN-L4-ZmUBILp-Cas9PTA-G7-R1 was subsequently constructed by Golden Gate cloning using pGG-A-ZmUBILp-B and the other Golden Gate entry clones pGG-B-Linker-C, pGG-C-Cas9PTA*-D, pGG-D-Linker-E, and pGG-E-G7T-F (LAMPROPOULOS *et al.*, 2013; DECAESTECKER *et al.*, 2019), and pEN-L4-AG-R1 (HOUBAERT *et al.*, 2018). The sgRNA Gateway (Thermo Fisher Scientific, Waltham, USA) entry clones pMR220 (attL1-attR5) and pMR221 (attL5-attL2) contain a sgRNA cassette similar to pMR185 (TRIPATHI *et al.*, 2019) with the OsU6 promoter followed by two *Bbs*I restriction sites and tracer RNA scaffold. They allow combining two sgRNA modules by appropriate recombination sites as previously described (RITTER *et al.*, 2017).

Complementary oligonucleotides generating 4 bp overhangs upon annealing, for the sgRNA targeting of exon 2 (5′-GTTGTTCGTGTTATTGAACGTT-3′ and 5′-AAACAACGTTCAAT-AACACGAA-3′) and for the sgRNA targeting exon 4 (5′-GTTGCTGAGAACATATGC-GATT-3′ and 5′-AAACAATCGCATATGTTCTCAG-3′), were inserted via a cut-ligation reaction with *Bbs*I (Thermo Fisher Scientific, Waltham, USA) and T4 DNA ligase (Thermo Fisher Scientific, Waltham, USA) in pMR220 and pMR221. The Gateway destination clone pBbm42GW7 (KARIMI *et al.* 2013) containing the *bar* gene under control of the double CaMV 35S promoter was used to combine the Cas9 module with the two sgRNA modules. The resulting expression vector was transferred to *Agrobacterium tumefaciens* strain EHA101, which was used for the transformation of the maize inbred line B104 (COUSSENS *et al.*, 2012). After transformation, genomic DNA was isolated from single leaves per regenerated plant. Oligonucleotide primers for TIDE tracking of indels by DEcomposition were designed using Primer 3 (<http://bioinfo.ut.ee/primer3-0.4/>) using standard parameters. Standard PCR reactions were performed using Phusion High-Fidelity DNA Polymerase (Thermo Fisher Scientific, Waltham, USA) to amplify 650 bp fragments including the two predicted Cas9 cut sites. Subsequently PCR amplicons were separated on 1% agarose gels and purified using the Monarch Gel Extraction Kit (NEB, Ipswich, MA, USA). The purified amplicons were sequenced by Sanger Sequencing. Quantitative sequence trace data were decomposed using

ICE (<https://ice.synthego.com/#/>). Furthermore, a fragment of ca. 1150 bp containing both Cas9 target sites was amplified to detect genomic deletions between these target sites. Cas9-specific primers were used for genotyping for the presence of the T-DNA insertion. Cas9 null segregants with novel Cas9-induced mutations at the *lrt1* locus were subsequently crossed with genotyped heterozygous and homozygous *lrt1-1* plants.

4.2.9 Identification of DWD proteins in maize

To identify all DWD proteins in maize, all annotated Maize WD40 proteins were retrieved from the UniProt protein database. In total 489 hits were retrieved after counting splice variants as a single protein. Among those, as identified by Scanprosite (<http://www.prosite.expasy.org/scannprosite>), 131 proteins displayed at least one WDxR motif, which is a basic requirement of DWD proteins for the interaction with DDB1 proteins. A subset of 55 of those proteins contained at least one 16 bp DWD motif ([ILVAMPWF]-[ILVAMPWFCS]-[AGSTPDNR]-[AGSTPDN]-[AGSTPDNLME]-x-[DELI]-x-x-[ILVAMPWFSG]-x-[ILVAMPWF]-[WY]-[DE]-[ILVAMPWFRT]-[RK]) (LEE *et al.*, 2008; modified by amino acids present in the DWD motif of LRT1 and LRT1-LIKE). The full-length protein sequences of these 55 proteins were subsequently used for alignment using the MUSCLE algorithm and the construction of an unrooted tree using the neighbor-joining method with the WAG+F substitution model in Mega X.

4.2.10 Expression analysis

For expression analysis via real-time PCR (qRT-PCR), seeds of the maize inbred line B73 and segregating seeds of *lrt1* and *rum1* were germinated in paper rolls (Anchor Paper, Saint Paul, MN, USA) for 4 to 14 days in a growth chamber in a 16 h light (28 °C)/ 8 h dark (8 °C) cycle as previously described (HETZ *et al.*, 1996).

Pools of ten roots per stage and genotype were harvested per biological replicate. Each experiment was performed in three biological replicates. Lateral roots were harvested by dipping primary roots, after forming lateral roots ~12 to 14 days after germination, in liquid nitrogen and scrapping off the lateral roots manually with a spatula.

For 2-4 cm primary roots four different tissues were sampled. First the apical 2 mm of the root were collected, containing the root cap and meristematic zone. Secondly, the zone adjacent to the root tip up to the part of the root where root hairs become visible was separated under the binocular, which corresponds to the elongation zone. Finally, the distal differentiation zone,

from the root hair zone up to the coleorhiza was mechanically separated into cortex and stele without damaging pericycle and endodermis cells as previously described (SALEEM *et al.*, 2009).

Three biological replicates, each consisting of 30 pooled root tissues from the same 30 seedlings were used. Crown roots and seminal roots were harvested at a length of 2-4 cm. The first leaf was harvested 9 days after germination.

All samples were immediately frozen in liquid nitrogen and stored at -80 °C until RNA extraction. Prior to RNA isolation, samples were pulverized in liquid nitrogen in pre-cooled mortars using pestles.

Total RNA was extracted from 80 mg of ground root tissue using the RNeasy Plant Mini Kit (Quiagen, Venlo, The Netherlands). RNA integrity was controlled on a 1% agarose gel. cDNA was synthesized from 400 ng total RNA using the qScriptcDNA SuperMix (Quantabio, Beverly, USA). Prior to qPCR, all cDNAs were diluted 1:2. qPCR was performed in a BioRad CFX 384 Real-Time System (Biorad, Hercules, CA, USA) for each biological replicate in three technical replications in 4 µl total reaction volume using the Quantabio PerfeCTa SYBR Green SuperMix (Quantabio, Beverly, USA). Oligonucleotide Primer efficiencies were tested in a dilution series (1, 1/2, 1/4, 1/8, 1/16, 1/32, 1/64, 1/128) and calculated as previously described (BUSTIN *et al.*, 2009): PCR amplification efficiency = $10^{-1/\text{slope}} - 1$. Primer efficiencies were between 85% and 100%, and R^2 was >0.95. Transcript levels were analyzed for all genes with respect to the expression level of the *homeobox-transcription factor 3 (hb3)* gene (Zm00001eb295800), a gene, which show consistent expression in all root tissues (BALDAUF *et al.*, 2016). Significant differences of means between each sample were calculated by Tukey's test ($p < 0.05$) and indicated with small letters.

4.2.11 Yeast two hybrid experiments

4.2.11.1 Construction of a cDNA library

For the construction of a cDNA library, RNA was isolated from 10-day-old primary roots of the maize inbred line B73. To this end, 15 primary roots were ground with mortar and pestle in liquid nitrogen. RNA isolation was performed using the RNeasy Plant Mini Kit (Quiagen, Hilden, Germany) according to manufacturer's protocol. An optional on-column DNase digestion using the RNase-free DNase set (Quiagen, Hilden, Germany) was performed according to manufacturer's protocol with an elongated incubation time of 30 min. After elution

of RNA in 30 μ l dH₂O RNA concentration was measured spectrometrically with NanoDrop (Thermo Fisher Scientific, Waltham, USA). RNA integrity and absence of DNA contamination was checked on a 1% agarose gel (100V, 30 min).

First-strand cDNA synthesis using CDSIII oligonucleotides, long distance PCR and cDNA purification with CHROMA SPIN+ columns was performed using the Mate and Plate library kit (ClonTech, Mountain View, CA, USA). Poly A⁺ RNA was used as positive control. cDNA quality and quantity was checked on a 1.2% agarose gel (120V, 60 min). In addition, cDNA concentration was measured spectrometrically.

Preparation and transformation of competent yeast cells was performed with the Yeast Transformation System 2 (ClonTech, Mountain View, CA, USA). The cDNA library was transformed into the yeast strain Y187 using 15 μ g of the prepared cDNA and 6 μ l of the linearized vector pGADT7-Rec. A decimal dilution series was plated onto SD- Leu and incubated together with the total transformed cells at 30 °C for four days to determine the number of independent clones in the library. Thereafter, transformed cells were harvested and aliquoted according to manufactures protocol and stored at -80 °C. A decimal dilution series of the pooled library transformants was plated onto SD- Leu and incubated at 30 °C for four days to determine the library titer in cfu/ml.

4.2.11.2 Construction of *lrt1* Bait construct

The full length CDS of *lrt1* containing two *Sma*I restriction sites and one additional base pair directly before start in order to maintain the reading frame in the destination vector was used for ligation into *Sma*I digested pGBKT7 and additionally for later control experiments also in *Sma*I digested pGADT7 vectors.

4.2.11.3 Test for autoactivation and toxicity of bait and prey constructs

All created constructs were tested for autoactivation and toxicity prior to following mating and co-transformation experiments. To test for autoactivation, all constructs containing either the bait vector pGBKT7 or the prey vector pGADT7 are plated onto the respective selection media SD-Trp or SD-Leu as well as on the respective reporter selection media SD-Trp/X, SD-Trp/X/A or SD-Leu/X, SD-Leu/X/A and DDO (SD-Leu-Trp). The positive control (pGBKT7-53 + pGADT7-T) was plated onto DDO/X/A as comparison.

To test for toxicity, the growth performance of all constructs were tested and compared to transformants containing empty pGBKT7 or pGADT7 vectors on SD-Trp or SD-Leu medium.

4.2.11.4 cDNA library screen using yeast mating

Mating procedure of the *lrt1*-pGBKT7 transformed strain Yeast Gold with the transformed cDNA library strain Y187 was performed according to the manufactures protocol ‘Two Hybrid Library Screening Using Yeast Mating’ (ClonTech, Mountain View, CA, USA).

4.2.11.5 Library screen using co-transformation of *lrt1* bait construct with cDNA library

Beside the Y2H assay using mating, a co-transformation of the *lrt1*-bait construct with a cDNA library was performed according to the protocol ‘Yeast Transformation System 2 - Library Scale’ (ClonTech, Mountain View, CA, USA). In brief, 15 µg of ds cDNA (procedure as described previously), 6 µL of the linearized vector pGADT7-Rec and 5 µg of the bait construct (*lrt1*-pGBKT7) were used for transformation of 600 µl competent Yeast Gold cells.

4.2.11.6 Interaction analysis of LRT1 and DDB1 homologs by Y2H co-transformation

Interaction between LRT1 and DDB1-LIKE1 as well as between LRT1 and DDB1-LIKE2 was tested by co-transforming of the respective constructs into PJ694A. Therefore, the full length CDS of LRT1 and both DDB1 proteins were cloned into pGADT7 and pGBKT7 respectively. Prior to co-transformation into PJ694A in construct combinations shown in Table 5, all constructs were sequenced by Sanger sequencing. Co-transformed yeast were subsequently plated onto DDO (SD-Leu-Trp) medium, incubated for three days before transferring onto dropout media with increasing intensity (DDO-His, DDO-His-Ade) as well as on DDO + X-α-Gal and DDO + X-α-Gal + Aureobasidin A. Growth capability on respective selective media were examined after four days of incubation at 30 °C.

Table 5 Co-transformed constructs for direct Y2H interaction analysis.

	pGBKT7 (Gal4 DNA-BD)	pGADT7 (Gal4 AD)
Interaction between LRT1 and DDB1-LIKE1	<i>lrt1</i>	<i>ddb1-like1</i>
	<i>ddb1-like1</i>	<i>lrt1</i>
Interaction between LRT1 and DDB1-LIKE2	<i>lrt1</i>	<i>ddb1-like2</i>
	<i>ddb1-like2</i>	<i>lrt1</i>
Positive control	BD	AD
Positive control	pGBKT7-53	pGADT7-T
Negative control	pGBKT7-Lam	pGADT7-T

In order to quantify the examined interactions between LRT1 and the DDB1 homologs, the β -Galactosidase activity was measured using an ortho-Nitrophenyl- β -galactoside (ONPG) assay and the pellet X-Gal (PXG) assay (MÖCKLI and AUERBACH, 2018). For both assays three clones per co-transformation were used as biological replicates.

For the ONPG assay a single colony per replicate was inoculated into 2 ml DDO media (SD-Leu-Trp) and incubated O/N on a spinning wheel at 28 °C. Next day 8 ml of YPD medium was added to the O/N cultures and incubated for additional 6 h before measuring the OD₆₀₀. Cells of 1 ml per culture were collected by centrifugation at full speed for 1 min. Subsequently the pellet was resuspended in 1 ml of Z-buffer (0.06 M Na₂HPO₄, 0.04 M NaH₂PO₄, 0.01 M KCl, 0.001 M MgSO₄, pH 7.0) centrifuged and resuspended again in 1 ml of fresh Z-buffer. In total, three washing steps were performed. After the last washing step, the pellets were resuspended into 300 μ l Z-buffer. Subsequently, cells were lysed by four freeze/thaw cycles using liquid nitrogen for ~20 sec and a water bath at 30 °C for 5 min alternately. Then 0.7 μ l of Z-buffer including 0.04 mM β -mercaptoethanol was added to the samples as well as to 300 μ l Z-buffer as blank. With adding of 160 μ l of Z-buffer containing ONPG (4 mg/ml) a timer was started. Cells were incubated at 30 °C and checked for a developing yellow color change every 5 min. After development of an obvious straw yellow color, 400 μ l of 1 M Na₂CO₃ was added to stop the reaction and the reaction time was recorded. Reaction tubes were centrifuged for 5 min at maximal speed to pellet cell debris. The absorption of the supernatant was measured at 420 nm relative to the blank. Finally, β -galactosidase units were calculated according to Formula 1.

$$\beta - galactosidase\ units = \frac{1000 * A_{420}}{(t * V * OD_{600})}$$

Formula 1 Calculation of β -galactosidase units. A₄₂₀ = Absorption of the supernatant containing the hydrolyzed product o-nitrophenol. t = incubation time where reaction takes place in min. V = volume of cells used. OD₆₀₀ = optical density of culture at 600 nm.

One unit of β -galactosidase is defined as the amount, which hydrolyzes 1 μ M of ONPG to o-nitrophenol and D-galactose per min per cell (Miller, 1972; Miller, 1992).

The PXG assay was performed according to MÖCKLI and AUERBACH (2018). As previously described, three independent colonies per co-transformation were used and inoculated into 5 ml of DDO medium and incubated O/N at 28 °C. One absorbance unit (A₆₀₀) was pelleted and the supernatant was discarded. Subsequently cell lysis was performed by two freeze-thaw cycles by using liquid nitrogen for 3 min and a water bath of 37 °C for 2 min alternately. After lysis, pellets were resuspended in 20 μ l dH₂O and transferred to a flat bottom 96-well microplate and

mixed with 100 μ l PBS buffer (pH 7.4) containing 500 μ g/ml X-gal and 0.005% β -mercaptoethanol and incubated at RT. β -galactose activity was measured by recording the color development of 5,5'-dibromo-4,4'-dichloro-indigo by measuring the absorbance at 680 nm in a 96-well microplatereader (CLARIOstar, BMG Labtech, Ortenberg, Germany) using a double orbital shaking of 10 s at 300 rpm before each cycle. The absorbance maxima of 5,5'-dibromo-4,4'-dichloro-indigo was previously determined by measuring the full absorbance spectrum between 220 and 700 nm of the positive control (pGBKT7-53 + pGADT7-T).

For the co-transformation as well as for the β -galactosidase assays pGBKT7-53 together with pGADT7-T were used as positive control. The vector pGBKT7-53 encodes the Gal4 DNA-BD fused with murine P53. The vector pGADT7-T encodes the Gal4 AD fused with SV40 large T-antigen. Both are interacting in yeast and thus are able to activate all four transporters. The vector pGADT7 together with pGBKT7-Lam, which encodes the Gal4BD fused with lamin and cannot interact with pGADT7-T, was used as negative control. BD and AD are two not yet published proteins fused to the Gal4 binding and activation domain respectively, which are known to show a weak interaction (GAUGLER, 2019).

4.2.12 Analysis of subcellular localization of LRT1 and DDB1 homologs using FRET co-localization

The subcellular localization of LRT1 and the DDB1 homologs DDB1-LIKE1 and DDB1-LIKE2 as potential subunits of the CUL4-E3 Ubiquitin ligase complex was analyzed using the binary 2in1 FRET vectors of HECKER *et al.* (2015). These vectors enable co-localization and dynamic protein interaction studies. In particular, the pFRETvr-2in1 vectors were used, where one protein of interest is fused to tagRFP and the second protein is fused to mVenus. As control for nuclear localization the chromatin-associated high mobility group protein A (HMGA, AT1G14900.1, LAUNHOLT *et al.*, 2006) was fused to tagRFP beside the respective GOI, which was fused to mVenus. tagRFP and mVenus protein fusions were generated by the MultiSite Gateway® system (Invitrogen, Waltham, USA). In the first step, the full CDS sequence of the genes were amplified using gene-specific oligonucleotide primers containing specific *attB*-site overhangs via PCR using cDNA as a template. The retrieved PCR products were gel purified using the Monarch DNA Gel Extraction Kit (NEB, Ipswich, USA). These purified PCR products were ligated into pJet1.2/Blunt using the CloneJet PCR Cloning Kit (Thermo Scientific, Waltham, USA) and were sequenced by Sanger sequencing using gene specific primers and the two pjet1.2 sequencing primers to get a complete sequence. To create entry clones, BP reaction with the BP-Clonase™ II enzyme mix (Invitrogen, Waltham, USA)

was performed using the MultiSite Pro Gateway Donor vectors pDONR™ 221 P1-P4 and pDONR™ 221 P3-P2 (Invitrogen, Waltham, USA) O/N at RT according to Table 6.

Table 6 Reaction mixture used for Gateway BP reaction

pDONR™ vector	75ng
PCR product with respective attB sites	molar ratio pDONR:PCR product of 1:1
dH ₂ O	to 4µl
BP-Clonase™ II enzyme mix	1µl
ProteinaseK (added after reaction)	0.5µl

Positive clones were confirmed by colony PCR and Sanger sequencing before producing the expression clones with LR-Clonase™ II enzyme mix (Invitrogen, Waltham, USA) using the destination vectors pFRETvr-2in1-NN, pFRETvr-2in1-NC, pFRETvr-2in1-CC and pFRETvr-2in1-CN from HECKER *et al.* (2015). The LR reaction was performed O/N at RT according to Table 7.

Table 7 Reaction mixture used for Gateway LR reaction

pENTR_B1_B4	molar ratio pENTR:pENTR:pDEST of 2:2:1
pENTR_B3_B2	
DEST vector	50 ng
dH ₂ O	to 4µl
LR clonase II enzyme mix	1µl
ProteinaseK (added after reaction)	0.5µl

Positive expression clones were selected on LBspec plates containing IPTG and X-Gal for blue-white selection and confirmed by colony PCR and Sanger sequencing.

Correct and confirmed expression plasmids were transformed into electrocompetent *Agrobacteria tumefaciens* strains AGL1 or C58C1. Positive clones were confirmed by colony PCR before transient transformation of tobacco leaves. *Agrobacterium tumefaciens* cultures were precipitated and dissolved in MMA solution (100 µM AS (5% sucrose, 0.01% Silvet, MgSO₄, Glucose, 450 µM Acetosyringone), 10 mM MgCl₂, 10 mM MES (pH 5.6)) and infiltrated into tobacco leaves. Transgene expression was analyzed three days after infiltration by confocal laser scanning microscopy (Zeiss LSM 780 attached to an Axio Observer Z1 with a

25x water-immersion and a 40x oil-immersion objective, Carl Zeiss Microscopy, Jena, Germany). TagRFP was excited at 543 nm using a Helium Neon laser and emission was detected with a 597 to 641 nm bandpass filter. mVenus was excited at 488 nm by the argon laser and emission was detected with a 514 to 554 nm bandpass filter. Chlorophyll autofluorescence was also detected with an excitation of 488 nm by the argon laser but in combination with the 686 to 711 nm bandpass filter. Images were further processed with ZEN 3.4 (Zeiss, Jena, Germany).

4.2.13 Analysis of Protein-protein interaction of LRT1 and DDB1 homologs using rBiFC

To examine a possible interaction between LRT1 and the DDB1 homologs DDB1L1 and DDB1L2, the rBiFC system of GREFEN and BLATT (2012) was used. BiFC in general is based on splitting an enhanced yellow fluorescence protein eYFP into two non-fluorescent peptides fused to two proteins of interest and their fluorophore complementation in case of an interaction between those two proteins. Using the rBiFC assay, in addition a simultaneous introduction of both fusion proteins on the same plasmid and the inclusion of an internal fluorescence marker (a monomeric red fluorescent protein1) for expression control and ratiometric quantification is possible. In total, four vectors were generated and also used in this interaction study, which offer the possibility to tag both genes of interest either N- or C-terminally with the nYFP or cYFP half. LRT1 and DDB1 fusion proteins with splitted YFP (cYFP and nYFP) were generated by the MultiSite Gateway® system (Invitrogen, Waltham, USA) as described in 4.3. For production of expression clones the destination vectors pBiFCt-2in1-NN, pBiFCt-2in1-NC pBiFCt-2in1-CN and pBiFCt-2in1-CC of GREFEN and BLATT (2012) were used. Procedures of cloning, selection and sequencing was performed as described in section 4.3. Correct and confirmed expression plasmids were transformed into electrocompetent *Agrobacterium tumefaciens* strains AGL1 or C58C1. Positive clones were confirmed by colony PCR before transient transformation of tobacco leaves as described in section 4.3. Confocal laser scanning microscopy was performed according to section 4.3 with the same settings for the excitation and emission detection of YFP, RFP and chlorophyll autofluorescence.

4.2.14 Analysis of Protein-protein interaction of LRT1 and DDB1L1 using FRET

In addition, a potential interaction between LRT1 and DDB1L1 was also analyzed in a FRET experiment. The principle of FRET is shown in Figure 10. An excited donor fluorophore (mVenus) is able to transfer the excitation energy to an adjacent acceptor fluorophore (RFP) by dipole-dipole coupling. Therefore, it is essential that the emission spectrum of the donor

fluorophore overlaps with the absorbance spectrum of the acceptor fluorophore, which is fulfilled for mVenus as donor and RFP as acceptor (FORSTER, 1946; HECKER *et al.*, 2015). Gateway-based cloning into the destination vectors pFRETvr-2in1-NN and pFRETvr-2in1-NC from HECKER *et al.* (2015), subsequent *Agrobacterium* transformation and transient tobacco transformation was performed as described in section 4.3. Transgene expression was analyzed three days after infiltration by confocal laser scanning microscopy (Zeiss LSM 780 attached to an Axio Oberver Z1 with a 25x water-immersion and a 40x oil-immersion objective, Carl Zeiss Microscopy, Jena, Germany). In order to confirm, that both genes are successfully expressed, first mVenus as well as tagRFP were excited at their respective excitation maxima. Therefore, mVenus was excited at 488 nm by the argon laser and emission was detected with a 514 to 554 nm bandpass filter. TagRFP was excited at 543 nm using a helium neon laser and emission was detected with a 597 to 641 nm bandpass filter. In a second step, emission was sensed only using the excitation at 488 nm without an excitation at 543 nm to check for FRET. Chlorophyll autofluorescence was also detected with an excitation of 488 nm by the argon laser but in combination with the 686 to 711 nm bandpass filter. Images were further processed with ZEN 3.4 (Zeiss, Jena, Germany).

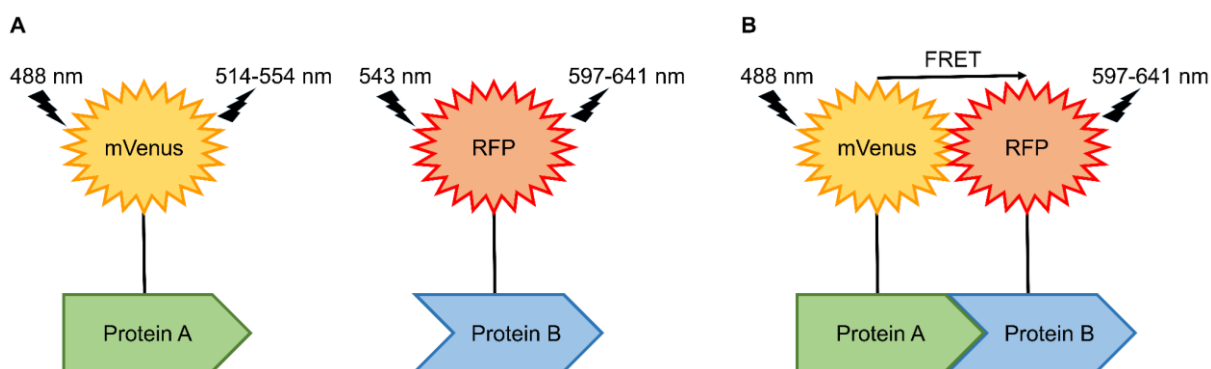


Figure 10 Schematic representation of the Fluorescence Resonance Energy Transfer (FRET) principle. A: Protein A is fused to a donor fluorophore (mVenus). Protein B is fused to an acceptor fluorophore (RFP). When Protein A is excited at a wavelength of 488 nm its emission can be observed between 517-533nm. If both proteins are not interacting the acceptor emission can only be detected when excited with 543 nm wavelength. B: When Protein A and B interact, the donor fluorophore mVenus (excited at 488nm) is able to transfer its excitation energy to the acceptor fluorophore RFP by FRET.

5 RESULTS

5.1 Phenotypic analysis of *lrt1*

A comparison of the primary root growth between homo- and heterozygous wild type *lrt1* seedlings showed no significant differences (Figure 11A). The primary root growth of homozygous *lrt1* mutant seedlings in comparison to homo- and heterozygous wild type *lrt1* seedlings showed a significant delay in primary root growth from day five after germination on, which consistently increases with a reduction in primary root length of 40% at 10 days after germination already (Figure 11A).

Analysis of the seminal root number showed a small but significant reduction in the *lrt1* mutant 10 days after germination (Figure 11B). No difference in seminal root number was observed between homozygous and heterozygous wild type plants.

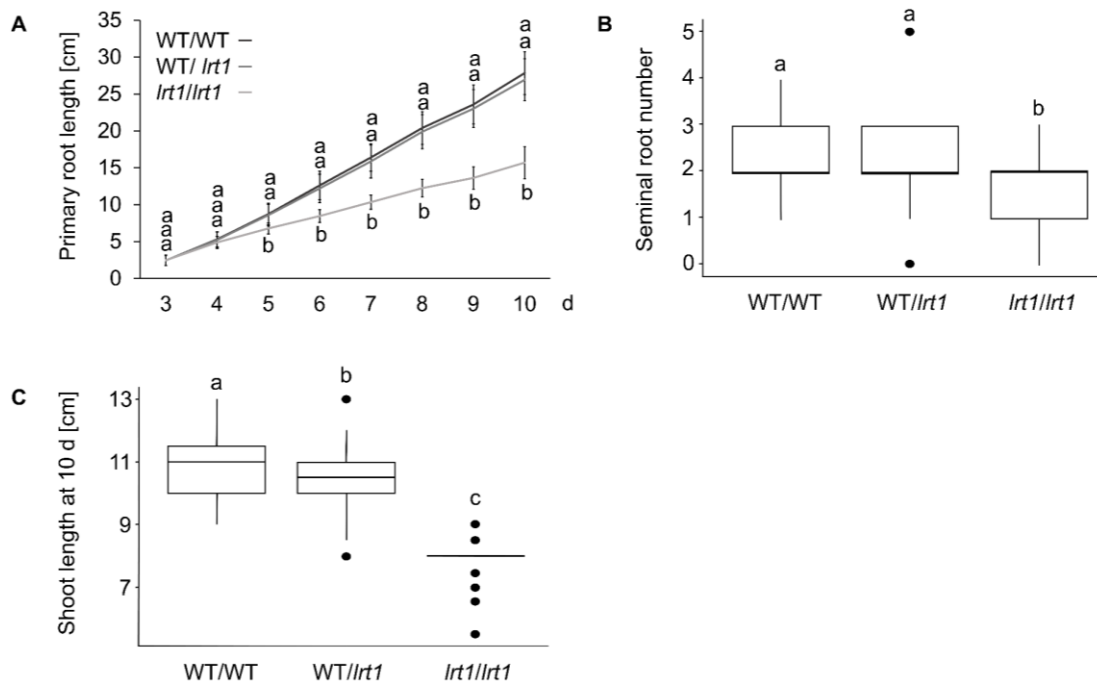


Figure 11 Phenotypic comparisons between WT/WT, WT/*lrt1* and *lrt1/lrt1* plants at seedling stage. **A:** Primary root growth until 10 days-after-germination. **B:** Seminal root number 10 days-after-germination. **C:** Shoot length 10 days-after-germination. Significant differences of means between each sample were calculated by Tukey's test ($p < 0.05$) and indicated with small letters.

A statistically significant reduction of shoot length in the *lrt1* mutant of ~30% was observed in young seedlings 10 days after germination (Figure 11C). Furthermore, a small but significant reduction of shoot length was also visible in heterozygous compared to homozygous wild type plants (Figure 11C).

The reduced development of the shoot and especially the root system continues until maturity. When comparing the plant height at maturity after pollination, a reduction of 55% was observed in *lrt1* mutants cultivated in soil pots in the greenhouse compared to wild type plants (Figure 12A). When growing the plants in hydroponics, *lrt1* mutants displayed only a reduction of 21% compared to wild type plants (Figure 12A). This is also reflected by the reduction in dry weight of shoot and root of *lrt1* plants grown in hydroponics compared to wild type plants (Figure 12B). The shoot dry weight was reduced by ~30% and root dry weight by ~50% in *lrt1* versus wild type plants.

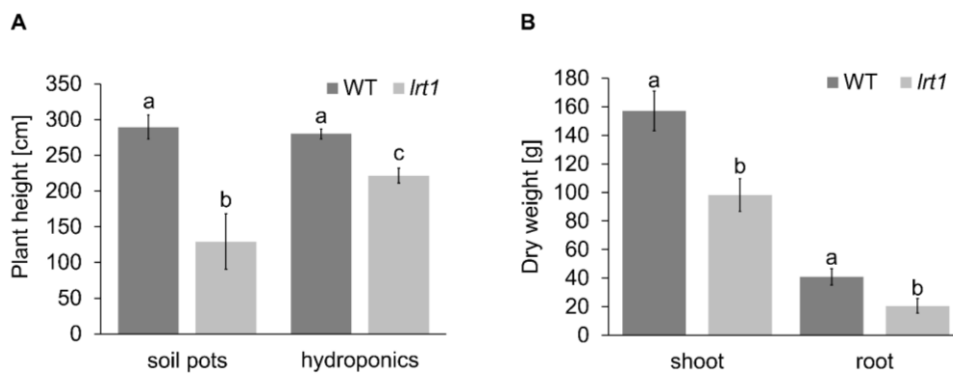


Figure 12 Phenotypic comparison of mature wild type and *lrt1* plants. **A:** Plant height of wild type and *lrt1* plants grown in soil pots and hydroponics at mature stage after pollination. **B:** Shoot and root dry weight of mature wild type and *lrt1* plants grown in hydroponics. Significant differences of means between each sample were calculated by Tukey's test ($p < 0.05$) and indicated with small letters. WT: wild type.

This reduction of root dry weight is also reflected by an obvious reduction of the whole root system complexity from seedling stage to maturity in the plants grown in hydroponics. 15-day-old *lrt1* mutants already showed a clear reduction of the root system reflected by less seminal roots, delayed crown root formation and fewer initiated lateral roots (Figure 13).

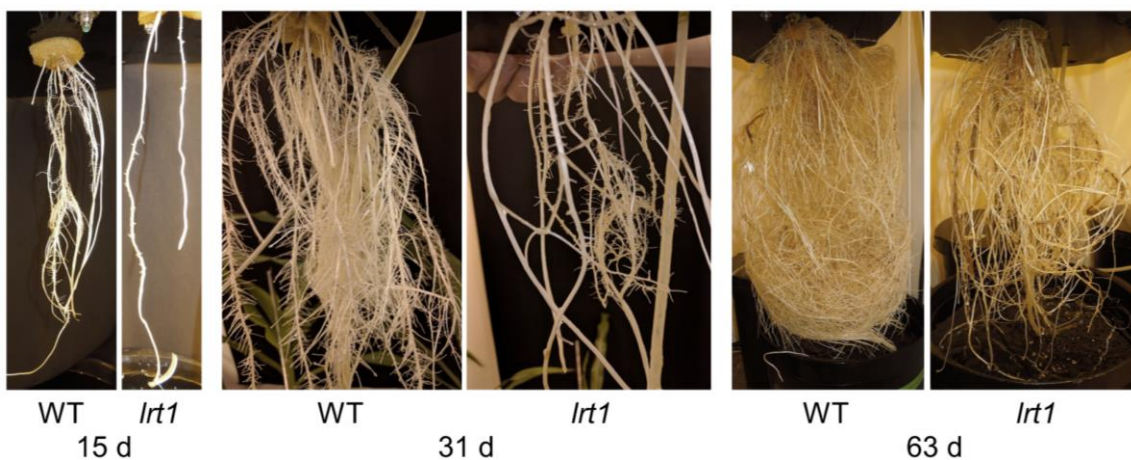


Figure 13 Comparison of wild type and *lrt1* root system grown in hydroponics at different stages 15, 31 and 63 days after germination. WT: wild type.

When looking at crown root development as part of the shoot born root system, *lrt1* mutant plants showed a delayed initiation (Figure 14, 23 days after germination) as well as a slower and reduced crown root development at the first shoot node (coleoptilar node) compared to wild type plants (Figure 14, 30 days after germination).

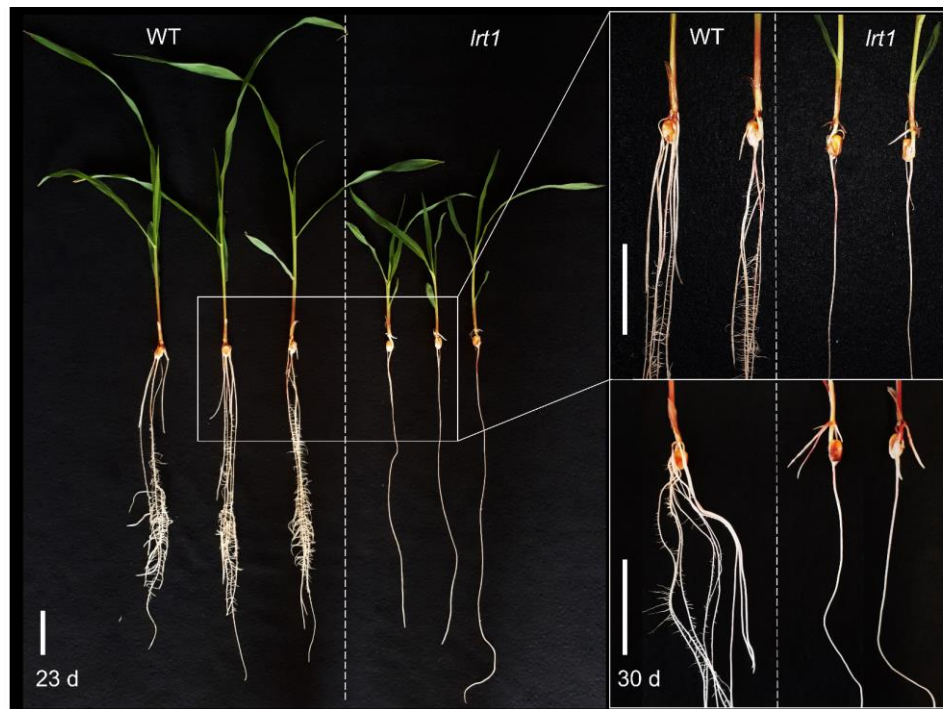


Figure 14 Comparison of crown root development at the coleoptilar node between wild type and *lrt1* plants 23 and 30 days after germination. Scale bar = 5 cm.

There was no significant difference in crown root number at the coleoptilar node between *lrt1* and wild type seedlings (Figure 15, A). When comparing the crown roots at the coleoptilar node of *lrt1* mutants with wild type seedlings at 23 and 30 days after germination, the mutants are significantly delayed and distinctly slower in development (Figure 14 and 15B).

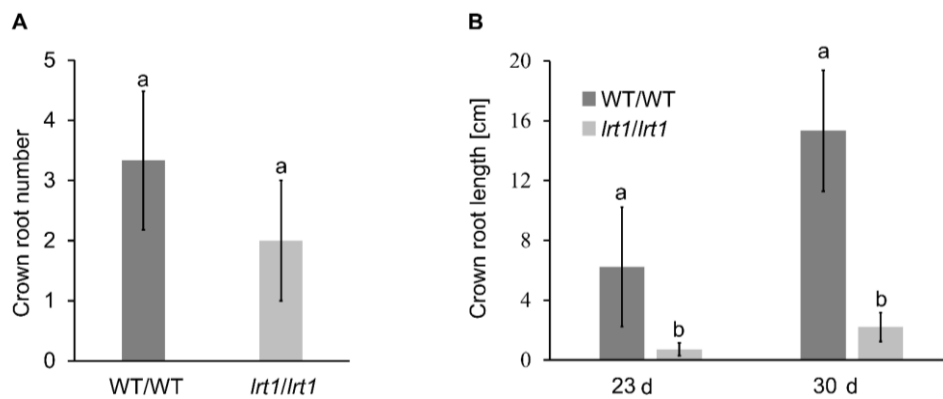


Figure 15 Crown root development of the *lrt1* mutant in comparison to wild type seedlings. **A:** Crown root number at the coleoptilar node 30 days after germination. **B:** Crown root length at the coleoptilar node 23 and 30 days after germination. Significant differences of means between each sample were calculated by Tukey's test ($p < 0.05$) and indicated with small letters.

In the seven-day period between 23 and 30 days after germination *lrt1* seedlings were still able to elongate their crown roots at the coleoptilar node. The *lrt1* seedlings elongated their crown roots by 3 times in comparison to wild type plants, which elongate their crown roots by 2.4 times in this period (Figure 15B).

5.2 Gravitropic response of *lrt1*

A comparison of the responsiveness of the primary root tip to gravity in a rotation experiment in rhizoboxes showed a transiently delayed response to a rotation of 90° for *lrt1* plants (Figure 16). This delay is significant between 3 and 12 h after rotation. From 24 h after rotation on, there was no difference between wild type and *lrt1* anymore.

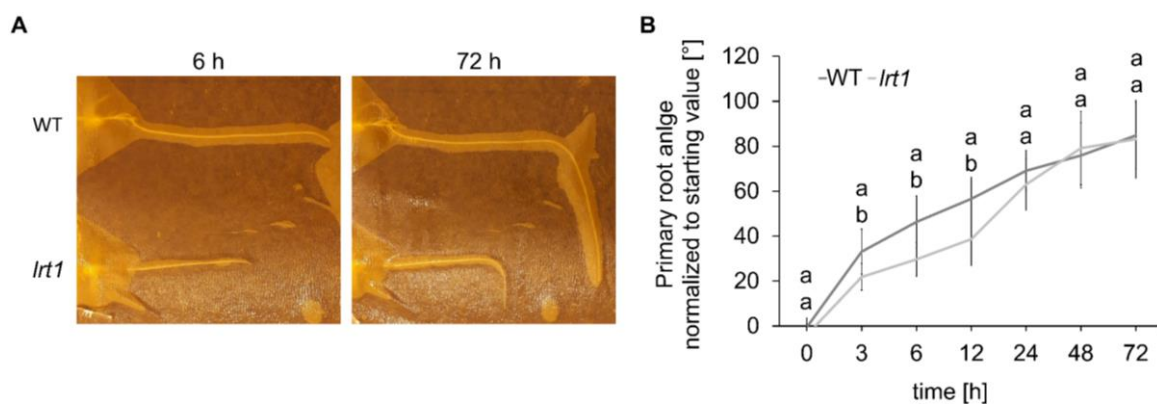


Figure 16 Gravitropic response of wild type and *lrt1* plants after rotation by 90°. **A:** Wild type and *lrt1* plant 6 and 72 h after rotation. **B:** Measurement of primary root tip angle after rotation by 90° over time. All measurements were normalized to the starting root tip angle. Significant differences of means between each sample were calculated by Tukey's test ($p < 0.05$) and indicated with small letters.

5.3 Skotomorphogenesis of *lrt1*

Maize seedlings, which are grown in the dark show skotomorphogenic growth including mesocotyl elongation (JOSSE and HALLIDAY, 2008; SAWERS *et al.*, 2002; FLINT, 1944). When comparing the expected mesocotyl elongation of dark grown wild type with *lrt1* seedlings it became obvious that the mesocotyl length of *lrt1* was significantly shorter than the wild type by ~50% (Figure 17A and B), whereas the coleoptile length was not affected. Seedlings grown in a day/night rhythm (16 h/8 h) did not show differences in mesocotyl and coleoptile length between wild type and *lrt1*. It was observed, that wild type plants grown in a day/night rhythm were faster in lateral root formation than wild type plants grown under dark conditions (Figure 17A). As expected, *lrt1* plants did not initiate lateral roots under both conditions seven days after germination.

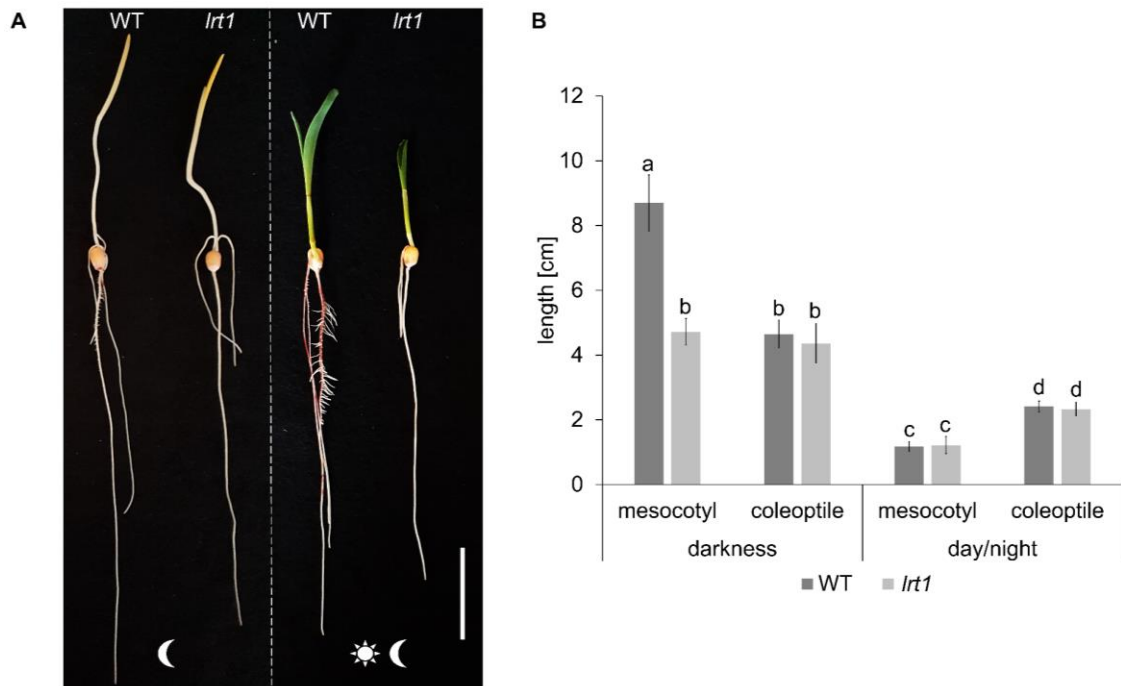


Figure 17 Comparison of wild type and *lrt1* seedlings grown in the dark (left) and day/night rhythm (right). **A:** Picture of wild type and *lrt1* seedlings grown in the dark (left side) and in the dark (right side) 7 days-after-germination. Scale bar = 5 cm. **B:** Measurement of mesocotyl and coleoptile length of wild type and *lrt1* seedlings grown in the dark (left) and in day/night rhythm (16 h/ 8 h). Significant differences of means between each sample were calculated by Tukey's test ($p < 0.05$) and indicated with small letters.

5.4 Effects of ethylene (ACC) on *lrt1*

It is known, that increased ethylene synthesis by exogenous application of 1-aminocyclopropane-1-carboxylic acid (ACC) is able to promote initiation of lateral root primordia in *Arabidopsis*. The application of high ACC concentrations however represses the initiation of lateral root primordia (IVANCHENKO et al., 2008). In proteome data from our laboratory an upregulation of a 1-Aminocyclopropane-1-carboxylic acid oxidase (ACCO) was identified in the primary root of *lrt1* mutants (YU, 2022). ACCO is the last key enzyme, which converts ACC to ethylene.

In order to analyze, if ethylene biosynthesis or signaling affects the deficiency of lateral root initiation in the *lrt1* mutant, the effect of exogenous application of the ethylene precursor 1-aminocyclopropane-1-carboxylic acid (ACC) in different concentrations from 1 μ M to 1 mM was tested. Both wild type and *lrt1* plants did not display any phenotypic differences when grown at 1, 5 and 10 μ M ACC in comparison to control dH₂O treatment (Figure 18). At a concentration of 1 mM ACC, both wild type and *lrt1* seedlings have significantly shorter primary and seminal roots as well as shorter shoots. At this ACC concentration, the primary roots also showed a curled structure, which was not observed in *lrt1*. ACC had no influence on

lateral root formation even at a concentration of 1 mM. For wild type plants the number and length of lateral roots were comparable to the control treatment at all ACC concentrations and the absence of lateral root formation in *lrr1* was not changed by any ACC concentration. Beside ACC, the effect of silver nitrate AgNO_3 , which inhibits ethylene receptors, was examined at 100 μM , 500 μM and 1 mM. Primary and seminal root length of wild type and *lrr1* seedlings was significantly reduced for all tested AgNO_3 concentrations compared to the control treatment. Lateral roots of wild type plants treated with AgNO_3 were longer in comparison to the control treatment. For *lrr1* no change in its lateral root defect was observed after AgNO_3 treatment (Figure 18).



Figure 18 Phenotypic characterization of wild type and *lrr1* seedlings grown at different concentrations of the ethylene inhibitor silver nitrate (AgNO_3) and the ethylene precursor 1-aminocyclopropane-1-carboxylic acid (ACC). Seedlings were grown for 14 days in the paper role system containing different AgNO_3 and ACC concentration. Seedlings grown in dH_2O were used as control. The picture was taken 14 days after germination showing a representative wild type (left) and *lrr1* (right) plant for each treatment. Scale bar = 2cm.

5.5 Effect of chemical treatments altering the peroxidase activity and ROS in *lrt1*

The analysis of proteome and metabolome data from a project of the laboratory regarding the regulation of lateral root initiation by arbuscular mycorrhizal fungi (AMF), pointed out, that a number of class III peroxidases are upregulated in the *lrt1* mutant in comparison to *lrt1* mutants treated with AMF.

Therefore, the effect of exogenous application of the two different peroxidase inhibitors KCN and SHAM was examined. Furthermore, exogenous application of the coumarin umbelliferone, which is able to modulate the peroxidase activity, as well as an application of H₂O₂ in different concentrations was analyzed to examine a potential connection between the class III peroxidase activity and the lateral root defect in the *lrt1* mutant.

The application of KCN at concentration of 10 µM showed no effect on wild type and *lrt1* mutant seedling (Figure 19A). At a concentration of 100 µM the primary root length of *lrt1* mutant and wild type seedlings were reduced in comparison to the control treatment with water. At 1 mM KCN concentration primary root length of *lrt1* and wild type was decreased by more than 80%. Initiation of lateral roots was visible in wild type plants for all tested KCN concentrations whereas the *lrt1* mutant always showed the lateral root defective phenotype.

The application of salicylhydroxamic acid (SHAM) also led to a reduction of primary root length from a concentration of 100 µM on (Figure 19B). At a concentration of 1mM primary root length was decreased by 50% in comparison to water control. Wild type as well as *lrt1* mutant seedlings showed no changes in lateral root formation by any SHAM concentration.

The application of the peroxidase activity modulator umbelliferone led to a reduction of primary root length from a concentration of 100 µM on (Figure 19C). At a concentration of 1mM umbelliferone wild type as well as the *lrt1* mutant showed a drastic reduction of primary root length by more than 80% as well. At this concentration the roots were also brownish with already necrotic root tips. No effect of umbelliferone on lateral root development of wild type and *lrt1* mutant seedlings was observed.

The application of H₂O₂ led to a reduction in primary root length of ~30% for wild type and <50% for *lrt1* mutant seedlings at a concentration of 1 mM H₂O₂ (Figure 19D). No effect was observed on lateral root formation in wild type and *lrt1* mutant seedlings at all tested concentrations.

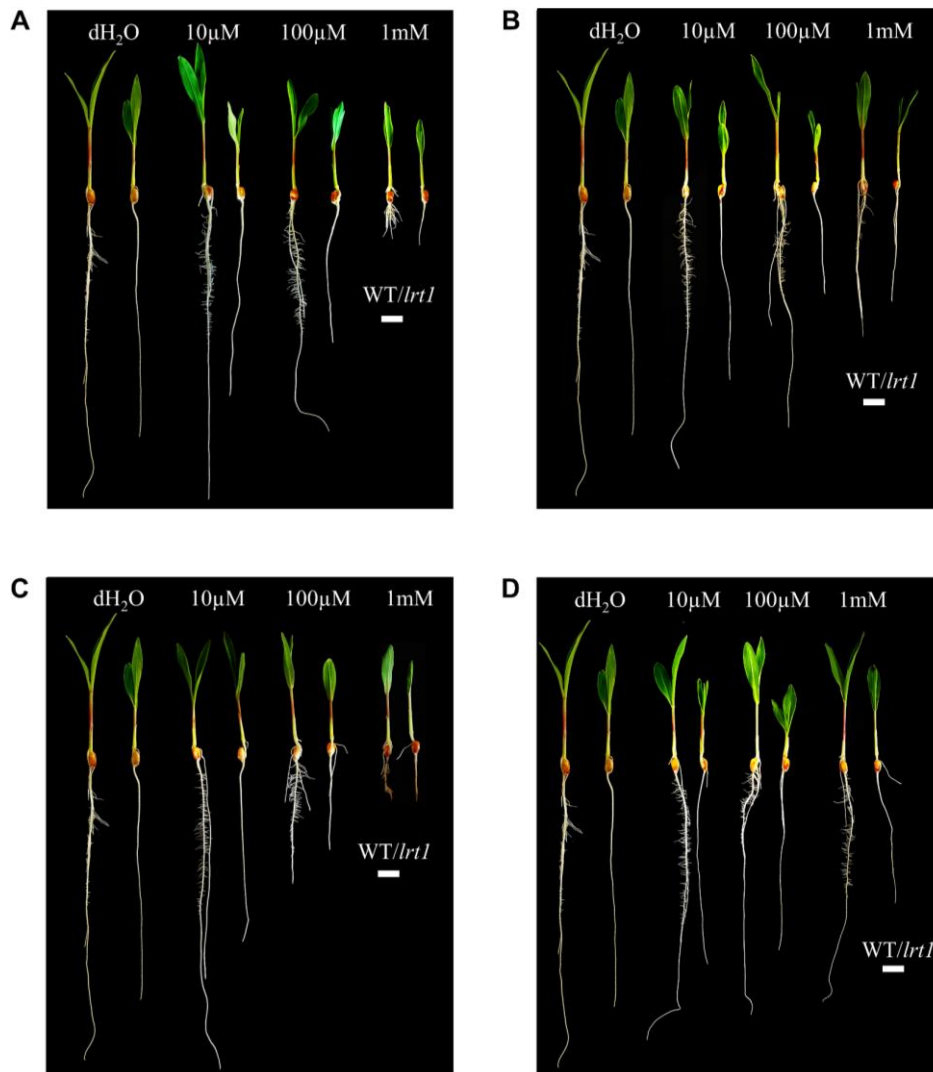


Figure 19 Phenotypic characterization of wild type and *lrt1* seedlings grown at different concentrations of the peroxidase inhibitors KCN (**A**) and SHAM (**B**) and the peroxidase activity modulator Umbelliferone (**C**) as well as H_2O_2 (**D**). Seedlings grown in dH_2O were used as control. The pictures were taken 14 days after germination showing a representative wild type (left) and *lrt1* (right) plant for each treatment. Scale bar = 2cm.

5.6 Cloning of the *lrt1* gene

The maize *lrt1-1* mutant was initially identified in a segregating F_2 -family of an EMS mutagenized population of the inbred line B73 (HOCHHOLDINGER and FEIX, 1998). Plants carrying the *lrt1-1* mutant allele in B73 background were crossed with wild type plants of the inbred line Mo17 and subsequently self-pollinated to generate a F_2 -mapping population. The *lrt1* gene was mapped on the long arm of chromosome 10 by testing 236 SSR markers dispersed along the 10 chromosomes on 92 homozygous mutant *lrt1* plants of the mapping population. Based on this information, an additional screen of 2,000 F_2 -plants with 15 additional SSR and SNP markers positioned the mutation downstream of marker bnlg1518, at a genetic distance of 0.8 cM (Figure 20).

A single *lrt1* mutant plant from the segregating mapping population was used to create a different mapping population, with the aim of identifying new recombination breakpoints flanking the left and right sides of the gene. Due to the absence of markers flanking the gene on the right side, a bulk segregant analysis followed by next generation sequencing (BSA-Seq) was adopted. Two DNA bulks were created by pooling DNA extracted from seven different *lrt1* mutants (*lrt1* pool) and seven different wild type plants (wild type pool) representing a mixture of heterozygous and homozygous wild type plants derived from an F₃-population created by self-pollinating F₂-plants of the above-mentioned mapping population.

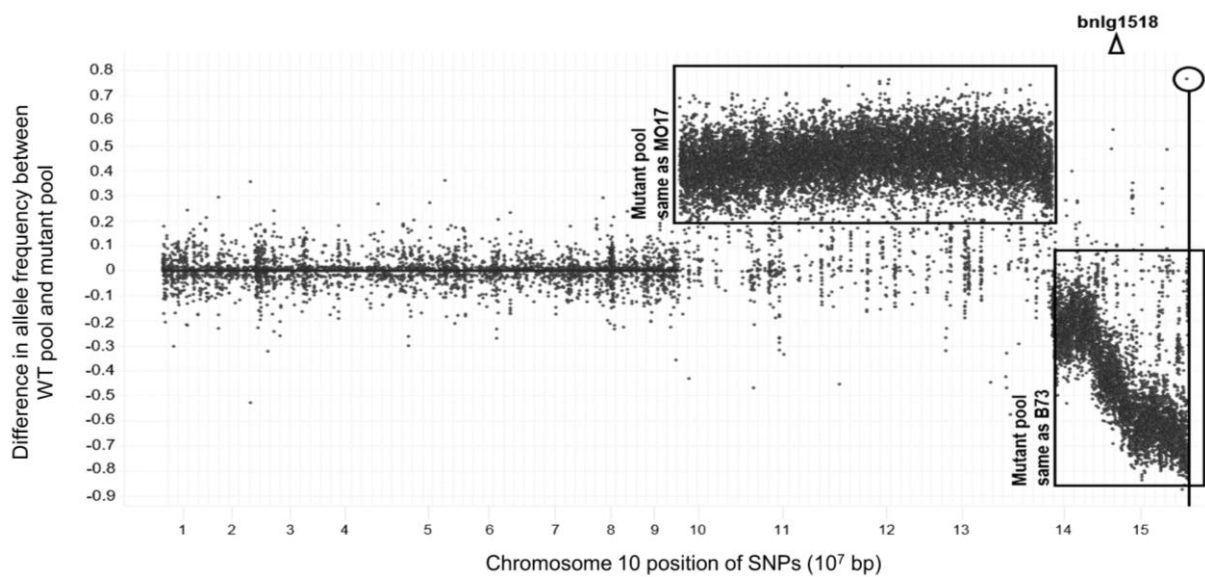


Figure 20 The allele frequency of each variant was calculated and recorded together with its nucleotide position, reference allele, alternate allele, and used to identify the region on chromosome 10 enriched for homozygous SNPs equal to B73, in linkage with the causative lesion. A comparison between the allele frequencies of mutant and wild type pools in the region linked to *lrt1* identified a G to A variant with a frequency of the allele G equal to 85% in the wild type pool, compared to a frequency of 10% in the mutant pool. This SNP is located in the sixth exon of gene Zm00001eb434410 and it creates a stop codon in the *lrt1* individuals that carry it. The presence of the allele G in the mutant pool could be explained by a possible inclusion of a non-*lrt1* mutant individual in one of the pools.

Three biological replicates per wild type and *lrt1* pool were used for sequencing using an Illumina HiSeq 2500 DNA sequencer with Illumina TruSeq SBS version 3 reagents. After initial base calling and filtering, the sequencing files generated by the Illumina pipeline were quality filtered through a custom pipeline, such that reads were trimmed at the 3' end beginning with the first base with a quality score <15 (Phred) down to a minimum read length of 24 bp. On average, ~663 million reads were generated from each pooled library and the sequences were mapped to the maize B73 reference genome sequence using Bowtie2 (LANGMEAD and SALZBERG, 2012). Variant calling was performed using a custom script that utilizes samtools

mpileup (DANECEK *et al.*, 2021). Non-variant positions were filtered out and only variant positions with coverage of 30x or more reads, were considered.

5.7 Validation of the *lrt1* candidate gene by CRISPR/Cas9

In maize, candidate genes are usually validated by independent mutant alleles. For the *lrt1* candidate gene several *Mu*- insertions were found in the public available sequenced indexed repository BonnMu (MARCON *et al.*, 2020), but all located within the 5' UTR or the first intron of *lrt1*, thus likely not causing a gene knockout. No mutant alleles were available in the recourses *UniformMu* (<http://www.maizegdb.org/uniformmu>) and *Mu-Illumina* (<http://teosinte.uoregon.edu/mu-illumina/>). Also the closest *Ac/DS* insertion (<http://acdstaggering.org/index.php>) which could provide a starting point for regional mutagenesis is at a distance of 205 kb and thus too far away from the *lrt1* candidate gene. Moreover, analysis of several putative *Mu*-insertions in the *lrt1* candidate gene from Pioneer's Trait Utility System of Corn (TUSC) (MEELEY and BRIGGS, 1995), which is another, yet not public, repository for reverse genetics potentially harboring insertions did not yield any novel mutant alleles. Most likely, the initially identified TUSC insertions were somatic mutations and not inherited to the next generation like germline mutations.

Hence, to be able to confirm that the gene with the Genbank Accession Zm00001eb434410 indeed corresponds to *lrt1*, novel mutant alleles were induced by CRISPR/Cas9 experiments. To this end, single guide RNAs (sgRNAs) were designed targeting exon 2 and exon 4 of the gene model (Figure 21). An expression vector containing the Cas9 module with the two sgRNA modules (see methods) was transformed into the maize inbred line B104. As a result, two novel mutant alleles referred to as *lrt1-2* and *lrt1-3* were generated (Figures 21 and 22). The mutant *lrt1-2* allele contains a single base insertion at the sgRNA binding site in exon 4, characteristic for sgRNAs induced double strand breaks repaired by error prone non-homologous end joining (NHEJ). As a consequence of this one base pair insertion, a frameshift resulting in a premature stop codon was introduced (Supplemental Table 2).



Figure 21 Gene model of *lrt1*. Exons are represented by black rectangles and introns are represented by connecting solid lines. Mutation sites of three mutant alleles with the assigned allele name of each mutation are indicated by arrows and a bracket, respectively.

The *lrt1-3* mutant allele contains a 531 bp deletion between the sgRNA binding sites in exon 2 and 4 (Supplemental Table 2). This suggests that both sgRNAs induced double strand breaks that were repaired after deleting the sequence between these sites. Both novel mutant alleles, *lrt1-2* and *lrt1-3* displayed the lateral rootless phenotype observed in the reference allele *lrt1-1*. These results were further substantiated by crosses between the reference mutant *lrt1-1* and the novel mutants *lrt1-2* and *lrt1-3*, each of which failed to complement the mutant phenotype and thus displayed the characteristic lateral rootless phenotype (Figure 22). These experiments confirmed that three mutants represent different alleles of the same gene and that Zm00001eb434410 is indeed the *lrt1* gene.

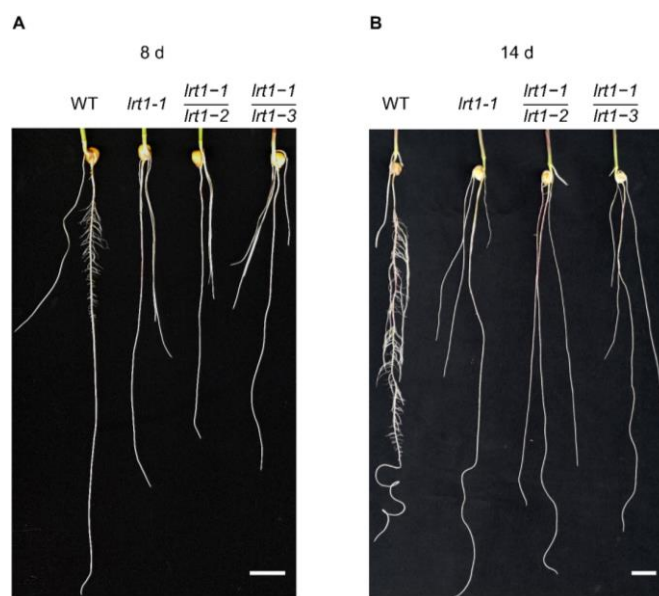


Figure 22 Confirmation of the *lrt1* gene by crossings of different *lrt1* alleles. Root phenotype of wild type, *lrt1-1* and crossed seedlings of *lrt1-1* with *lrt1-2* and *lrt1-3*, respectively 8 days after germination (A) and 14 days after germination (B). The original *lrt1-1* allele originated from an EMS treatment, *lrt1-2* and *lrt1-3* are generated CRISPR mutants. WT: Wild type. Scale bar = 2 cm.

5.8 Phylogeny and sequence analysis of LRT1

Phylogenetic analysis using the full length protein sequence of *lrt1* showed that LRT1 homologs are ubiquitously present in plants (Figure 23). Monocot and dicot LRT1 homologs are strictly separated into different phylogenetic clades. Homologs in green algae and non-vascular plants represent an additional clade. Monocots typically contain one LRT1 homolog, while maize contains two paralogs of this gene, which are designated as *lrt1* and *lrt1-like* (Figure 23). While *lrt1* is located on maize subgenome 2, *lrt1-like* belongs to maize subgenome 1. Syntenic homologs located on the two subgenomes resulted from an ancient whole genome duplication, indicating that this gene was already present in a maize progenitor more than 5

million years ago (compare with Figure 1, SCHNABLE and LYONS (2011), SCHNABLE *et al.*, (2011)).

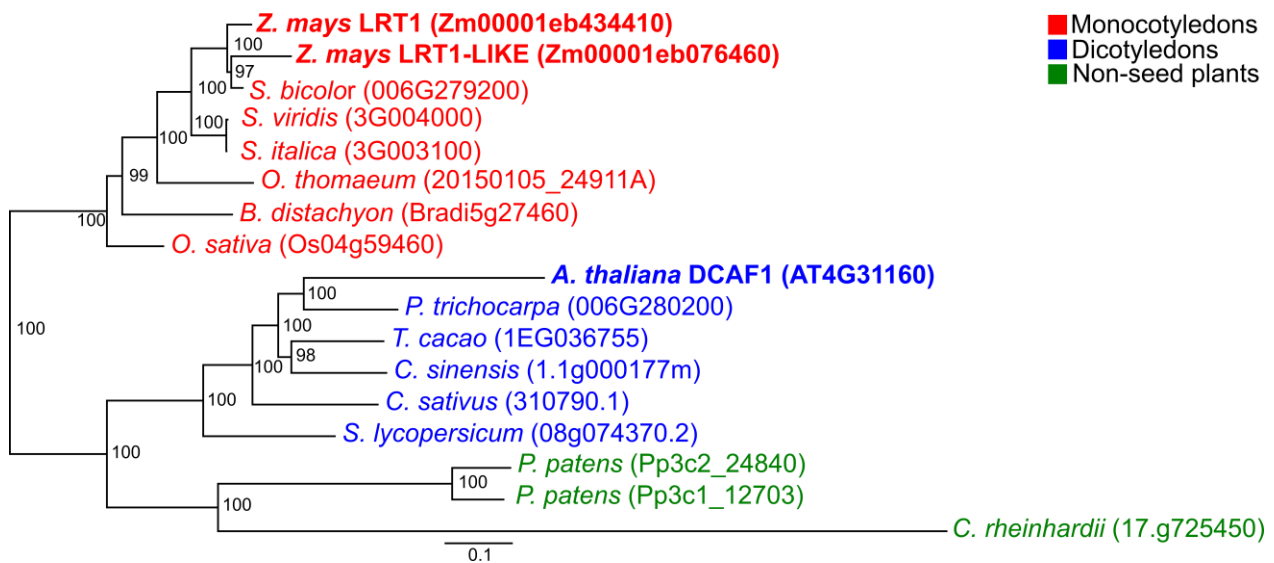


Figure 23 Phylogenetic tree for LRT1 and homologous proteins from selected plant species. After alignment of full-length protein sequences with the MUSCLE algorithm using MEGA X, the tree was constructed with 4 chains and 1 M generations using MrBayes. Bootstrap values are shown for all clades. Dicot species: blue, monocot species: red, green algae and vascular plants: green.

In version 3 of the B73 annotation, the *lrt1* gene has the maizedb.org accession GRMZM2G348735. Sequence analyses by sequencing and aligning gDNA and cDNA sequences of the B73 allele of the *lrt1* gene revealed, that the database sequence of the *lrt1* gene GRMZM2G348735 did not cover the complete sequence of this gene. Actually, the sequenced sequence was bridging a gap between GRMZM2G348735 and GRMZM2G110869, indicating that these two accessions belong to a single gene. From version 4 of the B73 annotation on, this sequence gap was resolved and the *lrt1* gene had the accession Zm00001d026691.

In version 5 the *lrt1* gene has the accession Zm00001eb434410 without any sequence changes (Supplemental Table 1). The *lrt1* gene contains 14 exons which translate into a 209 kDa protein of 1915 amino acids (Figure 24). According to *in silico* protein domain searches, the LRT1 protein is predicted to contain a LisH domain and a WD40 domain (Figure 24). The LisH domain is a protein-protein interaction motif. In maize, 75 proteins harboring a LisH motive were identified by a motive search using Uniprot.

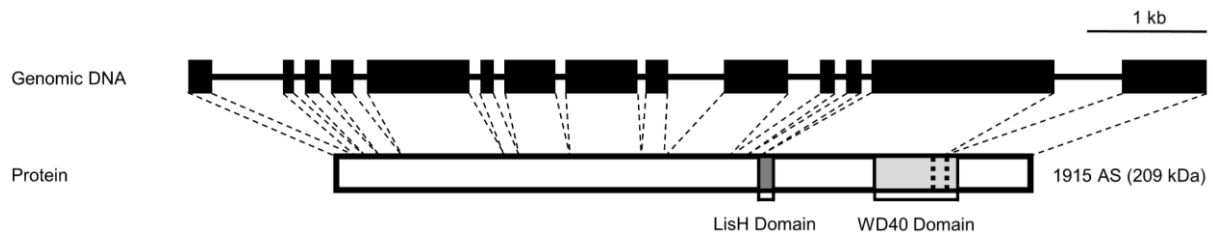


Figure 24 Protein structure of LRT1. Two WDxR motifs within the WD40 Domain are indicated by dashed lines.

The WD40 domain in the LRT1 protein harbors two DWD motifs (Figure 25) characteristic for DDB1-CUL4 ASSOCIATED FACTOR (DCAF) proteins.

	WDxR 1																WDxR 2															
	1	2	3	4	5	6	7	8	9	10	11	12	13	14	15	16	1	2	3	4	5	6	7	8	9	10	11	12	13	14	15	16
DWD-Motif	Hy	Hy	Sm	Sm	Sm	X	D/E	X	X	Hy	X	Hy	W/Y	D/E	Hy	R/K	Hy	Hy	Sm	Sm	Sm	X	D/E	X	X	Hy	X	Hy	W/Y	D/E	Hy	R/K
LRT1	P	S	D	T	M	L	L	W	N	G	V	L	W	D	T	R	P	A	G	N	E	V	I	L	N	S	E	V	W	D	L	R
LRT1-LIKE	P	S	D	T	M	L	L	W	N	G	V	L	W	D	T	R																
<i>S. bicolor</i> (006G279200)	P	S	D	T	M	L	L	W	N	G	B	L	W	D	T	R	P	A	G	N	E	V	I	L	N	S	E	V	W	D	L	R
<i>S. viridis</i> (3G004000)	P	S	D	T	M	L	L	W	N	G	V	L	W	D	T	R	P	A	G	N	E	V	I	L	N	S	E	V	W	D	L	R
<i>S. italica</i> (3G003100)	P	S	D	T	M	L	L	W	N	G	V	L	W	D	T	R	P	A	G	N	E	V	I	L	N	S	E	V	W	D	L	R
<i>O. thomaeum</i> (20150105_24911A)	P	D	D	Q	K	L	L	W	N	G	V	L	W	D	M	R	P	A	G	N	E	V	I	L	N	S	E	V	W	D	L	R
<i>B. distachyon</i> (Bradi5g27460)	P	S	D	D	M	F	L	W	N	G	V	L	W	D	I	R	P	A	G	N	E	V	I	I	N	S	E	V	W	D	L	R
<i>O. sativa</i> (Os04g59460)	P	S	D	T	M	L	L	W	N	G	V	L	W	D	R	R	P	A	G	N	E	V	I	I	N	S	E	V	W	D	L	R
DCAF1	P	C	D	T	L	I	L	W	N	G	V	L	W	D	R	R	P	S	R	N	E	V	I	I	N	S	E	I	W	D	M	R
<i>P. trichocarpa</i> (006G280200)	P	S	D	T	M	L	L	W	N	G	V	L	W	D	R	R	P	A	G	N	E	V	I	I	N	S	E	V	W	D	L	R
<i>T. cacao</i> (1EG036755)	P	S	D	T	M	L	L	W	N	G	V	L	W	D	R	R	P	A	G	N	E	V	I	I	N	S	E	V	W	D	L	R
<i>C. sinensis</i> (1.1g000177m)	P	S	D	T	M	L	L	W	N	G	I	L	W	D	R	R	P	A	G	N	E	V	I	I	N	S	E	V	W	D	L	R
<i>C. sativus</i> (310790.1)	P	S	D	T	M	L	L	W	N	G	V	L	W	D	R	R	P	A	G	N	E	V	I	I	N	S	E	V	W	D	L	R
<i>S. lycopersicum</i> (08g074370.2)	P	S	D	N	M	L	L	W	N	G	V	L	W	D	T	R	P	A	G	N	E	V	I	I	N	S	E	V	W	D	L	R
<i>P. patens</i> (Pp3c2_24840)	P	D	D	V	L	V	L	W	S	G	V	L	W	D	P	R	P	A	G	N	E	V	I	I	N	S	E	V	W	D	L	R
<i>P. patens</i> (Pp3c1_12703)	P	D	D	I	L	V	L	W	S	G	V	L	W	D	H	R	P	A	G	N	E	V	I	I	N	S	E	V	W	D	L	R
<i>C. reinhardtii</i> (17.g725450)																	P	A	G	L	E	V	I	L	N	S	E	V	W	D	L	R

Figure 25 Alignment of the DWD motifs of the LRT1 homologs from selected plant species (*Arabidopsis thaliana*, *Brachypodium distachyon*, *Chlamydomonas reinhardtii*, *Cucumis sativus*, *Camellia sinensis*, *Oropetium thomaeum*, *Oryza sativa*, *Physcomitrella patens*, *Populus trichocarpa*, *Setaria italica*, *Setaria viridis*, *Solanum lycopersicum*, *Sorghum bicolor*, *Theobroma cacao* and *Zea mays*) with reference to the DWD-motif definition by HE *et al.* (2006). Hy: any hydrophobic AS, SM: any small AS, X: any AS. All AS according to the DWD-motif showing 100% identity to the Arabidopsis DCAF1 are marked in dark green. All AS according to the DWD-motif but with differences to each other are marked in light green. All AS not according to the DWD-motif are marked in yellow. LRT1-LIKE and the homolog in the green algae *C. reinhardtii* only have one DWD motif.

DCAF proteins are receptors binding specific substrate proteins to CULLIN4-based E3 ubiquitin ligase (CRL4) complexes destined to degradation via the 26S proteasome.

In maize, 55 proteins containing one or two WD40 domains were identified which potentially encode for DCAF proteins. After identification, their phylogenetic relationship was determined and displayed in a phylogenetic tree (Figure 26).

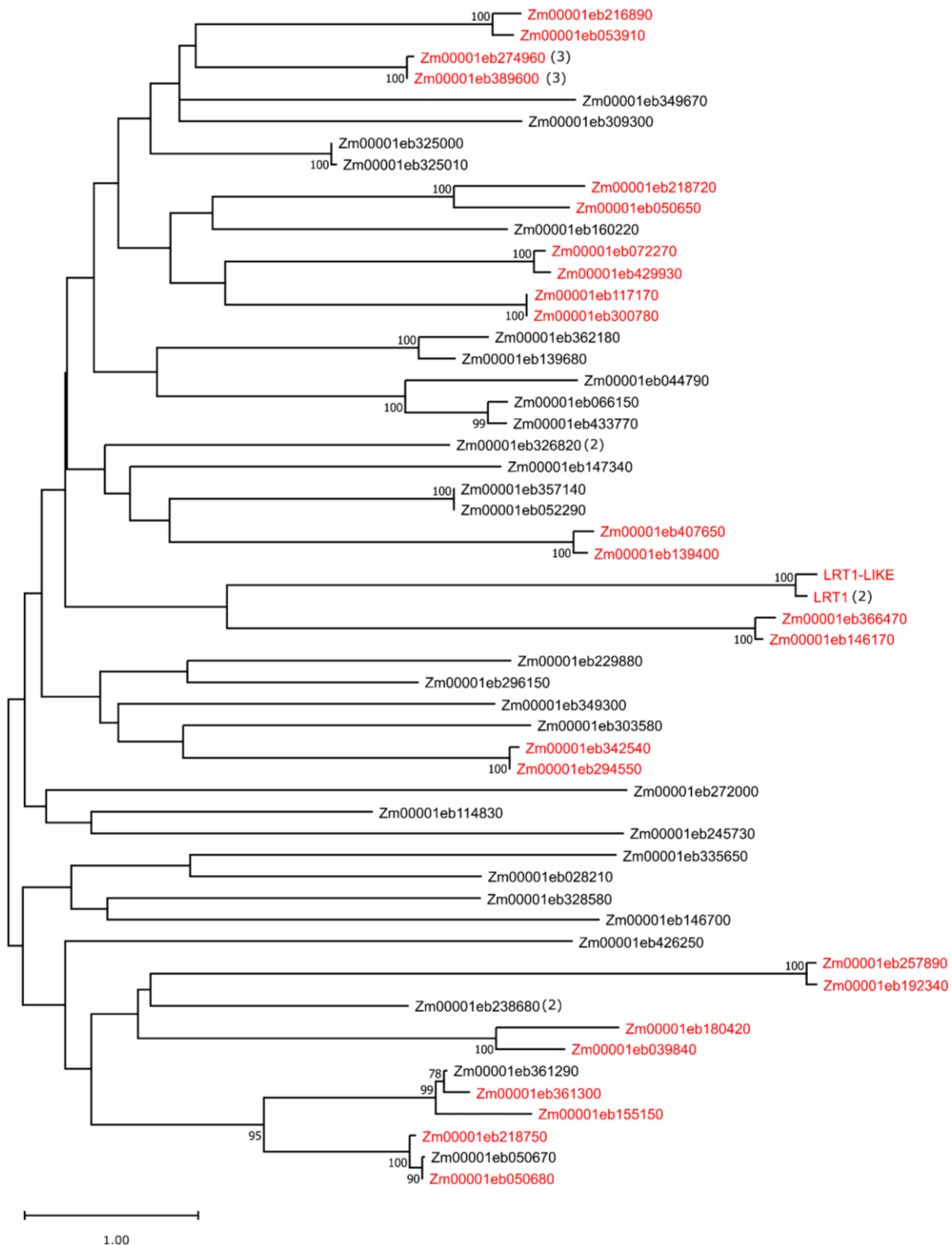


Figure 26 Phylogenetic tree based on DWD motifs in *Zea mays*. All WD 40 full-length protein sequences containing at least one DWD motif were aligned with the MUSCLE algorithm using MEGA X. An unrooted tree was constructed using the neighbor-joining method in Mega X. Bootstrap support for 1000 replicates higher than 50% is indicated at respective nodes. Scale bar indicates number of changes per site. All genes contain one DWD motif, unless another number is indicated in brackets. Genes belonging to subgenome 1 and 2 according to Schnable *et al.* (2011) are highlighted in bold and normal font, respectively. Genes not assigned to one of the maize subgenomes are printed in italics. Duplicated gene pairs are highlighted in red.

These potential DCAF protein candidates display only little sequence similarity outside the WD40 domains as indicated by their phylogenetic reconstruction (Figure 26). While LRT1 contains two DWD motifs characteristic for DCAF proteins, its paralog LRT1-LIKE contains only one DWD motif (Figures 25, 26).

About half of the identified proteins are gene pairs, which are present in both maize subgenomes. For the remaining genes there is only one copy in one of the subgenomes or they could not be assigned to subgenome and are therefore non-syntenic genes.

5.9 Expression analysis

5.9.1 Root-type and tissue specific expression of *lrt1* and *lrt1-like*

The expression of *lrt1* and *lrt1-like* was determined relative to *hb3* via qRT-PCR in different root types and leaves (Figure 27A and B) and root tissues (Figure 27C and D).

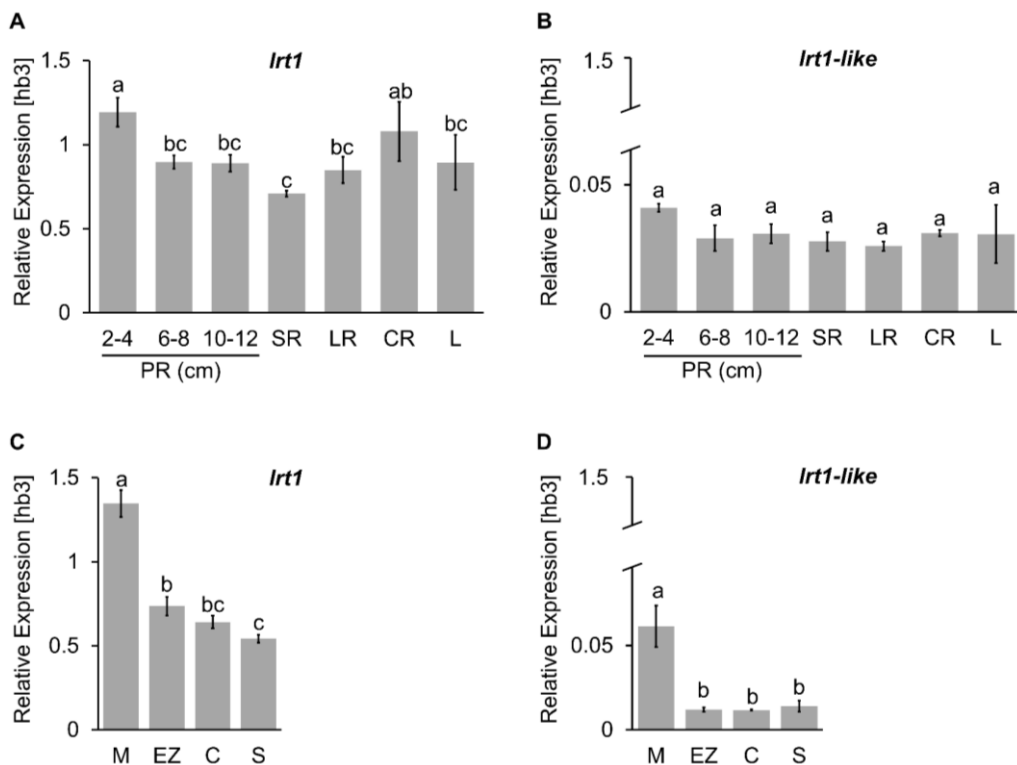


Figure 27 Expression of *lrt1* and *lrt1-like* in different root-types and tissues. Relative expression of *lrt1* and *lrt1-like* was analyzed via qRT-PCR relative to the *homeobox-transcription factor 3* (*hb3*) in primary roots (PR) at different developmental stages, seminal roots (SR), lateral roots (LR), crown roots (CR) and leaves (L) (A, B) and in different primary root tissues (C, D). Significant differences of means between each sample were calculated by Tukey's test ($p < 0.05$) and indicated with small letters.

In primary roots of different length, *lrt1* showed the highest expression in young roots of 2-4 cm length, while significantly less expression was detected in older 6-8 cm and 10-12 cm long roots (Figure 27A). Moreover, *lrt1* expression in 2-4 cm primary roots was significantly higher

than in seminal and lateral roots, while expression in crown roots was only significantly higher than in seminal roots compared to all root types (Figure 27A). Leaves displayed similar expression levels of *lrt1* compared to all root-types except young 2-4 cm primary roots, which displayed higher expression. In contrast to *lrt1*, *lrt1-like* did not display any significant expression variation between the different root-types or root-types and leaves (Figure 27B). When different root tissues of the primary root were surveyed for expression, both *lrt1* and *lrt1-like* displayed significantly higher expression in the meristematic zone than in the elongation zone and cortex and stele of the differentiation zone (Figure 27C and D).

In general, *lrt1* expression levels were on average 25-times higher in all root-types and tissues compared to *lrt1-like* (Figure 27). When comparing the expression of *lrt1* and *lrt1-like* in different root types and root tissues, a significant correlation between both genes was observed (Figure 28). A coefficient of determination of $R^2 = 0.839$ and a Pearson correlation coefficient of $R = 0.92$ ($P \leq 0.001$) was calculated.

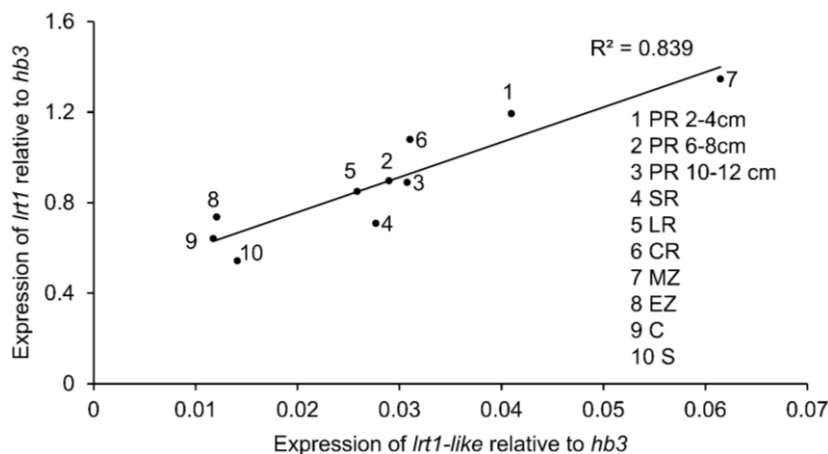


Figure 28 Correlation between *lrt1* and *lrt1-like* expression in different root types and root tissues. Expression of *lrt1* and *lrt1-like* was analyzed via qRT-PCR relative to the *homeobox-transcription factor 3 (hb3)* PR: primary root, SR: seminal root, LR: lateral root, CR: crown root, MZ: meristematic zone, EZ: elongation zone, C: cortex, S: stele.

5.9.2 Expression of *lrt1* and *lrt1-like* in the *lrt1* mutant

Furthermore, expression of *lrt1* and *lrt1-like* was compared in seven day old primary roots of homozygous and heterozygous wild type and in mutant *lrt1* plants (Figure 29A and B). The expression of *lrt1* was significantly reduced in heterozygous wild type and even more reduced in homozygous mutant *lrt1* primary roots compared to homozygous wild type plants (Figure 29A). The expression of *lrt1-like* was independent of the *lrt1* mutation and is thus likely not regulated by this gene (Figure 29B).

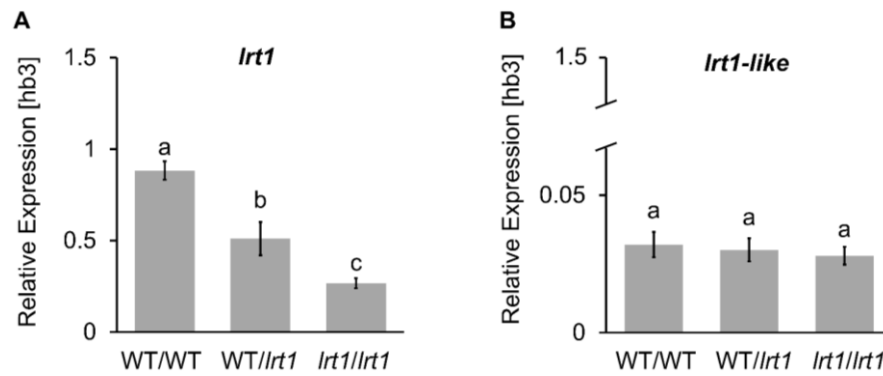


Figure 29 Expression of *lrt1* and *lrt1-like* in primary roots of WT/WT, WT/*lrt1* and *lrt1/lrt1* plants 7 days after germination. Relative expression of *lrt1* (A) and *lrt1-like* (B) was analyzed via qRT-PCR relative to the homeobox-transcription factor 3 (*hb3*). Significant differences of means between each sample were calculated by Tukey's test ($p < 0.05$) and indicated with small letters.

5.9.3 Expression of *lrt1* in the seminal- and lateral root defective mutant *rum1*

Furthermore, *lrt1* expression was analyzed in the seminal- and lateral root defective mutant *rum1* (Figure 30A). No difference was observed in primary roots of 10-12 cm between wild type and *rum1* mutants. The expression levels were comparable to those measured in the experiments before (Figure 27 A, C). When comparing the expression of *rum1* in homozygous *lrt1* with wild type plants (Figure 30B), *lrt1* expression was significantly downregulated in *rum1* mutants by ~30%.

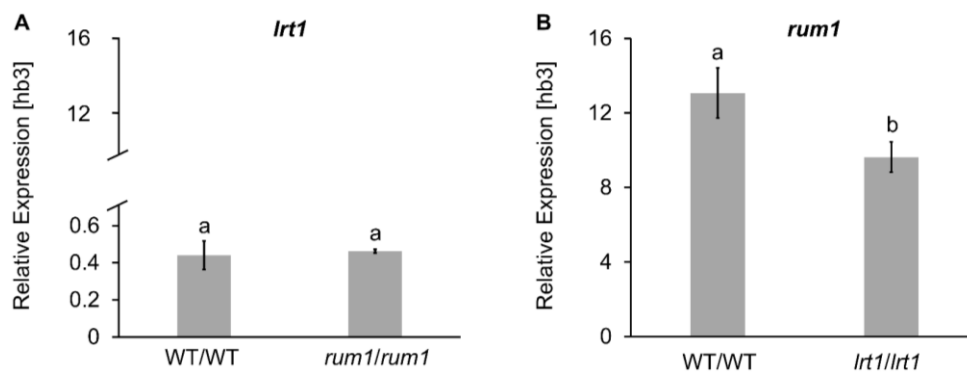


Figure 30 Expression of *lrt1* in wild type and *rum1* mutants (A) and *rum1* expression in wild type and *lrt1* mutants (B). Expression of *lrt1* and *rum1* was analyzed via qRT-PCR relative to the homeobox-transcription factor 3 (*hb3*) in primary roots 10 days after germination. Significant differences of means between each sample were calculated by Tukey's test ($p < 0.05$) and indicated with small letters. WT: wild type.

5.9.4 Expression of *lrt1* in the seminal- and crown root defective mutant *rtcs*

In addition, the expression of *lrt1* was measured in the *rtcs* (*rootless concering crown and seminal roots*) mutant and compared with wild type (Figure 31). The expression in the *rtcs* mutant was significantly reduced by 27%.

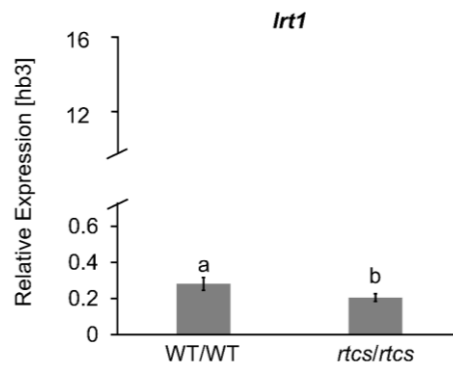


Figure 31 Expression of *lrt1* in wild type and *rtcs* mutants. Expression was analyzed via qRT-PCR relative to the *homeobox-transcription factor 3* (*hb3*) in primary roots 10 days after germination. Significant differences of means between each sample were calculated by Tukey's test ($p < 0.05$) and indicated with small letters. WT: wild type.

5.10 Subcellular localization of LRT1

LRT1 is predicted to be a DCAF protein homolog (Figure 23) within the CUL4-based E3 Ligase, which targets proteins for degradation and therefore acts in the nucleus. Using the subcellular localization prediction tool LOCALIZER (SPERSCHNEIDER *et al.*, 2017), three nuclear localization signals were identified (Figure 32, NLS1-3).



Figure 32 Nuclear localization signals (NLS) in LRT1. NLS1 (KRKLSRAPSRRLRVK GK), NLS2 (RRQFSGIQIPRRDRH), NLS3 (RRNLDDVTSSINARRVRH) were identified using LOCALIZER (SPERSCHNEIDER *et al.*, 2017).

To verify the predicted subcellular localization, LRT1 was fused to mVenus within a 2in1 FRET vector, where the Arabidopsis transcription factor HMGA (chromatin-associated high mobility group protein A) was fused to tagRFP and served as a nuclear localization control. HMGA and LRT1 were fused either N- or C-terminally to investigate the influence of the fusion site on the subcellular localization. When mVenus was fused N-terminally to LRT1 it was exclusively expressed in the nucleus (Figure 33A and B) while the expression signal of the C-terminal fusions was not localized in the nucleus. The signal likely indicates a peroxisomal localization in this case (Figure 33C and D). HMGA-tagRFP fusions showed exclusive nuclear localization for C- and N-terminal fusions (Figure 33A and D).

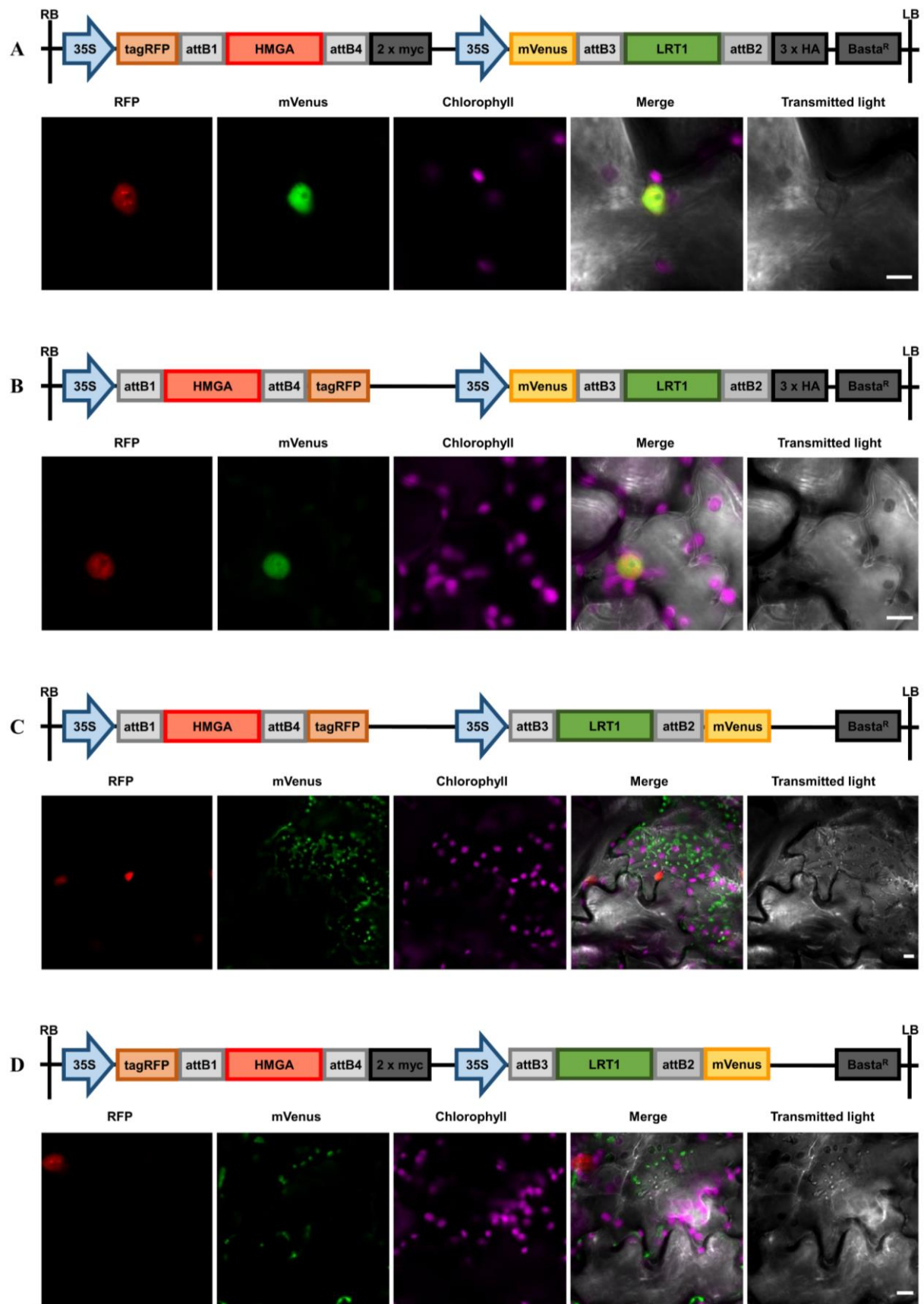


Figure 33 Subcellular localization of LRT1-mVenus fusion protein in transiently transformed tobacco leaves. HMGA as nuclear control gene was fused to tagRFP. LRT was fused to mVenus. Scale bar = 10 μ m.

5.11 Phylogeny and sequence analyses of DDB1 homologs in maize

Blasting the *Arabidopsis* DDB1A (AT4G05420) amino acid sequence against all maize gene model protein sequences followed by phylogenetic analyses using the full protein sequences of the BLAST hits identified five possible homologs in maize from which the two closest related are referred to as DDB1-LIKE 1 and DDB1-LIKE 2 (Figure 34). DDB1-LIKE 1 and DDB1-LIKE 2 represent a paralogous gene pair with DDB1-LIKE1 assigned to subgenome 1 and DDB1-LIKE 2 assigned to subgenome 2.

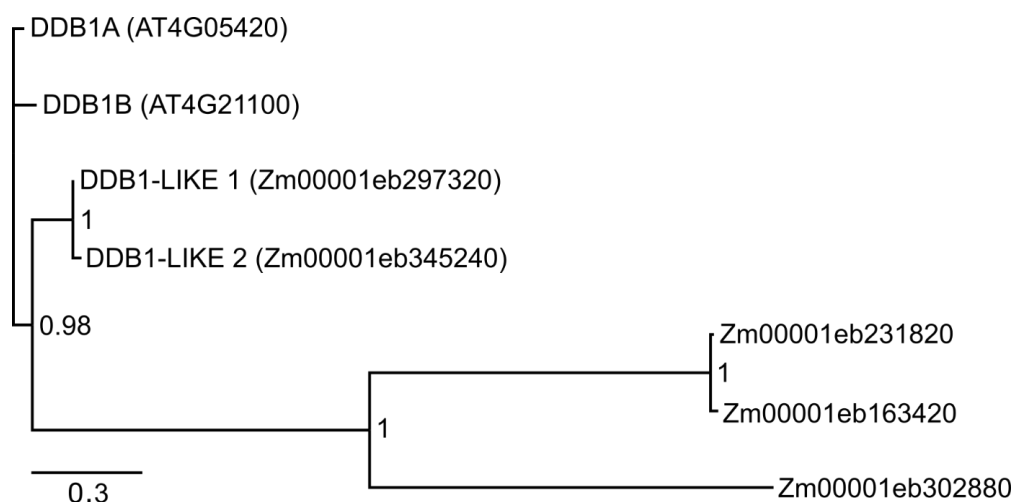


Figure 34 Phylogenetic tree of DDB1 homologs in maize. After alignment of full-length protein sequences with MUSCLE algorithm using MEGA X, the tree was constructed with 2 chains and 1 M generations using MrBayes. Bootstrap values are shown for all clades.

Furthermore, the AS sequences of the potential DDB1 homologs were compared in more detail. A comparison of the protein domains showed that DDB1A and DDB1B from *Arabidopsis* as well as all potential maize homologs exhibit a WD40/ YVTN-repeat-containing domain as well as N- and C- terminal Cleavage/polyadenylation specificity factor A subunits (Figure 35).

Maize DDB1-LIKE 1 and DDB1-LIKE 2 showed the strongest similarity to the *Arabidopsis* homologs regarding the position and length of the mentioned domains and also the same protein length of 1088 AS as the *Arabidopsis* proteins. (Figure 35).

The two homologs with the accessions Zm00001eb231820 and Zm00001eb302880 do also show a similar domain structure compared to DDB1A but with differences in position and length of the domains and also in the length of AS sequence. The potential homolog with the accession Zm00001eb163420 also contains the mentioned domains but only very short fragments of them resulting in a protein length of only 264 AS.

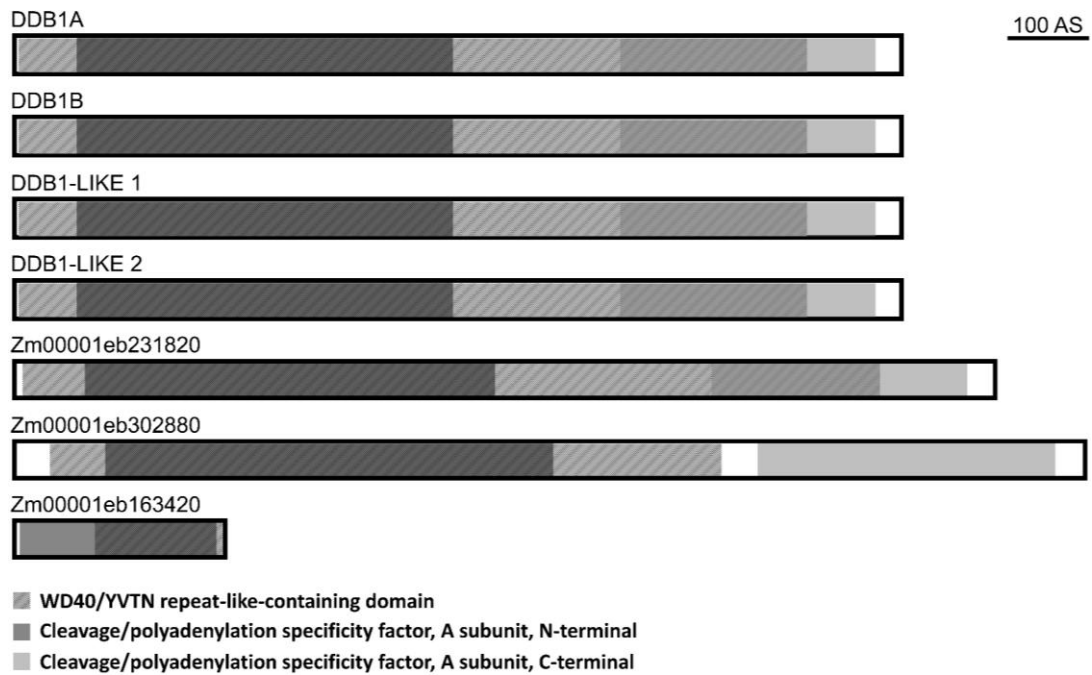


Figure 35 Protein sequence models of DDB1 homologs. Complete AS of DDB1A, DDB1B of *Arabidopsis* as well as the potential homologs in maize are shown.

Comparison of the identity and similarity of the potential DDB1A homologs in maize supports the notion that DDB1-LIKE 1 and DDB1-LIKE 2 are the closest homologs to DDB1A in *Arabidopsis* with a similarity of 91% and 90% and an identity of 83% and 82% respectively (Table 8).

Table 8 Identity/similarity matrix of DDB1 homologs in percent identity (blue) or similarity (brown). Full protein sequences were aligned using the muscle algorithm in Mega X. Identity and similarity of the aligned sequences were calculated with Ident and Sim (STOTHARD, 2000).

identity similarity	<i>A.t.</i>	<i>A.t.</i>	<i>Z.m.</i>	<i>Z.m.</i>	Zm0000eb		
	DDB1A	DDB1B	DDB1-L 1	DDB1-L 2	231820	163420	302880
<i>A.t.</i> DDB1A		91	83	82	21	6	17
<i>A.t.</i> DDB1B	96		81	79	21	6	18
<i>Z.m.</i> DDB1-L 1	91	90		98	20	7	16
<i>Z.m.</i> DDB1-L 2	90	89	99		20	6	16
Zm00001eb231820	39	39	40	40		21	15
Zm00001eb163420	11	10	11	11	21		4
Zm00001eb302880	34	34	33	33	33	8	

The other possible homologs show similarities of <40% and identities of <21%, suggesting that these proteins have different functions and do not act as DDB1 proteins in maize.

Based on these results, subsequent experiments were performed using DDB1-LIKE 1 and DDB1-LIKE 2 as DDB1 homologs in maize, the other possible homologs described were neglected.

5.12 Subcellular localization of DDB1L1 and DDB1L2

The two DDB1 homologs DDB1-LIKE1 and DDB1-LIKE2 are assumed to be also localized in the nucleus which would enable their role in acting in nuclear localized complexes, specifically as part of the CUL4-DDB1-DCAF complex.

Using the subcellular prediction tool Predict Protein (BERNHOFER *et al.*, 2021) a nuclear localization for both DDB1 homologs was predicted with a probability of 10%. The use of different localization prediction tools led to different and ambiguous results as summarized in Table 9. Plant-mSubP (SAHU *et al.*, 2019) predicted both DDB1 homologs to be localized in the cytosol and the nucleus. Using the subcellular localization prediction tool LOCALIZER (SPERSCHNEIDER *et al.*, 2017) one chloroplast transit peptide (AS 1-40) with a probability of 79% was identified for DDB1L1. For DDB1L2 no transit peptides or NLS were identified.

Table 9 Prediction of subcellular localization for DDB1 homologs using different subcellular localization prediction tools.

	Predict Protein	Plant-mSubP	Localizer
DDB1L1	nuclear localization (10%)	cytosolic and nuclear localization (52%)	chloroplastic localization (79%)
DDB1L2	nuclear localization (10%)	cytosolic and nuclear localization (43%)	-

In order to verify the subcellular localization of both DDB1 homologs, N- and C- terminal fusions of DDB1L1 as well as DDB1L2 to mVenus were created. For DDB1L1 (Figure 36) as well as for DDB1L2 (Figure 37) a nuclear and cytosolic expression was observed. HMGA-tagRFP as nuclear localization control was expressed in the nucleus exclusively in both, N- and C-terminal fusions (Figures 36, 37).

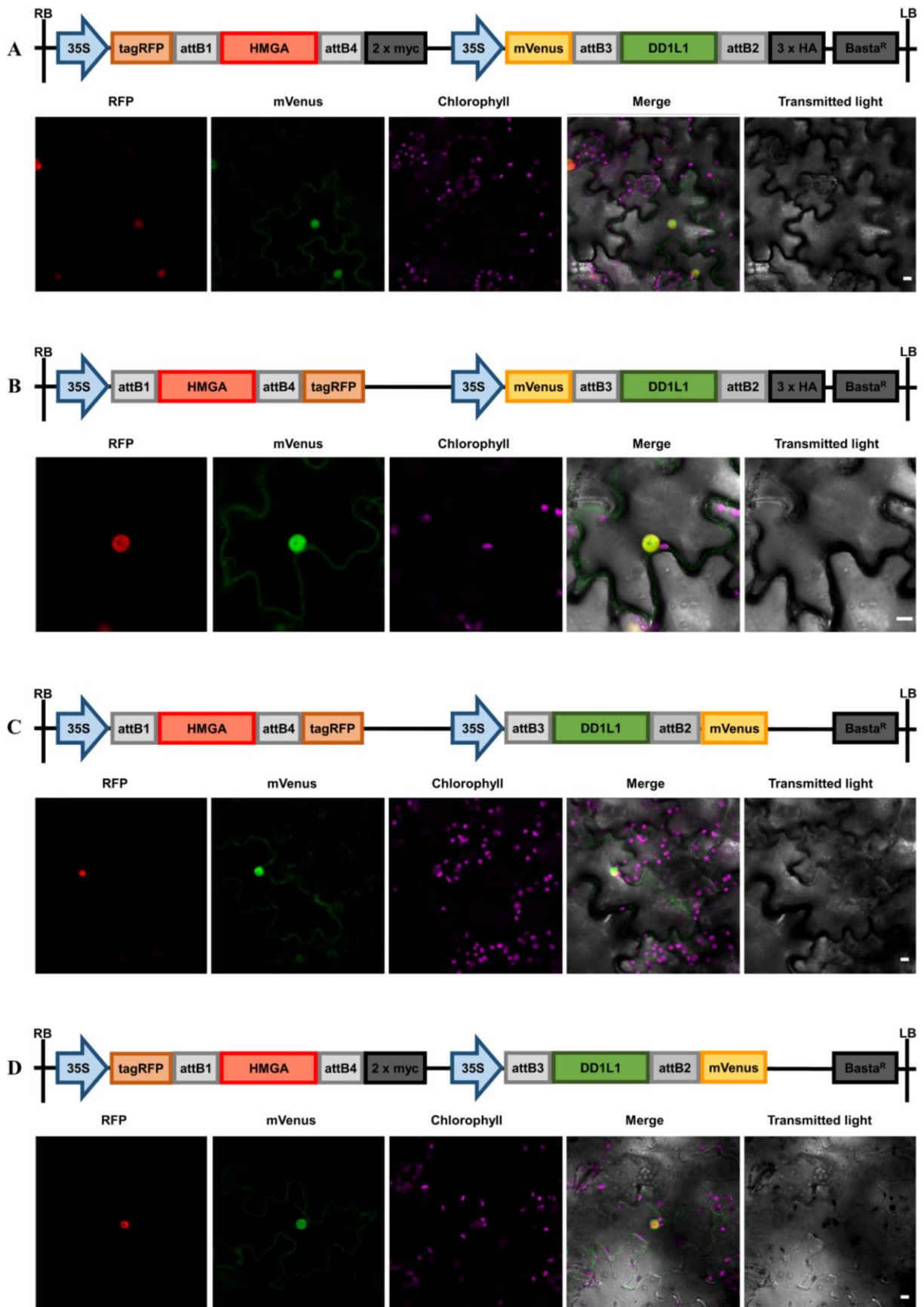


Figure 36 Subcellular localization of DDB1-L1-mVenus fusion protein in transiently transformed tobacco leaves. HMGA as nuclear control gene was fused to tagRFP. DDB1-LIKE1 was fused to mVenus. Scale bar = 10 μ m.

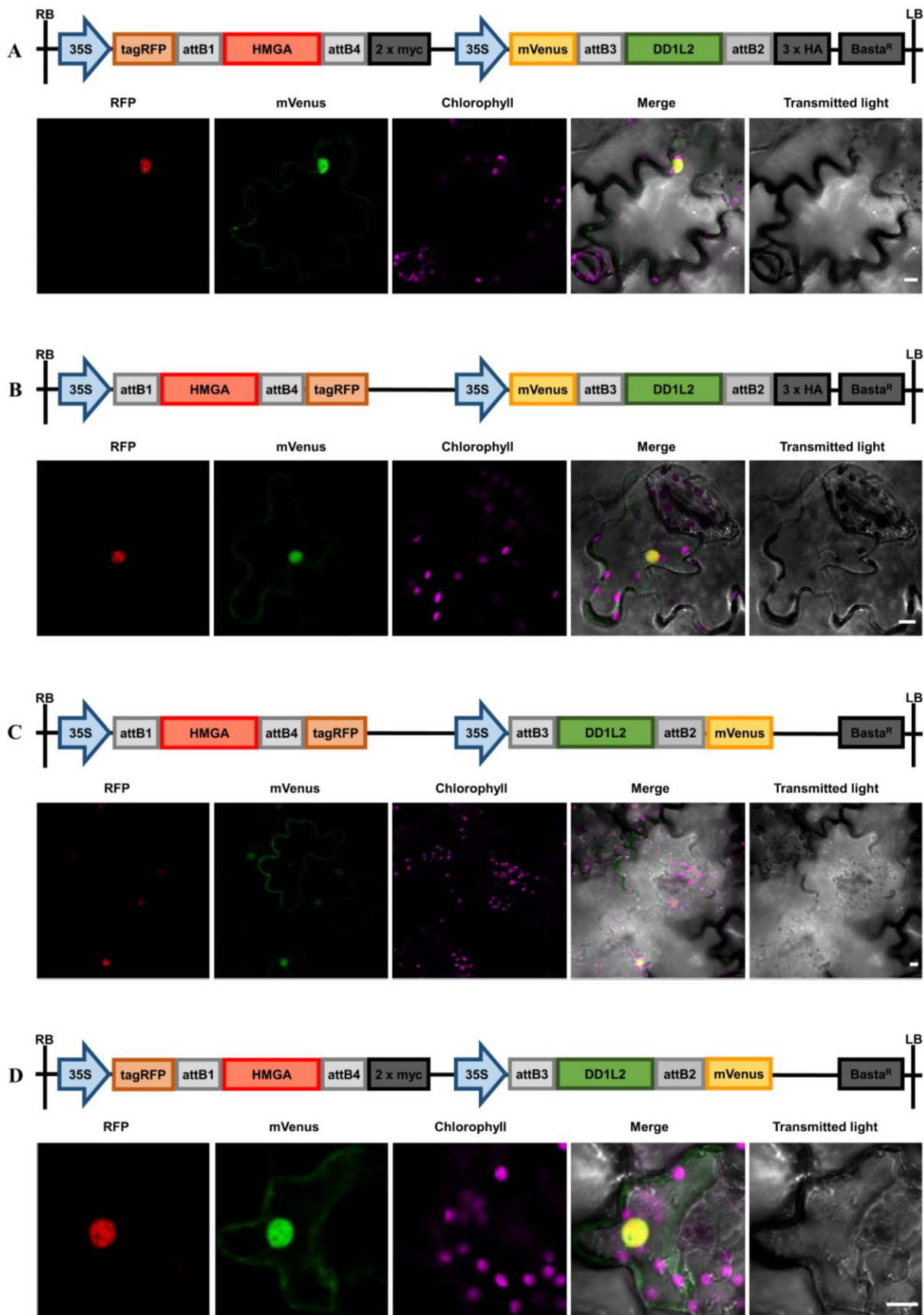


Figure 37 Subcellular localization of DDB1-L-2-mVenus fusion protein in transiently transformed tobacco leaves. HMGA as nuclear control gene was fused to tagRFP. DDB1-LIKE2 was fused to mVenus. Scale bar = 10 μ m.

5.13 Analysis of the protein-protein interaction between LRT1 and DDB1 homologs















To test if LRT1 is able to interact with DDB1-LIKE1 and or DDB1-LIKE 2, a direct interaction test was performed using the Y2H system by co-transforming two constructs fused to the Gal4 binding (pGBKT7) or Gal4-DNA activation domain (pGADT7) respectively. As shown in Table 10, neither a co-transformation of DDB1-LIKE1 with LRT1 nor of DDB1-LIKE2 with LRT1 led to a reporter gene activation. Consequently, the co-transformed yeast was neither able to grow on quadruple dropout medium (SD-Leu-Trp-His-Ade) nor on double dropout media supplemented with the antibiotic aureobasidin A. Moreover, the co-transformed yeast was not able to hydrolyze the colorless X- α -Gal into the blue end product, which implies that the reporter gene which encodes for the secreted enzyme alpha-galactosidase was not activated. Co-transformation with pGBKT7-53 which encodes the Gal4 DNA-BD domain fused with murine P53 and pGADT7-T which encodes the Gal4 AD fused with the SV40 large antigen were used as positive controls because both proteins are known to interact (LI and FIELDS, 1993; IWABUCHI *et al.*, 1993). As expected the positive controls showed growth on all dropout media and were able to hydrolyze X- α -Gal. Co-transformation of pGBKT7-lam, which encodes the GAL4 DNA-BD domain fused with lamin which cannot interact with pGADT7-T was used as negative control and was only able to grow on DDO. A second positive control consisting of two not yet published weakly interacting proteins fused to the Gal4 DNA-BD and Gal4 AD were also co-transformed (GAUGLER, 2019). These co-transformants were able to grow on triple (SD-Leu-Trp-His) and quadruple (SD-Leu-Trp-His-Ade) dropout medium but failed to grow on DDO containing aureobasidin A and were not able to hydrolyze X- α -Gal.

Table 10 Growth of co-transformed constructs of DDB1-LIKE 1 and DDB1-LIKE2 with LRT1 in Yeast. Growth: X; no growth: O; DDO: SD-Leu-Trp; X: X- α Gal; A: aureobasidin A; pGBKT7-53 encodes the Gal4 DNA-BD fused with murine P53; pGADT7-T encodes the Gal4 AD fused with SV40 large T-antigen. pGBKT7-53 and pGADT7-T are interacting in yeast and thus activate all four reporters and are used as positive control. pGBKT7-Lam encodes the Gal4BD fused with lamin and cannot interact with pGADT7-T and is used as negative control. BD and AD are two not yet published proteins fused to the Gal4 binding and activation domain respectively, which are known to show a weak interaction (GAUGLER, 2019).

Cotransformed constructs	Selective media				
	DDO	SD-Leu-Trp-His	SD-Leu-Trp-His-Ade	DDO/X	DDO/X/A
DDB1L1_pGADT7 + LRT1_pGBKT7	X	X	O	O	O
LRT1_pGADT7 + DDB1L1_pGBKT7	X	X	O	O	O
DDB1L2_pGADT7 + LRT1_pGBKT7	X	X	O	O	O
LRT1_pGADT7 + DDB1L2_pGBKT7	X	X	O	O	O
pGBKT7-53 + PGADT7-T	X	X	X	X	X
BD +AD	X	X	X	O	O
pGBKT7-Lam + PGADT7-T	X	O	O	O	O

To further test for possible weak interactions between LRT1 and DDB1-LIKE1 and or DDB1-LIKE2 and to quantify these potential interactions, the β -galactosidase activity was measured in yeast cells, co-transformed with the same constructs as described before for the growth assay, using the ONPG assay and the PXG assay (Table 11). In the ONPG assay, the chromogenic substrate o-nitrophenyl-D-galactosidase which mimics lactose is hydrolyzed into galactose and O-nitrophenol, which causes the yellow color. Only for the positive control of pGBKT5-53 and pGADT7-T a β -galactosidase activity was observed. Neither for DDB1-LIKE1 and DDB1-LIKE2 with LRT1 nor for the control BD + AD, a β -galactosidase activity was observed. The same result was observed for the pellet X-Gal (PXG) assay, where β -galactosidase activity is measured by the hydrolyzation of X-gal to 5-bromo-4chloro-3-hydroxyindole which spontaneously dimerizes and oxidizes to the blue product 5,5'-dibromo-4,4'-dichloro-indigo (Table 11).

Table 11 β -Galactosidase assays of co-transformed DDB1-LIKE1, DDB1-LIKE2 and LRT1 constructs in yeast. ONPG: o-Nitrophenyl- β -D-galactopyranosid; PXG-assay: Pellet X-Gal assay. Indicated are Miller Units for ONPG assays and Absorption at 680 nm for PXG-Assay with standard deviations in brackets respectively. pGBKT7-53 encodes the Gal4 DNA-BD fused with murine P53; pGADT7-T encodes the Gal4 AD fused with SV40 large T-antigen. pGBKT7-53 and pGADT7-T are interacting in yeast and thus activate all four reporters and are used as positive control. pGBKT7-Lam encodes the Gal4BD fused with lamin and cannot interact with pGADT7-T and is used as negative control. BD and AD are two not yet published proteins fused to the Gal4 binding and activation domain respectively, which are known to show a weak interaction (GAUGLER, 2019).

	ONPG assay [Miller Units]			PXG assay [A_{680}]		
	#1	#2	#3			
DDB1L1_pGADT7 + LRT1_pGBKT7	0 (0.2)	0 (0.0)	0 (0)		0.0 (0.0)	
LRT1_pGADT7 + DB1L1_pGBKT7	0 (0.3)	0 (0.2)	4 (1.9)		-0.3 (0.1)	
DDB1L2_pGADT7 + LRT1_pGBKT7	1 (1.2)	0 (0.0)	2(0.6)		-0.3 (0.0)	
LRT1_pGADT7 + DDB1L2_pGBKT7	1 (0.6)	0 (0.0)	5 (1.1)		-0.3 (0.0)	
+ pGBKT7-53 + PGADT7-T	256 (27.0)	84 (7.1)	216 (54.5)		1.3 (0.1)	
+ BD + AD	1 (1.1)	0 (0.0)	4 (1.6)		-0.2 (0.0)	
- pGBKT7-Lam + PGADT7-T	1 (1.3)	0 (0.0)	3 (3.2)		-0.3 (0.0)	

5.14rBiFC and FRET analysis of interaction between LRT1 and DDB1 homologs

To investigate the possibility of LRT1 acting as a substrate receptor (DCAF protein) in a CUL4-DDB1-E3 ubiquitin ligase complex, the putative interaction of LRT1 with DDB1L1 and DDB1L2 was analyzed using the rBiFC 2in1 system (GREFEN and BLATT 2012). Therefore, all four possible split YFP-tag orientations of the genes of interest were tested for both protein partner combinations. A YFP fluorescence signal indicating the fusion of the splitted YFP halves ($nYFP + cYFP = eYFP$) was not detected for any of the constructs, neither for the interaction of LRT1 with DDB1L1 (Figure 38) nor for an interaction of LRT1 with DDB1L2 (Figure 39). For all construct combinations, a clear nuclear and cytosolic RFP fluorescence signal was observed, indicating a successful transformation and expression of the internal control mRFP1 (Figures 38 and 39).

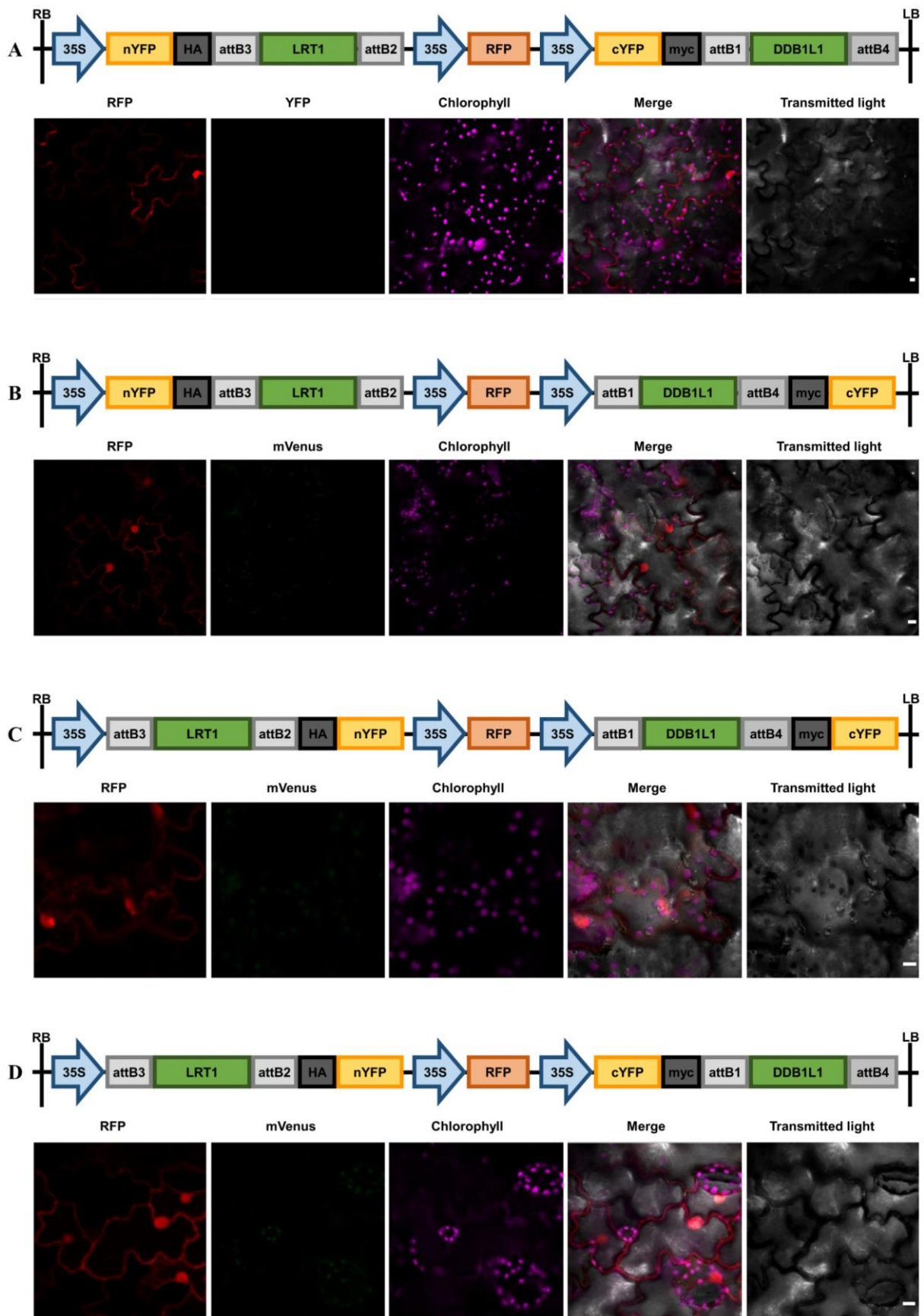


Figure 38 BiFC assay of LRT1 and DDB1L1 in transiently transformed tobacco leaves. LRT1 is fused to nYFP, either N- or C- terminally. DDB1L1 is fused to cYFP, either N- or C-terminally. Scale bar = 10 μ m

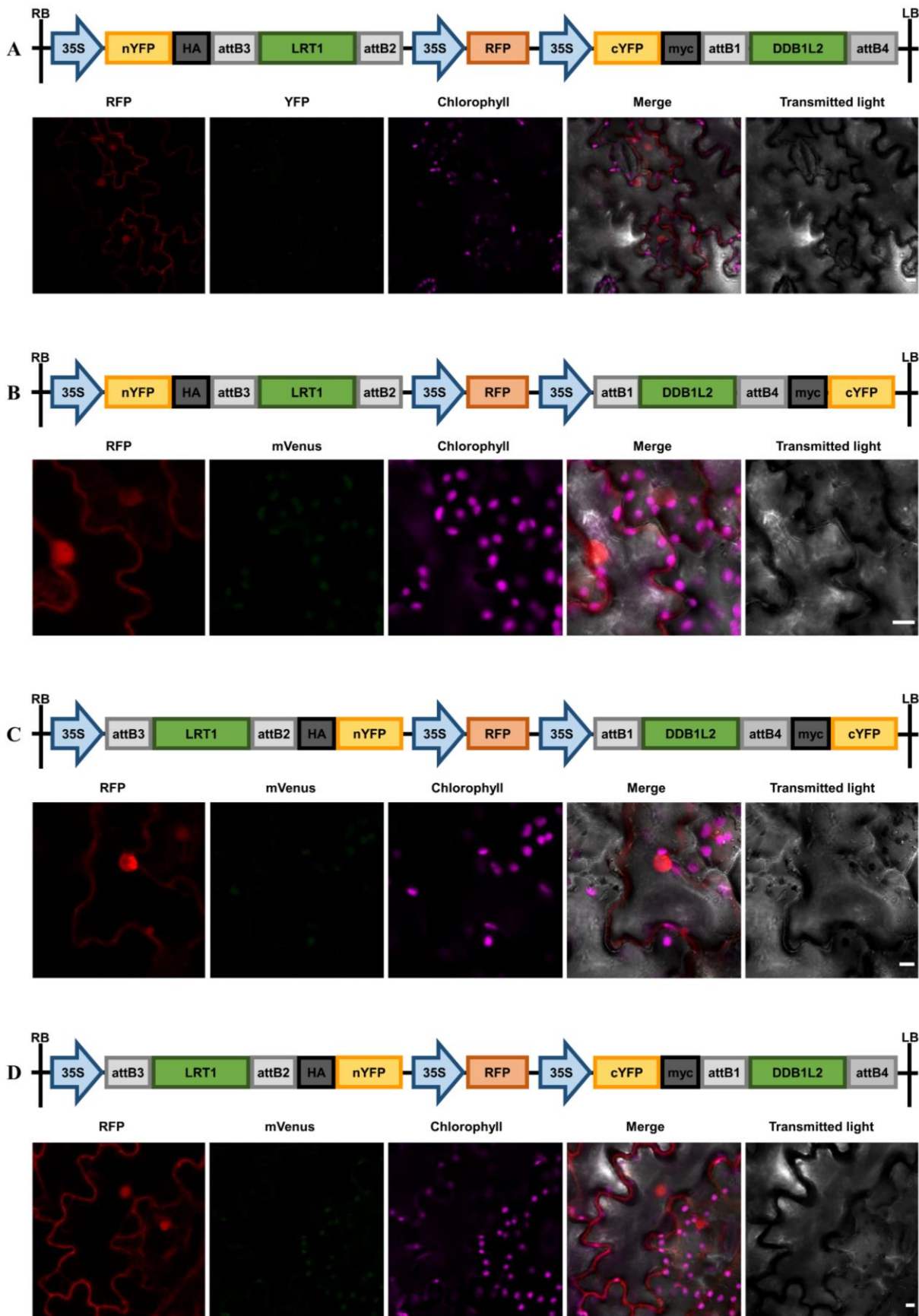


Figure 39 BiFC assay of LRT1 and DDB1L2 in transiently transformed tobacco leaves. LRT1 is fused to nYFP, either N- or C-terminally. DDB1L1 is fused to cYFP, either N- or C-terminally. Scale bar = 10 μ m

In addition, a potential interaction of LRT1 and DDB1-L1 was also analyzed by a FRET experiment. Therefore, both genes were fused C-terminally to the split YFP- tags in the FRET 2 in 1 system. Two different constructs, with a N-terminal mVenus at LRT1 in combination with a N-terminal (Figure 40A) or a C-terminal (Figure 40B) RFP fusion at DDB1L1, were tested. When excited at 488 and 543 nm, a clear fluorescence signal for RFP and mVenus was detected, indicating an expression of LRT1 (Figure 40, mVenus) and DDB1L1 (Figure 40, RFP) in both tested constructs. In accordance with the FRET results for the nuclear localization experiments, the LRT1 mVenus fluorescence signal was localized in the nucleus (Figure 33) and the DDB1L1 RFP fluorescence signal was localized in both, the nucleus and the cytosol (Figure 36), whereas the nuclear signals was stronger. When imaging without excitation at 543 nm, no fluorescence signal observed with the 579 to 633 nm bandpass filter, indicating that the donor mVenus was not able to transfer energy to the acceptor RFP due to the missing interaction between LRT1 and DDB1L1.

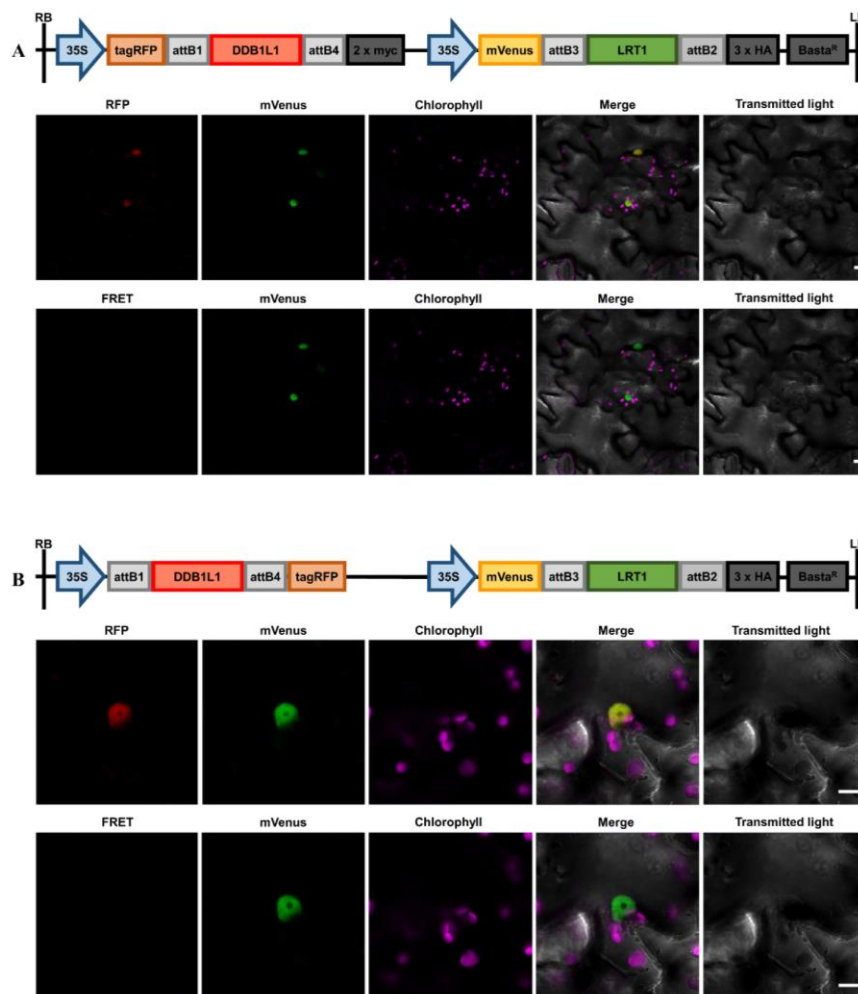


Figure 40 FRET analysis of protein-protein interaction between LRT1 and DDB1L1 in transiently transformed tobacco leaves. LRT1 is fused C-terminally to mVenus and DDB1L1 is either fused C-terminally (A) or N-terminally to tagRFP (B). Scale bar = 10µm.

5.15 Identification of potential LRT1 interaction partners

In the present study, a Y2H cDNA library originating from maize B73 primary roots was screened using LRT1 as bait protein to identify possible interaction partners. Although the library screen was performed by mating as well as co-transformation, it was not possible to detect any potential candidates by this method. To exclude any technical problems during the experimental procedures, control experiments were performed according to the manufacturer's information, which indicated that library preparation, yeast transformations and library screen were performed successfully (MatchmakerGold Yeast Two-Hybrid System, Takara, Kusatsu, Japan).

6 DISCUSSION

6.1 LRT1 affects different aspects of root development and reduces aboveground plant performance

The maize mutant *lrt1* was initially identified by its lack of lateral root formation in the embryonic primary and seminal root system in an EMS mutation screening (HOCHHOLDINGER and FEIX, 1998). The *lrt1* and *rum1* gene display the defective lateral root phenotype only in embryonic roots while postembryonic shoot-borne roots display normal lateral root formation (HOCHHOLDINGER and FEIX, 1998; WOLL *et al.*, 2005). Furthermore, the *lrt1* primary root showed an impaired primary root elongation in comparison to wild type with a reduced primary root length by ~40%, 10 days after germination (Figure 11 A), which is in accordance with the description by HUSAKOVA *et al.* (2013). A similar phenotype was also observed in the mutant *rum1* (WOLL *et al.*, 2005). The *lrt1* mutant is also defective in crown root formation at the coleoptilar node, forming only rudimentary crown root structures (HOCHHOLDINGER and FEIX 1998). In the current work, delayed but functional crown root formation was observed from 23 days after germination (Figure 14). These crown roots were significantly shorter in comparison to wild type plants 30 days after germination (Figure 15 B). Beside the defects in lateral root formation and primary root development, seminal root number of *lrt1* homozygous plants was also significantly reduced (Figure 11 B). While in *lrt1* the seminal root number is decreased, the maize lateral root mutant *rum1* (WOLL *et al.*, 2005) and the maize shoot-borne root defective mutant *rtcs* (Hetz *et al.*, 1996) are completely lacking seminal roots.

Aboveground development of *lrt1*, is already significantly decreased in 10-day-old seedlings as illustrated by a reduction of shoot length by ~30% (Figure 11 C). This is in accordance with the description of the phenotype by HUSAKOVA *et al.* (2013).

At maturity, the *lrt1* plant showed a reduction of plant height by >50% when grown in soil pots under controlled conditions in the greenhouse, whereas this reduction was only ~20% when grown in an aerated hydroponic system compared to wild type plants (Figure 12 A). Nevertheless, shoot and root dry weight was decreased by ~50% also for *lrt1* plants grown in hydroponics (Figure 12 B). This could be explained by slender appearance of *lrt1* plants in general. For *lrt1* plants grown in the field also a clear reduction in plant height and a less complex root system of the mature plant is described (HOCHHOLDINGER and FEIX, 1998). When comparing the mature root system of *lrt1* with wild type grown in the aerated hydroponics system the reduced complexity of the root system is also obvious (Figure 13).

Considering the root system of *lrt1* grown in hydroponics, lateral roots became visible 14 days after germination, but showed a rather irregular distribution in comparison to wild type (Figure 13, 15 days after germination). In line with this, the number of initiated lateral root primordia in *lrt1* is not different from wild type, but these lateral root primordia did typically not emerge from the primary root (HUSAKOVA *et al.*, 2013). This is also consistent during later development until maturity (Figure 13, 63 days after germination). Similarly, the maize mutant *rum1* is also affected during the early stages of lateral root development (WOLL *et al.*, 2005).

6.2 Exogenous application of auxin and ethylene failed to recover the *lrt1* mutant

Auxin biosynthesis, transport and signaling play essential roles in the regulation of root system architecture including primary root elongation, gravitropism and lateral root initiation as well as lateral root primordium development in dicots like *Arabidopsis* and in monocots like maize (ALARCÓN *et al.*, 2019; LAVENUS *et al.*, 2013; PERET *et al.*, 2009).

Auxin response maxima are essential for lateral root formation in monocots and dicots (JANSEN *et al.*, 2012). Many mutants, defective in lateral root formation connected to auxin signaling and transport were identified in maize and rice (reviewed in YU *et al.*, 2016). Dose-dependent exogenous application of auxin is able to initiate lateral root formation, while auxin inhibitors are able to suppress lateral root formation (ALARCÓN *et al.*, 2019; JANSEN *et al.*, 2012; REED *et al.*, 1998).

HOCHHOLDINGER and FEIX (1998) showed that exogenous application of auxin was not able to recover the mutant phenotype of *lrt1*. Also no changes in PIN1 auxin efflux transporter localization were observed (SCHLICHT *et al.*, 2006). Polar auxin transport specifically affects lateral root initiation and primordium development (CASIMIRO *et al.*, 2001; CASIMIRO *et al.*, 2003). Auxin transported from the root tip basically to the shoot is required for the initiation of lateral root primordia, whereas apical auxin transport from the shoot into the root enables further lateral root primordia development (BHALERAO *et al.*, 2002).

Auxin immunolocalization experiments showed, that the *lrt1* mutant in contrast to *rum1* is not impaired in polar transcellular auxin transport (SCHLICHT *et al.*, 2006).

Auxin and ethylene are tightly connected in root system architecture regulation. Auxin is able to enhance ethylene production by upregulation of ACC synthase (ALARCON *et al.*, 2014).

Low levels of ethylene in turn upregulates auxin biosynthesis and promotes lateral root initiation, whereas increasing ethylene levels interact with auxin in the root tip and inhibit lateral root initiation (IVANCHENKO *et al.*, 2008). In the current work, a potential involvement of ethylene biosynthesis and signaling on the *lrt1* phenotype was analyzed by exogenous supply

of the ethylene precursor ACC as well as by inhibiting ethylene receptors by silver nitrate. No impact on LR formation in the *lrt1* mutant was observed by those treatments using different concentrations of both reagents (Figure 18). Although exogenous application of auxin (HOCHHOLDINGER and FEIX, 1998) and an ethylene precursor in this study failed to complement the *lrt1* phenotype, an involvement of *lrt1* within auxin and, or ethylene biosynthesis and signaling cannot be excluded.

6.3 Changes in *lrt1* peroxidase activity and ROS do not directly affect the *lrt1* phenotype

LRT1 most likely indirectly affects different biosynthetic pathways related to lateral root formation.

As already described, a higher peroxidase activity was observed in the primary root of the *lrt1* mutant (HUSAKOVA *et al.*, 2013). Also an L-ascorbate peroxidase (APX) was identified to preferentially accumulate in the *lrt1* primary root (HOCHHOLDINGER *et al.*, 2004). Furthermore, a higher expression of different class III peroxidases (PRXs) in the primary root of *lrt1* compared to arbuscular mycorrhizal fungi (AMF) treated *lrt1* plants was observed (YU, 2022). These previously described changes in peroxidase activity and thus associated changes in ROS led to the hypothesis of a potential involvement of LRT1 on the proportion between proliferation and differentiation and further processes as lignification and endogenous auxin degradation by its direct or indirect involvement (Figure 6).

In order to validate this function of LRT1, treatments with the peroxidase inhibitors KCN (BESTWICK *et al.*, 1997) and salicylhydroxamic acid (SHAM; BROUWER *et al.*, 1986) as well as exogenous H₂O₂ application and promotion of H₂O₂ production by the coumarin umbelliferone (KRYLOV *et al.*, 1996) were performed in order to understand the function of peroxidases in the *lrt1* mutant their impact on the *lrt1* phenotype and thereby their role in lateral root formation in general.

The performed phenotyping after respective exogenous chemical application showed no effect on the lateral root defect in the *lrt1* mutant. This suggests, that the already described alteration in peroxidase activity in the *lrt1* mutant is not directly causing the lateral root defect, since the modification of peroxidase activity and ROS levels by the applied chemicals did not have any effect on the lateral root formation in the *lrt1* mutant.

Thus, the observed differences in the peroxidase activity in the *lrt1* mutant (HUSAKOVA *et al.*, 2013), especially class III peroxidases (PRX, YU, 2022) and L-ascorbate peroxidase (APX, HOCHHOLDINGER *et al.*, 2004) are most likely an additional secondary effect of the *lrt1* mutation and not directly connected to lateral root formation.

6.4 The *lrt1* gene encodes a DCAF protein homolog

Molecular cloning showed that *lrt1* encodes a homolog of a DCAF subunit of the CUL4-based E3 ubiquitin ligase (CRL4) complex. The *rum1* gene, which is the only previously cloned maize gene affecting lateral root formation, encodes an Aux/IAA gene, which is a central regulator of auxin signal transduction (VON BEHRENS *et al.*, 2011).

DCAF proteins are characterized by the presence of WD40 repeats with at least one, in most cases two repeats ending in a WDxR motif ending in an arginine (CHOI *et al.* 2014). The LRT1 protein contains two WDxR motifs while the paralogous LRT1-LIKE protein contains only one WDxR motif within the WD40 domain. DDB1 BINDING WD40 (DWD)-boxes are a conserved 16-17 amino acid motif within WD40 domains, which are involved in the interaction of DCAF proteins with DDB1 proteins (LEE *et al.* 2008). The LRT1 protein contains two 16 aa DWD boxes while LRT1-LIKE contains only one 16 aa DWD box (Figure 25). The shared DWD-box of LRT1 and LRT1-LIKE displays 100% identity along the 16 aa sequence (Figure 25).

The presence of the CRL4 E3 ligase complexes throughout all plants (BIEDERMANN and HELLMANN, 2011) is also reflected by the phylogenetic relationship of the LRT1 and LRT1-LIKE DCAF subunits identified in this study. The maize genome encodes 55 WD40 proteins that contain one to three DWD motifs (Figure 26). This class of proteins is conserved between monocots like rice with 78 and dicots like *Arabidopsis* with 85 WD40 repeat proteins containing one or two copies of the DWD motif (LEE *et al.*, 2008). Despite the presence of the DWD motifs in all 55 proteins, they are phylogenetically only distantly related (Figure 26). The high degree of evolutionary conservation of the LRT1 protein is supported by the observation that even single-cell green algae such as *Chlamydomonas reinhardtii* and early land plants such as the moss *Physcomitrella patens* contain LRT1 homologs. Phylogenetic analyses demonstrated that the monocot and dicot subclades are strictly separated (Figure 26). This observation suggests that this gene family diversified along monocot, dicot, and non-seed plant evolution. Among the surveyed monocot and dicot LRT1 homologs, the maize *lrt1* and *lrt1-like* genes are the only ones that underwent a duplication. Their assignment to maize subgenome 1 (*lrt1-like*) and subgenome 2 (*lrt1*) suggests that they emerged as a consequence of the last whole genome duplication of maize ~5 to 12 million years ago (SWIGONOWA *et al.*, 2004; Figure 1), shortly after the divergence of the maize and sorghum lineages (SCHNABLE *et al.*, 2011). This also explains why LRT1-LIKE and the homolog of the unduplicated Sorghum genome (Genbank AC: 006G279200) map very closely together in the phylogenetic tree. Hence, *lrt1* and *lrt1-like*

are syntenic genes that are evolutionarily old and can be traced back to a maize progenitor already before the separation of maize and sorghum. Since these genes have survived more than 5 million years of natural selection, they likely have crucial functions in maize development.

CRL4 complexes play a variety of functions in plants including development, response to stress, phytohormone signaling or DNA repair (reviewed in CHOI *et al.*, 2014). The functional diversity of CRL4 complexes is not surprising given the large number of WD40 domain containing DCAF proteins and their low phylogenetic conservation even within a single species.

To date, the only close LRT1 and LRT1-LIKE relative that has been functionally characterized is the *Arabidopsis* DCAF1 protein (ZHANG *et al.*, 2008). Two homozygous *dcaf1* T-DNA insertion mutants were embryo lethal at the globular stage, indicating that *Arabidopsis* DCAF1 is essential for plant embryogenesis (ZHANG *et al.*, 2008). Transgenic lines in which DCAF1 protein abundance was downregulated displayed multiple developmental defects. Mutant plants and their vegetative and generative organs were overall smaller and irregularly shaped. (ZHANG *et al.*, 2008). The root phenotypes of these weak *Arabidopsis* mutant alleles were not studied. In contrast to the strong *Arabidopsis* DCAF1 mutants, the maize mutant alleles *lrt1-1* to *lrt1-3* were not lethal although these mutations introduced premature stop codons, frame shifts or substantial deletions, which likely inactivated the encoded protein. In contrast to *Arabidopsis*, the maize DCAF1 homolog is present in a pair of paralogous genes. It can be hypothesized that a partial functional redundancy of the paralogous genes *lrt1* and *lrt1-like* might explain the weaker phenotype of the maize *lrt1* mutant alleles compared to *Arabidopsis* knock out alleles of DCAF1 (ZHANG *et al.*, 2008). The maize *lrt1* mutant also displays a semi dwarf phenotype for the aboveground part of the plant, which is reflected by the smaller plant height. This is in line with the observed phenotype for weak *Arabidopsis* DCAF1 mutant alleles (Zhang *et al.*, 2008). However, in contrast to weak *Arabidopsis* DCAF1 mutant alleles, maize *lrt1* mutants are not affected in phylotaxy (HOCHHOLDINGER and FEIX, 1998) or the number of leaves (HOCHHOLDINGER, 1999). The class of WD40 proteins of maize that contain one or two DWD motifs can possibly act as receptors to bind specific substrate proteins to CRL4 complexes. They display only a very weak sequence conservation outside the WD40 domains, which makes them difficult to compare. In *Arabidopsis*, known mutations in WD40 genes resulted in shorter primary roots (LEE *et al.*, 2008, 2010) but not in lateral root defects. In *Arabidopsis*, mutations that result in reduced levels of the CULLIN4 (CUL4) subunit of CRL4 E3 ubiquitin ligases

resulted among other defects in reduced lateral root growth (BERNHARDT *et al.*, 2006; CHEN *et al.*, 2006).

6.5 The *lrt1* gene is preferentially expressed in the primary root meristematic zone

Expression analyses of *lrt1* and *lrt1-like* demonstrated that *lrt1* is on average substantially higher expressed than *lrt1-like* in all surveyed tissues (Figure 27). On the level of whole roots, *lrt1* was significantly higher expressed in young 2-4 cm long primary roots than in most other root types and developmental stages analyzed. This is in line with the observation that *lrt1* is preferentially expressed in the meristem of roots which is significantly overrepresented in short 2-4 cm root compared to older and longer roots. The *Arabidopsis DCAF1* homolog of *lrt1* did also display an expression peak in the root meristem as demonstrated in GUS reporter lines (ZHANG *et al.* 2008). Moreover, the *Arabidopsis DCAF1* gene displayed very strong expression in the stele of the primary root compared to the cortex tissue (ZHANG *et al.* 2008). The maize *lrt1* gene did not display any difference in expression between cortex and stele.

The *lrt1-like* gene did not display any expression differences between the different root types and developmental stages of the primary root (Figure 27B and D). However, the *lrt1-like* gene and its paralog *lrt1* is preferentially expressed in the primary root meristem compared to other tissues. In contrast, the *rum1* gene, identified in the lateral and seminal rootless mutant *rum1*, showed the highest expression in the stele and cortex of 3 day-old primary roots and the lowest expression in the elongation zone of the primary root (ZHANG *et al.*, 2016).

Finally, the expression of *lrt1* and *lrt1-like* in wild type, heterozygous and mutant *lrt1* primary roots were analyzed. As expected the *lrt1* gene displayed reduced expression in heterozygous and even less expression in mutant *lrt1* roots (Figure 29). This can be explained by nonsense-mediated mRNA decay (NMD) in which premature stop codons are recognized and the corresponding mRNA degraded to prevent from translation of shorter and non-functional proteins (KERVESTIN and JACOBSON, 2012; RAYSON *et al.*, 2012).

In contrast, *lrt1-like* expression was not influenced by the presence of the *lrt1* gene, suggesting that *lrt1* and *lrt1-like* act in independent molecular pathways. For the homologous gene of *rum1*, *rum1-like1* (*rul1*) it was also shown that its expression is independent of *rum1* and therefore might not be controlled by *rum1* (ZHANG *et al.*, 2016).

Typically, genes of the subgenome 1 are expressed at higher levels than their homologous genes in subgenome 2 (SCHNABLE *et al.*, 2011). Contrary to this, *lrt1* (subgenome 2) showed on average a 25-fold higher expression than *lrt1-like* (subgenome 1). Although a correlation

between the *lrt1* and *lrt1-like* expression patterns was observed (Figure 28), the remarkable difference in the expression level of *lrt1* and *lrt1-like* suggests distinct functions of these homologous genes.

The expression of *rum1* was downregulated in the *lrt1* mutant (Figure 30B). The *rum1* gene encodes a Aux/IAA protein which interacts with the auxin responsive factors ARF25 and ARF34 and is required for the initiation of seminal and lateral roots on the primary root (VON BEHRENS *et al.*, 2011). Since the *lrt1* gene is likely auxin independent, as exogenous auxin supplementation was not able to restore the *lrt1* phenotype (HOCHHOLDINGER AND FEIX, 1998) and also no changes in auxin transport were detected (SCHLICHT *et al.*, 2006), the *rum1* gene is likely not directly related to the *lrt1* gene.

Both mutants, *lrt1* and *rum1* are showing a very similar phenotype in post-embryonic lateral root formation only on embryonic roots. The *rum1* mutant is completely defective in the initiation of seminal roots (VON BEHRENS *et al.*, 2011), while in the *lrt1* mutant the seminal root number is only reduced (Figure 11B). This could indicate, that the *lrt1* gene is acting upstream of the *rum1* gene and thereby causing the similar phenotypes of *lrt1* and *rum1*.

Furthermore, the expression of *lrt1* was downregulated in the *rtcs* mutant (Figure 31), which is impaired in the initiation of seminal roots and the post-embryonic shoot-borne root system (TARAMINO *et al.*, 2007). The auxin responsive gene *rtcs* is involved in the early initiation and maintenance of seminal and shoot-borne root primordia (TARAMINO *et al.*, 2007), but has no effect on lateral root formation. The downregulation of *lrt1* in the *rtcs* mutant thereby seems to be a secondary effect and not due to a direct interaction between both genes.

6.6 Subcellular localization of LRT1 and the DDB1 homologs

The subcellular localization of LRT1 and the DDB1 homologs DDB1L1 and DDB1L2 was analyzed using FRET co-localization experiments in order to confirm a predicted nuclear localization for those proteins. This would be a basic requirement for the involvement in a nuclear E3 ubiquitin ligase complex.

When mVenus was fused to the N-terminus of LRT1 a clear co-localization with the nuclear control protein HMGA (LAUNHOLT *et al.*, 2006) in the nucleus was observed (Figure 32 A, B). C-terminal fusions however showed a different subcellular localization (Figure 32 C, D). This suggests a mislocalization for this fusion orientation. A transient overexpression of GFP-labeled Arabidopsis DCAF1 in *Allium cepa* showed an exclusive nuclear localization (ZHANG *et al.*, 2008).

Using the subcellular prediction tool LOCALIZER (SPERSCHNEIDER *et al.*, 2017) three nuclear localization signals (NSLs) were identified within the LRT1 sequence (RRQFSGIQIPRRDRH, KRKLSRAPSRRLRVKGG, RRNLDDVTSSINARRVRH) also supporting a nuclear localization of LRT1 (Figure 31).

Most proteins exhibit their targeting signal peptides at the N-terminus, whereas N-terminal fluorescent protein fusions are often masking those peptides and lead to a mislocalization of those proteins (PALMER AND FREEMAN, 2004; WIEMANN *et al.*, 2001). However, proteins containing C-terminal targeting signals are often mislocalized due to C-terminal fusions (HUH *et al.*, 2003). So it is likely, that the potential mislocalization of LRT1, when mVenus was fused to the C-terminus (Figure 32, C, D), could be explained by masking of the two C-terminal nuclear localization signals within the WD40 domain of the LRT1 protein.

The DDB1 homologs DDB1L1 and DDB1L2 were localized to the nucleus and the cytosol, which is reflected by a nuclear and cytosolic mVenus signal for all examined fusion proteins (Figure 35 and 36). In accordance with this finding, the transient overexpression of GFP-labeled *Arabidopsis* DDB1A and DDB1B in *Allium cepa* showed also a nuclear and cytoplasmic localization for both proteins (ZHANG *et al.*, 2008).

In addition, the results of the performed localization analysis using FRET vectors indicate, that LRT1 is localized in the nucleus together with DDB1L1 and DDB1L2, which are also localized in the cytoplasm. This suggests a possible role of those proteins within a nuclear E3 ubiquitin ligase complex.

6.7 Interaction between LRT1 and the DDB1 homologs DDB1L1 and DDB1L2

Based on the strong homology of LRT1 with its ortholog DCAF1 in *Arabidopsis* (Figure 23, ZHANG *et al.*, 2008), we hypothesized, that in maize LRT1 is also part of the CUL4-based DDB1 E3 ubiquitin ligase complex. The differences between the phenotype of a homozygous *Arabidopsis dcaf1* mutant with an embryo lethal phenotype (ZHANG *et al.*, 2008) and the homozygous *lrt1* mutant with the lateral root defect during early postembryonic development, suggests different functions of the dicot DCAF1 and the monocot LRT1 protein. Furthermore, the *lrt1* gene has been duplicated during whole genome duplication in maize, generally leading to homologs harboring different and specialized functions (SCHNABLE *et al.*, 2011).

In the present work, a possible interaction of LRT1 with DDB1L1 or DDB1L2 was analyzed to be able to demonstrate the role of LRT1 as a DCAF protein within the CUL4-DDB1-E3 Ubiquitin ligase complex as described for the DCAF1 gene in *Arabidopsis* (Zhang *et al.*, 2008).

To this end, first heterologous Y2H co-transformation experiments were performed. All tested combinations of co-transformations, where LRT1 was fused to the GAL4 BD domain and the respective DDB1 homolog to the GAL4 AD domain and *vice versa*, were able to grow on the SD-His selection medium (Table 10). In contrast, the pGBKT7-53 + pGAT7-T positive control grew on all examined selective media. BD + AD proteins (GAUGLER, 2019) grew on DDO - His-Ade. This suggests that LRT1 does not or does only weakly interact with DDB1L1 and DDB1L2. In order to further quantify these interactions, two β -Galactosidase activity assays were performed. Both assays, the ONPG and the PXG-assay did not succeed in verifying these interactions (Table 11). Protein-protein interactions in plants can rely on posttranslational modifications like glycosylation, phosphorylation, ubiquitination, sulfenylation, myristoylation and isoprenylation and thereby render their detection impossible by heterologous systems like Y2H. This could be a possible explanation for the lack of interactions of LRT1 with DDB1L1 and DDB1L2 in Y2H co-transformation assays (XING *et al.*, 2016; VIDALAIN *et al.*, 2015). A further problem of Y2H co-transformation could be that the interaction of bait and prey proteins is hindered by the GAL4 domain fusions and thereby preventing a physiologically existing interaction. Using one vector pair for Y2H only allows for detection of 20-30% of all protein-protein interactions (VIDALAIN *et al.*, 2015). Although both BD and AD vector combinations were tested for the interaction of LRT1 with the DDB1 homologs (bait-prey swapping), in both vectors the proteins of interest were fused C-terminally to the GAL4 domains. Creation of N- and C-terminal fusions, which were not provided by the used Y2H kit, could improve the possibility to detect an interaction in prospective experiments (CAUFIELD *et al.*, 2012).

Beside the Y2H co-transformation experiments, BiFC experiments were performed to examine the formation of a protein-protein interaction between LRT1 and the DDB1 homologs DDB1L1 and DDB1L2. Overall, it was not possible to show any interaction between those proteins in all tested C- and N-terminal fusions combinations (Figure 38, 39). Furthermore, the interaction between LRT1 and DDB1-L1 was also tested using the FRET 2 in 1 system. Even though the LRT1-mVenus signal was localized in the nucleus and the DDB1L1-RFP fluorescence signal was localized in the nucleus and the cytosol in accordance with the previously performed FRET co-localization experiments, it was not possible to detect an energy transfer from the donor fluorophore mVenus to the acceptor RFP (Figure 40). Thus, by using the two fluorescence-based methods BiFC and FRET it was not possible to show an interaction between the examined proteins LRT1 and DDB1L1 and DDB1L2. In order to reduce the possibility of masking the interaction sides by the used fluorophore tags in both vector systems, which could hinder a

protein-protein interaction detection, C- as well as N- terminal fusion proteins were already used in the current work (GREFEN and BLATT, 2012).

6.8 Future Protein-protein interaction analyses

Since the Y2H assay, BiFC and FRET experiments in the current work failed to identify any potential protein-binding partners of LRT1 or to confirm an interaction with the DDB1 homologs DDB1L1 and DDB1L2, further protein-protein identification methods are essential to identify protein-binding partners of LRT1. Thereby it would also be possible to figure out, if LRT1 is working as a DCAF protein like its homolog DCAF1 in *Arabidopsis thaliana* (ZHANG *et al.*, 2008), Particularly by identifying possible substrates of LRT1 and by confirming LRT1 participating in the CUL4 DDB1 E3 ligase complex. Promising alternative protein-protein interaction analyzing methods for the future could be protein immunoprecipitation (IP) and affinity purification (AP) experiments, both *in vitro* techniques.

Co-immunoprecipitation (Co-IP) is using highly specific antibodies coupled to a sedimentable matrix in order to identify the binding partners of a specific protein including the identification of protein binding complexes, when coupled with mass spectrometry analysis (XING *et al.*, 2016; STEWART and FISHER, 2012). Co-IP can also be performed using the transformation of tagged proteins and antibody against the tag (HE *et al.*, 2009) to avoid difficulty and costs of creating highly specific antibodies but making a transformation unalterable, which on the other hand is more difficult in monocots like maize in comparison to dicots like *Arabidopsis*. In general, it is difficult to detect weak and transient interactions using CoIP (XING *et al.*, 2016), although cross-linking can be used to stabilize protein complexes (GARCIA-MOLINA *et al.*, 2014). In maize, protein immunoprecipitation was already successfully used to identify cellular protein complexes in combinations with mass spectrometry (ABRAHAM-JUÁRES, 2019; GUMBER *et al.*, 2019; ZHANG and GUY, 2006). For the examination of interaction between specific proteins like LRT1 and DDB1 the advanced co-IP technique real-time single-molecule coIP could be used, which enables also the detection of weak and transient protein-protein interactions (LEE *et al.*, 2013). Also Co-IP based protoplast transient expression has already been successfully used in rice to this end (YANG *et al.*, 2014).

The second *in vitro* technique, which also enables the identification of so far unknown binding partners and whole protein complexes, is affinity purification coupled with MS. It is highly sensitive, specific, efficient and accurate, which makes this strategy very applicable for studying protein interactions of protein complexes. The combination of AP and MS ensures

highly reliable protein interaction information, which allows the differentiation between specific protein interactors from nonspecific background proteins (KAAKE *et al.*, 2010).

Induced by the development of new affinity tags and antibodies, affinity purification coupled with MS has become one major strategy for the study of multi-subunit protein complexes consisting of stable as well as of transient and weak interactions (TAGWERKER *et al.*, 2006). Especially tandem affinity purification enables the identification of cooperative binding components within a protein complex. Tandem affinity purification is able to reduce nonspecific binding proteins more strictly but also reduces the ability of detecting transient interactions. Thus, single-step affinity purification should be used to capture those proteins under native conditions even if a detection of nonspecific binding proteins is associated with this. By using quantitative mass spectrometry, it is possible to distinguish between specific and nonspecific binding proteins for example by comparing the relative abundance of the proteins in purified extracts containing the tagged bait version with a control without the tag in label-free AP-QMS (KAAKE *et al.*, 2010). In maize, NELISSEN *et al.* (2015) were able to show the dynamics of ANGUSTIFOLIA 3-interacting proteins within the growing leaf using tandem affinity purification followed by mass spectrometry.

7 CONCLUSIONS

The *lrt1* mutant is transiently defective in lateral root formation in the embryonic primary and seminal roots during early development. Furthermore, the seminal root number is slightly reduced and crown root formation at the coleoptilar node is delayed in the *lrt1* mutant. Based on the present results, the *lrt1* phenotype is not directly related to auxin and ethylene and the *lrt1* mutation does not affect the root gravitropic response or mesocotyl elongation during photomorphogenesis sustainable.

Map based cloning identified an *lrt1* candidate gene (Zm00001eb434410). This gene was validated by the generation of independent mutant alleles by CRISPR/Cas9 in the present study.

Based on the strong similarity and identity to the *Arabidopsis* DCAF1 protein we hypothesized that LRT1 could also act as a CUL4-based E3 ubiquitin ligase in maize. In line with this, LRT1 is exclusively localized in the nucleus whereas its potential interaction partners DDB1-LIKE1 and DDB1-LIKE2 are localized in both the nucleus and cytoplasm.

Expression analyses demonstrated that the *lrt1* gene is preferentially expressed in the primary root meristem and substantially higher than its homolog *lrt1-like*. The *lrt1* gene displayed reduced expression in the *lrt1* mutant, whereby *lrt1-like* expression was not influenced. Although a correlation between the *lrt1* and *lrt1-like* expression pattern was observed, the distinct differences in expression level of both homologs suggests distinct functions of these genes.

Among the surveyed monocot and dicot LRT1 homologs, the maize *lrt1* and *lrt1-like* genes are the only ones that underwent a duplication. Since these genes have survived more than 5 million years of natural selection, both likely have crucial functions in maize development. Thus, future studies should also continue focusing on both syntenic genes.

The gene *lrt1* cloned in the present study encodes an important regulator of lateral root development in maize. The underlying molecular pathway still needs to be evaluated. In the future, this can be achieved by additional protein-protein interaction analysis techniques such as co-immunoprecipitation and tandem affinity purification coupled to mass spectrometric analyses, which ideally would enable the identification of a whole protein complex.

8 REFERENCES

- Abraham-Juárez, M.J. (2019).** Protein immunoprecipitation in maize. *Bio-protocol*, 9(11).
- Ahn, J.-H., Keum, J.-W. and Kim, D.-M. (2011).** Expression screening of fusion partners from an *E. coli* genome for soluble expression of recombinant proteins in a cell-free protein synthesis system. *PLoS ONE*, 6(11), e26875.
- Alarcón, M.V., Lloret, P.G. and Salguero, J. (2014).** The development of the maize root system: role of auxin and ethylene. *Soil Biology*, 40, 75–103.
- Alarcón, M.V., Salguero, J. and Lloret, P.G. (2019).** Auxin modulated initiation of lateral roots is linked to pericycle cell length in maize. *Frontiers in Plant Science*, 10(11).
- Arrietabaez, D. and Stark, R. (2006).** Modeling suberization with peroxidase-catalyzed polymerization of hydroxycinnamic acids: cross-coupling and dimerization reactions. *Phytochemistry*, 67(7), 743–753.
- Ashby, A.M., Watson, M.D., Loake, G.J. and Shaw, C.H. (1988).** Ti plasmid-specified chemotaxis of *Agrobacterium tumefaciens* c58c1 toward vir-inducing phenolic compounds and soluble factors from monocotyledonous and dicotyledonous plants. *Journal of Bacteriology*, 170(9), 4181–4187.
- Baldauf, J., Marcon, C., Paschold, A. and Hochholdinger, F. (2016).** Nonsyntenic genes drive tissue-specific dynamics of differential, nonadditive and allelic expression patterns in maize hybrids. *Plant Physiology*, 171(2), 1144–1155.
- Bell, J.K. and McCully, M.E. (1970).** A histological study of lateral root initiation and development in *Zea mays*. *Protoplasma*, 70(2), 179–205.
- Bernhardt, A., Lechner, E., Hano, P., Schade, V., Dieterle, M., Anders, M., Dubin, M.J., Benvenuto, G., Bowler, C., Genschik, P. and Hellmann, H. (2006).** CUL4 associates with DDB1 and DET1 and its downregulation affects diverse aspects of development in *Arabidopsis thaliana*. *The Plant Journal*, 47(4), 591–603.

Bernhofer, M., Dallago, C., Karl, T., Satagopam, V., Heinzinger, M., Littmann, M., Olenyi, T., Qiu, J., Schütze, K., Yachdav, G., Ashkenazy, H., Ben-Tal, N., Bromberg, Y., Goldberg, T., Kajan, L., O'Donoghue, S., Sander, C., Schafferhans, A., Schlessinger, A. and Vriend, G. (2021). PredictProtein – Predicting protein Structure and function for 29 Years. *bioRxiv*, doi:10.1101/2021.02.23.432527.

Bestwick, C.S., Brown, I.R., Bennett, M.H. and Mansfield, J.W. (1997). Localization of hydrogen peroxide accumulation during the hypersensitive reaction of lettuce cells to *Pseudomonas syringae* pv *phaseolicola*. *The Plant Cell*, 9(2), 209–221.

Bhalerao, R.P., Eklöf, J., Ljung, K., Marchant, A., Bennett, M. and Sandberg, G. (2002). Shoot-derived auxin is essential for early lateral root emergence in arabidopsis seedlings. *The Plant Journal*, 29(3), 325–332.

Biedermann, S. and Hellmann, H. (2011). WD40 and CUL4-based E3 ligases: lubricating all aspects of life. *Trends in Plant Science*, 16(1), 38–46.

Brouwer, K.S., van Valen, T., Day, D.A. and Lambers, H. (1986). Hydroxamate-stimulated O₂ uptake in roots of *Pisum sativum* and *Zea mays*, mediated by a peroxidase: Its consequences for respiration measurements. *Plant Physiology*, 82(1), 236–240.

Buccitelli, C. and Selbach, M. (2020). mRNAs, proteins and the emerging principles of gene expression control. *Nature Reviews Genetics*, 21(10), 630–644.

Bustin, S.A., Benes, V., Garson, J.A., Hellemans, J., Huggett, J., Kubista, M., Mueller, R., Nolan, T., Pfaffl, M.W., Shipley, G.L., Vandesompele, J. and Wittwer, C.T. (2009). The MIQE guidelines: Minimum information for publication of quantitative real-Time PCR experiments. *Clinical Chemistry*, 55(4), 611–622.

Casimiro, I., Beeckman, T., Graham, N., Bhalerao, R., Zhang, H., Casero, P., Sandberg, G. and Bennett, M.J. (2003). Dissecting arabidopsis lateral root development. *Trends in Plant Science*, 8(4), 165–171.

Casimiro, I., Marchant, A., Bhalerao, R.P., Beeckman, T., Dhooge, S., Swarup, R., Graham, N., Inzé, D., Sandberg, G., Casero, P.J. and Bennett, M. (2001). Auxin transport promotes arabidopsis lateral root initiation. *The Plant Cell*, 13(4), 843–852.

- Caufield, J.H., Sakhawalkar, N. and Uetz, P. (2012).** A comparison and optimization of yeast two-hybrid systems. *Methods*, 58(4), 317–324.
- Chen, H., Shen, Y., Tang, X., Yu, L., Wang, J., Guo, L., Zhang, Y., Zhang, H., Feng, S., Strickland, E., Zheng, N. and Deng, X.W. (2006).** Arabidopsis CULLIN4 forms an E3 ubiquitin ligase with RBX1 and the CDD complex in mediating light control of development. *The Plant Cell*, 18(8), 1991–2004.
- Choi, C.M., Gray, W.M., Mooney, S. and Hellmann, H. (2014).** Composition, roles, and regulation of cullin-based ubiquitin E3 ligases. *The Arabidopsis Book*, 12, e0175.
- Ciechanover, A., Finley, D. and Varshavsky, A. (1984).** Ubiquitin dependence of selective protein degradation demonstrated in the mammalian cell cycle mutant ts85. *Cell*, 37(1), 57–66.
- Cluet, D., Amri, I., Vergier, B., Léault, J., Audibert, A., Grosjean, C., Calabrési, D. and Spichy, M. (2020).** A quantitative tri-fluorescent yeast two-hybrid system: From flow cytometry to *in cellula* affinities. *Molecular & Cellular Proteomics*, 19(4), 701–715.
- Cosio, C. and Dunand, C. (2009).** Specific functions of individual class III peroxidase genes. *Journal of Experimental Botany*, 60(2), 391–408.
- Cosio, C., Vuillemin, L., De Meyer, M., Kevers, C., Penel, C. and Dunand, C. (2009).** An anionic class III peroxidase from zucchini may regulate hypocotyl elongation through its auxin oxidase activity. *Planta*, 229(4), 823–836.
- Coussens, G., Aesaert, S., Verelst, W., Demeulenaere, M., De Buck, S., Njuguna, E., Inzé, D. and Van Lijsebettens, M. (2012).** *Brachypodium distachyon* promoters as efficient building blocks for transgenic research in maize. *Journal of Experimental Botany*, 63(11), 4263–4273.
- Decaestecker, W., Buono, R.A., Pfeiffer, M.L., Vangheluwe, N., Jourquin, J., Karimi, M., Van Isterdael, G., Beeckman, T., Nowack, M.K. and Jacobs, T.B. (2019).** CRISPR-TSKO: A technique for efficient mutagenesis in specific cell types, tissues, or organs in arabidopsis. *The Plant Cell*, 31(12), 2868–2887.
- de Folter, S. (2005).** Comprehensive interaction map of the Arabidopsis MADS box transcription factors. *The Plant Cell*, 17(5), 1424–1433.

- Danecek, P., Bonfield, J.K., Liddle, J., Marshall, J., Ohan, V., Pollard, M.O., Whitwham, A., Keane, T., McCarthy, S.A., Davies, R.M. and Li, H. (2021).** Twelve years of SAMtools and BCFtools. *GigaScience*, 10(2).
- De Las Rivas, J. and Fontanillo, C. (2010).** Protein–protein interactions essentials: Key concepts to building and analyzing interactome Networks. *PLoS Computational Biology*, 6(6), e1000807.
- Decaestecker, W., Buono, R.A., Pfeiffer, M.L., Vangheluwe, N., Jourquin, J., Karimi, M., Van Isterdael, G., Beeckman, T., Nowack, M.K. and Jacobs, T.B. (2019).** CRISPR-TSKO: A technique for efficient mutagenesis in specific cell types, tissues, or organs in arabidopsis. *The Plant Cell*, 31(12), 2868–2887.
- Ding, X., Richter, T., Chen, M., Fujii, H., Seo, Y.S., Xie, M., Zheng, X., Kanrar, S., Stevenson, R.A., Dardick, C., Li, Y., Jiang, H., Zhang, Y., Yu, F., Bartley, L.E., Chern, M., Bart, R., Chen, X., Zhu, L. and Farmerie, W.G. (2009).** A rice kinase-protein interaction map. *Plant Physiology*, 149(3), 1478–1492.
- Ding, Z. and Kihara, D. (2019).** Computational identification of protein-protein interactions in model plant proteomes. *Scientific Reports*, 9, 8740.
- Dreze, M., Carvunis, A.-R., Charloteaux, B., Galli, M., Pevzner, S.J., Tasan, M., Ahn, Y.-Y., Balumuri, P., Barabási, A.-L., Bautista, V., Braun, P., Byrdsong, D., Chen, H., Chesnut, J.D., Cusick, M.E., Dangl, J.L., de los Reyes, C., Dricot, A., Duarte, M. and Ecker, J.R. (2011).** Evidence for network evolution in an arabidopsis interactome map. *Science*, 333(6042), 601–607.
- Ehlert, A., Weltmeier, F., Wang, X., Mayer, C.S., Smeekens, S., Vicente-Carbajosa, J. and Dröge-Laser, W. (2006).** Two-hybrid protein-protein interaction analysis in arabidopsis protoplasts: Establishment of a heterodimerization map of group C and group S bZIP transcription factors. *The Plant Journal*, 46(5), 890–900.
- Eljebbawi, A., Guerrero, Y. del C.R., Dunand, C. and Estevez, J.M. (2021).** Highlighting reactive oxygen species as multitaskers in root development. *iScience*, 24(1), 101978.
- Ferro, E. and Trabalzini, L. (2013).** The yeast two-hybrid and related methods as powerful tools to study plant cell signalling. *Plant Molecular Biology*, 83(4-5), 287–301.

- Fields, S. and Song, O. (1989).** A novel genetic system to detect protein–protein interactions. *Nature*, 340(6230), 245–246.
- Flint, L.H. (1944).** Light and the elongation of the mesocotyl in corn. *Plant Physiology*, 19(3), 537–543.
- Forster, T. (1946).** Energiewanderung und Fluoreszenz. *Die Naturwissenschaften*, 33(6), 166–175.
- Fuentes, M., Mateo, C., Pessela, B.C.C., Batalla, P., Fernandez-Lafuente, R. and Guisán, J.M. (2007).** Solid phase proteomics: Dramatic reinforcement of very weak protein–protein interactions. *Journal of Chromatography B*, 849(1-2), 243–250.
- Fukao, Y. (2012).** Protein-protein interactions in plants. *Plant and Cell Physiology*, 53(4), 617–625.
- Garcia-Molina, A., Xing, S. and Huijser, P. (2013).** A Conserved KIN17 curved DNA-binding domain protein assembles with SQUAMOSA PROMOTER-BINDING PROTEIN-LIKE7 to adapt arabidopsis growth and development to limiting copper availability. *Plant Physiology*, 164(2), 828–840.
- Gaugler, P. 2019,** personal communication
- Ghosh, I., Hamilton, A.D. and Regan, L. (2000).** Antiparallel leucine zipper-directed protein reassembly: Application to the green fluorescent protein. *Journal of the American Chemical Society*, 122(23), 5658–5659.
- Grefen, C. (2013).** The split-ubiquitin system for the analysis of three-component interactions. *Methods in Molecular Biology*, 659–678.
- Grefen, C. and Blatt, M. (2012).** A 2in1 cloning system enables ratiometric bimolecular fluorescence complementation (rBiFC). *BioTechniques*, 53(5).
- Gumber, H.K., McKenna, J.F., Tolmie, A.F., Jalovec, A.M., Kartick, A.C., Graumann, K. and Bass, H.W. (2019).** MLKS2 is an ARM domain and F-actin-associated KASH protein that functions in stomatal complex development and meiotic chromosome segregation. *Nucleus*, 10(1), 144–166.

Haberer, G., Young, S., Bharti, A.K., Gundlach, H., Raymond, C., Fuks, G., Butler, E., Wing, R.A., Rounsley, S., Birren, B., Nusbaum, C., Mayer, K.F.X. and Messing, J. (2005). Structure and architecture of the maize genome. *Plant Physiology*, 139(4), 1612–1624.

Hake, S. and Ross-Ibarra, J. (2015). Genetic, evolutionary and plant breeding insights from the domestication of maize. *ELife*, 4(25), e05861

Hall, T.A. (1999). BioEdit: a user-friendly biological sequence alignment editor and analysis program for Windows 95/98/NT. *Nucleic Acids Symposium Series*, 10(5), 95–98.

Harper, J.W., Adami, G.R., Wei, N. and Elledge, S.J. (1993). The p21 Cdk-interacting protein Cip1 is a potent inhibitor of G1 cyclin-dependent kinases. *Cell*, 75(4), 805–816.

He, X.-J., Hsu, Y.-F., Zhu, S., Wierzbicki, A.T., Pontes, O., Pikaard, C.S., Liu, H.-L., Wang, C.-S., Jin, H. and Zhu, J.-K. (2009). An effector of RNA-directed DNA methylation in arabidopsis is an ARGONAUTE 4- and RNA-binding protein. *Cell*, 137(3), 498–508.

He, Y.J., McCall, C.M., Hu, J., Zeng, Y. and Xiong, Y. (2006). DDB1 functions as a linker to recruit receptor WD40 proteins to CUL4–ROC1 ubiquitin ligases. *Genes and Development*, 20(21), 2949–2954.

Hecker, A., Wallmeroth, N., Peter, S., Blatt, M.R., Harter, K. and Grefen, C. (2015). Binary 2in1 vectors improve in planta (co)localization and dynamic protein interaction studies. *Plant Physiology*, 168(3), 776–787.

Hershko, A. and Ciechanover, A. (1998). The ubiquitin system. *Annual Review of Biochemistry*, 67(1), 425–479.

Hiraga, S., Sasaki, K., Ito, H., Ohashi, Y. and Matsui, H. (2001). A large family of class III plant peroxidases. *Plant and Cell Physiology*, 42(5), 462–468.

Hochholdinger, F. (2004 a). Genetic dissection of root formation in maize (*Zea mays*) reveals root-type specific developmental programmes. *Annals of Botany*, 93(4), 359–368.

Hochholdinger, F., Guo, L. and Schnable, P.S. (2004 b). Lateral roots affect the proteome of the primary root of maize (*Zea mays* L.). *Plant Molecular Biology*, 56(3), 397–412.

- Hochholdinger, F. (1999).** Isolierung und Charakterisierung von Mais-Mutanten mit Defekten in der frühen postembryonalen Wurzelentwicklung. *PhD dissertation, University of Freiburg.*
- Hochholdinger, F. and Feix, G. (1998).** Early post-embryonic root formation is specifically affected in the maize mutant *lrt1*. *The Plant Journal*, 16(2), 247–255.
- Hochholdinger, F., Park, W.J. and Feix, G.H. (2001).** Cooperative action of SLR1 and SLR2 is required for lateral root-specific cell elongation in maize. *Plant Physiology*, 125(3), 1529–1539.
- Hochholdinger, F. and Tuberosa, R. (2009).** Genetic and genomic dissection of maize root development and architecture. *Current Opinion in Plant Biology*, 12(2), 172–177.
- Hochholdinger, F., Yu, P. and Marcon, C. (2018).** Genetic control of root system development in maize. *Trends in Plant Science*, 23(1), 79–88.
- Hose, E., Clarkson, D.T., Steudle, E., Schreiber, L. and Hartung, W. (2001).** The exodermis: A variable apoplastic barrier. *Journal of Experimental Botany*, 52(365), 2245–2264.
- Houbaert, A., Zhang, C., Tiwari, M., Wang, K., de Marcos Serrano, A., Savatin, D.V., Urs, M.J., Zhiponova, M.K., Gudesblat, G.E., Vanhoutte, I., Eeckhout, D., Boeren, S., Karimi, M., Betti, C., Jacobs, T., Fenoll, C., Mena, M., de Vries, S., De Jaeger, G. and Russinova, E. (2018).** POLAR-guided signalling complex assembly and localization drive asymmetric cell division. *Nature*, 563(7732), 574–578.
- Hu, C.-D. and Kerppola, T.K. (2003).** Simultaneous visualization of multiple protein interactions in living cells using multicolor fluorescence complementation analysis. *Nature Biotechnology*, 21(5), 539–545.
- Huh, W.-K., Falvo, J.V., Gerke, L.C., Carroll, A.S., Howson, R.W., Weissman, J.S. and O’Shea, E.K. (2003).** Global analysis of protein localization in budding yeast. *Nature*, 425(6959), 686–691.
- Husakova, E., Hochholdinger, F. and Soukup, A. (2013).** Lateral root development in the maize (*Zea mays*) *lateral rootless 1* mutant. *Annals of Botany*, 112(2), 417–428.

- Ivanchenko, M.G., Muday, G.K. and Dubrovsky, J.G. (2008).** Ethyleneauxin interactions regulate lateral root initiation and emergence in *Arabidopsis thaliana*. *The Plant Journal*, 55(2), 335–347.
- Iwabuchi, K., Li, B., Bartel, P. and Fields, S. (1993).** Use of the two-hybrid system to identify the domain of p53 involved in oligomerization. *Oncogene*, 8(6), 1693–1696.
- James, P., Halladay, J. and Craig, E.A. (1996).** Genomic libraries and a host strain designed for highly efficient two-hybrid selection in yeast. *Genetics*, 144(4), 1425–1436.
- Jansen, L., Roberts, I., De Rycke, R. and Beeckman, T. (2012).** Phloem-associated auxin response maxima determine radial positioning of lateral roots in maize. *Philosophical Transactions of the Royal Society B: Biological Sciences*, 367(1595), 1525–1533.
- Jiao, Y., Peluso, P., Shi, J., Liang, T., Stitzer, M.C., Wang, B., Campbell, M.S., Stein, J.C., Wei, X., Chin, C.-S., Guill, K., Regulski, M., Kumari, S., Olson, A., Gent, J., Schneider, K.L., Wolfgruber, T.K., May, M.R., Springer, N.M. and Antoniou, E. (2017).** Improved maize reference genome with single-molecule technologies. *Nature*, 546(7659), 524–527.
- Josse, E.-M., Foreman, J. and Halliday, K.J. (2008).** Paths through the phytochrome network. *Plant, Cell and Environment*, 31(5), 667–678.
- Kaake, R.M., Wang, X. and Huang, L. (2010).** Profiling of protein interaction networks of protein complexes using affinity purification and quantitative mass spectrometry. *Molecular and Cellular Proteomics*, 9(8), 1650–1665.
- Karimi, M., Depicker, A. and Hilson, P. (2007).** Recombinational cloning with plant gateway vectors. *Plant Physiology*, 145(4), 1144–1154.
- Karimi, M., Inzé, D., Van Lijsebettens, M. and Hilson, P. (2013).** Gateway vectors for transformation of cereals. *Trends in Plant Science*, 18(1), 1–4.
- Kerppola, T.K. (2006).** Design and implementation of bimolecular fluorescence complementation (BiFC) assays for the visualization of protein interactions in living cells. *Nature Protocols*, 1(3), 1278–1286.

- Kervestin, S. and Jacobson, A. (2012).** NMD: a multifaceted response to premature translational termination. *Nature Reviews Molecular Cell Biology*, 13(11), 700–712.
- Krylov, S.N. and Dunford, H.B. (1996).** Accelerating effect of umbelliferone on peroxidase-catalyzed oxidation of indole-3-acetic acid at neutral pH. *The Journal of Physical Chemistry*, 100(50), 19719–19727.
- Kudla, J. and Bock, R. (2016).** Lighting the way to protein-protein interactions: Recommendations on best practices for bimolecular fluorescence complementation analyses. *The Plant Cell*, 28(5), 1002–1008.
- Kumar, S., Stecher, G., Li, M., Knyaz, C. and Tamura, K. (2018).** MEGA X: Molecular evolutionary genetics analysis across computing platforms. *Molecular Biology and Evolution*, 35(6), 1547–1549.
- Langmead, B. and S.L. Salzberg. (2012).** Fast gapped-read alignment with Bowtie 2. *Nature Methods*, 9(4), 357–359
- Lampropoulos, A., Sutikovic, Z., Wenzl, C., Maegele, I., Lohmann, J.U. and Forner, J. (2013).** GreenGate - A novel, versatile, and efficient cloning system for plant transgenesis. *PLoS ONE*, 8(12), e83043.
- Launholt, D., Merkle, T., Houben, A., Schulz, A. and Grasser, K.D. (2006).** Arabidopsis chromatin-associated HMGA and HMGB use different nuclear targeting signals and display highly dynamic localization within the nucleus. *The Plant Cell*, 18(11), 2904–2918.
- Lavenus, J., Goh, T., Roberts, I., Guyomarc'h, S., Lucas, M., De Smet, I., Fukaki, H., Beeckman, T., Bennett, M. and Laplaze, L. (2013).** Lateral root development in arabidopsis: Fifty shades of auxin. *Trends in Plant Science*, 18(8), 450–458.
- Lazo, G.R., Stein, P.A. and Ludwig, R.A. (1991).** A DNA transformation-competent arabidopsis genomic library in agrobacterium. *Bio/Technology*, 9(10), 963–967.
- Lee, H.-W., Kyung, T., Yoo, J., Kim, T., Chung, C., Ryu, J.Y., Lee, H., Park, K., Lee, S., Jones, W.D., Lim, D.-S., Hyeon, C., Do Heo, W. and Yoon, T.-Y. (2013).** Real-time single-molecule co-immunoprecipitation analyses reveal cancer-specific *ras* signalling dynamics. *Nature Communications*, 4, 1505.

- Lee, J. and Zhou, P. (2007).** DCAFs, the missing link of the CUL4-DDB1 ubiquitin ligase. *Molecular Cell*, 26(6), 775–780.
- Lee, J.-H., Terzaghi, W., Gusmaroli, G., Charron, J.-B.F., Yoon, H.-J., Chen, H., He, Y.J., Xiong, Y. and Deng, X.W. (2008).** Characterization of Arabidopsis and rice DWD proteins and their roles as substrate receptors for CUL4-RING E3 ubiquitin ligases. *The Plant Cell*, 20(1), 152–167.
- Lee, J.-H., Yoon, H.-J., Terzaghi, W., Martinez, C., Dai, M., Li, J., Byun, M.-O. and Deng, X.W. (2010).** DWA1 and DWA2, two Arabidopsis DWD protein components of CUL4-based E3 ligases, act together as negative regulators in ABA signal transduction. *The Plant Cell*, 22(6), 1716–1732.
- Li, B. and Fields, S. (1993).** Identification of mutations in p53 that affect its binding to SV40 large T antigen by using the yeast two-hybrid system. *The FASEB Journal*, 7(10), 957–963.
- Ma, F., Wang, L., Li, J., Samma, M.K., Xie, Y., Wang, R., Wang, J., Zhang, J. and Shen, W. (2013).** Interaction between HY1 and H2O2 in auxin-induced lateral root formation in Arabidopsis. *Plant Molecular Biology*, 85(1-2), 49–61.
- Marcon, C., Altrogge, L., Win, Y.N., Stöcker, T., Gardiner, J.M., Portwood, J.L., Opitz, N., Kortz, A., Baldauf, J.A., Hunter, C.T., McCarty, D.R., Koch, K.E., Schoof, H. and Hochholdinger, F. (2020).** *BonnMu*: A sequence-indexed resource of transposon-induced maize mutations for functional genomics studies. *Plant Physiology*, 184(2), 620–631.
- Maruta, N., Trusov, Y., Brenya, E., Parekh, U. and Botella, J.R. (2015).** Membrane-localized extra-large G proteins and G $\beta\gamma$ of the heterotrimeric G proteins form functional complexes engaged in plant immunity in arabidopsis. *Plant Physiology*, 167(3), 1004–1016.
- Marzec, M., Melzer, M. and Szarejko, I. (2015).** Root hair development in the grasses: What we already know and what we still need to know. *Plant Physiology*, 168(2), 407–414.
- Mase, K. and Tsukagoshi, H. (2021).** Reactive oxygen species link gene regulatory networks during arabidopsis root development. *Frontiers in Plant Science*, 12.
- Michael, T.P. (2014).** Plant genome size variation: bloating and purging DNA. *Briefings in Functional Genomics* 13(4), 308–317.

- Miller, J.P., Lo, R.S., Ben-Hur, A., Desmarais, C., Stagljar, I., Noble, W.S. and Fields, S. (2005).** Large-scale identification of yeast integral membrane protein interactions. *Proceedings of the National Academy of Sciences*, 102(34), 12123–12128.
- Möckli, N. and Auerbach, D. (2004).** Quantitative β -galactosidase assay suitable for high-throughput applications in the yeast two-hybrid system. *BioTechniques*, 36(5), 872–876.
- Moriwaki, T., Miyazawa, Y., Fujii, N. and Takahashi, H. (2012).** Light and abscisic acid signalling are integrated by MIZ1 gene expression and regulate hydrotropic response in roots of *Arabidopsis thaliana*. *Plant, Cell & Environment*, 35(8), 1359–1368.
- Morsy, M., Gouthu, S., Orchard, S., Thorneycroft, D., Harper, J.F., Mittler, R. and Cushman, J.C. (2008).** Charting plant interactomes: possibilities and challenges. *Trends in Plant Science*, 13(4), 183–191.
- Musungu, B., Bhatnagar, D., Brown, R.L., Fakhoury, A.M. and Geisler, M. (2015).** A predicted protein interactome identifies conserved global networks and disease resistance subnetworks in maize. *Frontiers in Genetics*, 6(201).
- Nelissen, H., Eeckhout, D., Demuyne, K., Persiau, G., Walton, A., van Bel, M., Vervoort, M., Candaele, J., De Block, J., Aesaert, S., Van Lijsebettens, M., Goormachtig, S., Vandepoele, K., Van Leene, J., Muszynski, M., Gevaert, K., Inzé, D. and De Jaeger, G. (2015).** Dynamic changes in ANGUSTIFOLIA3 complex composition reveal a growth regulatory mechanism in the maize leaf. *The Plant Cell*, 27(6), 1605–1619.
- Nooren, I.M.A. and Thornton, J.M. (2003).** New member's review: Diversity of protein-protein interactions. *The EMBO Journal*, 22(14), 3486–3492.
- Offenborn, J.N., Waadt, R. and Kudla, J. (2015).** Visualization and translocation of ternary Calcineurin-A/Calcineurin-B/Calmodulin-2 protein complexes by dual-color trimolecular fluorescence complementation. *New Phytologist*, 208(1), 269–279.
- Pagan, J., Seto, T., Pagano, M. and Cittadini, A. (2013).** Role of the ubiquitin proteasome system in the heart. *Circulation Research*, 112(7), 1046–1058.

- Palmer, E. and Freeman, T. (2004).** Investigation into the use of C- and N-terminal GFP fusion proteins for subcellular localization studies using reverse transfection microarrays. *Comparative and Functional Genomics*, 5(4), 342–53.
- Paschold, A., Larson, N.B., Marcon, C., Schnable, J.C., Yeh, C.-T., Lanz, C., Nettleton, D., Piepho, H.-P., Schnable, P.S. and Hochholdinger, F. (2014).** Nonsyntenic genes drive highly dynamic complementation of gene expression in maize hybrids. *The Plant Cell*, 26(10), 3939–3948.
- Passardi, F., Penel, C. and Dunand, C. (2004).** Performing the paradoxical: how plant peroxidases modify the cell wall. *Trends in Plant Science*, 9(11), 534–540.
- Paszkowski, U. and Boller, T. (2002).** The growth defect of *lrt1*, a maize mutant lacking lateral roots, can be complemented by symbiotic fungi or high phosphate nutrition. *Planta*, 214(4), 584–590.
- Pawson, T. (2003).** Assembly of cell regulatory systems through protein interaction domains. *Science*, 300(5618), 445–452.
- Péret, B., De Rybel, B., Casimiro, I., Benková, E., Swarup, R., Laplaze, L., Beeckman, T. and Bennett, M.J. (2009).** Arabidopsis lateral root development: an emerging story. *Trends in Plant Science*, 14(7), 399–408.
- Phizicky, E.M. and Fields, S. (1995).** Protein-protein interactions: methods for detection and analysis. *Microbiological Reviews*, 59(1), 94–123.
- Popescu, S.C., Snyder, M. and Dinesh-Kumar, S.P. (2007).** Arabidopsis protein microarrays for the high-throughput identification of protein-protein interactions. *Plant Signaling & Behavior*, 2(5), 416–420.
- Ramírez-Sánchez, O., Pérez-Rodríguez, P., Delaye, L. and Tiessen, A. (2016).** Plant proteins are smaller because they are encoded by fewer exons than animal proteins. *Genomics, Proteomics & Bioinformatics*, 14(6), 357–370.
- Rao, V.S., Srinivas, K., Sujini, G.N. and Kumar, G.N.S. (2014).** Protein-protein interaction detection: methods and analysis. *International Journal of Proteomics*, 2014, 1–12.

- Rayson, S., Arciga-Reyes, L., Wootton, L., De Torres Zabala, M., Truman, W., Graham, N., Grant, M. and Davies, B. (2012).** A role for nonsense-mediated mRNA decay in plants: Pathogen responses are induced in *Arabidopsis thaliana* NMD mutants. *PLoS ONE*, 7(2), e31917.
- Reed, R.C., Brady, S.R. and Muday, G.K. (1998).** Inhibition of auxin movement from the shoot into the root inhibits lateral root development in *Arabidopsis*. *Plant Physiology*, 118(4), 1369–1378.
- Ritter, A., Iñigo, S., Fernández-Calvo, P., Heyndrickx, K.S., Dhondt, S., Shi, H., De Milde, L., Vanden Bossche, R., De Clercq, R., Eeckhout, D., Ron, M., Somers, D.E., Inzé, D., Gevaert, K., De Jaeger, G., Vandepoele, K., Pauwels, L. and Goossens, A. (2017).** The transcriptional repressor complex FRS7-FRS12 regulates flowering time and growth in *Arabidopsis*. *Nature Communications*, 8, 15235.
- Rogers, E.D. and Benfey, P.N. (2015).** Regulation of plant root system architecture: implications for crop advancement. *Current Opinion in Biotechnology*, 32, 93–98.
- Ronquist, F. and Huelsenbeck, J.P. (2003).** MrBayes 3: Bayesian phylogenetic inference under mixed models. *Bioinformatics*, 19(12), 1572–1574.
- Sahu, S.S., Loaiza, C.D. and Kaundal, R. (2019).** Plant-mSubP: a computational framework for the prediction of single and multi-target protein subcellular localization using integrated machine-learning approaches. *AoB PLANTS*, 12(3).
- Saleem, M., Lamkemeyer, T., Schützenmeister, A., Madlung, J., Sakai, H., Piepho, H.-P., Nordheim, A. and Hochholdinger, F. (2010).** Specification of cortical parenchyma and stele of maize primary roots by asymmetric levels of auxin, cytokinin, and cytokinin-regulated proteins. *Plant Physiology*, 152(1), 4–18.
- Sawers, R.J.H., Linley, P.J., Farmer, P.R., Hanley, N.P., Costich, D.E., Terry, M.J. and Brutnell, T.P. (2002).** *Elongated mesocotyl1*, a phytochrome-deficient mutant of maize. *Plant Physiology*, 130(1), 155–163.

Schlicht, M., Strnad, M., Scanlon, M.J., Mancuso, S., Hochholdinger, F., Palme, K., Volkmann, D., Menzel, D. and Baluška, F. (2006). Auxin immunolocalization implicates vesicular neurotransmitter-like mode of polar auxin transport in root apices. *Plant Signaling & Behavior*, 1(3), 122–133.

Schnable, J.C. and Lyons, E. (2011). Comparative genomics with maize and other grasses: from genes to genomes. *Maydica*, 56(2), 183-199.

Schnable, J.C., Springer, N.M. and Freeling, M. (2011). Differentiation of the maize subgenomes by genome dominance and both ancient and ongoing gene loss. *Proceedings of the National Academy of Sciences, USA* 108(10), 4069–4074.

Schnable, P.S., Ware, D., Fulton, R.S., Stein, J.C., Wei, F., Pasternak, S., Liang, C., Zhang, J., Fulton, L., Graves, T.A., Minx, P., Reily, A.D., Courtney, L., Kruchowski, S.S., Tomlinson, C., Strong, C., Delehaunty, K., Fronick, C., Courtney, B. and Rock, S.M. (2009). The B73 maize genome: Complexity, diversity, and dynamics. *Science*, 326(5956), 1112–1115.

Schneider, C.A., Rasband, W.S. and Eliceiri, K.W. (2012). NIH image to ImageJ: 25 years of image analysis. *Nature Methods*, 9(7), 671–675.

Schoonheim, P.J., Veiga, H., da Costa Pereira, D., Friso, G., van Wijk, K.J. and de Boer, A.H. (2006). A comprehensive analysis of the 14-3-3 interactome in barley leaves using a complementary proteomics and two-hybrid approach. *Plant Physiology*, 143(2), 670–683.

Sharma, P. and Dubey, R.S. (2007). Involvement of oxidative stress and role of antioxidative defense system in growing rice seedlings exposed to toxic concentrations of aluminum. *Plant Cell Reports*, 26(11), 2027–2038.

Smith, S.E. and Read, D.J. (1997). *Mycorrhizal Symbiosis*. 2nd edition, Academic Press, San Diego, USA. Chapter 5, 126-160

Song, G., Olatunji, D., Montes, C., Clark, N.M., Pu, Y., Kelley, D.R. and Walley, J.W. (2021). Quantitative proteomics reveals extensive lysine ubiquitination in the arabidopsis root proteome and uncovers novel transcription factor stability states. *bioRxiv*, DOI: 10.1101/2021.01.07.425780

- Sperschneider, J., Catanzariti, A.-M., DeBoer, K., Petre, B., Gardiner, D.M., Singh, K.B., Dodds, P.N. and Taylor, J.M. (2017).** LOCALIZER: subcellular localization prediction of both plant and effector proteins in the plant cell. *Scientific Reports*, 7(1).
- Stewart, A. and Fisher, R.A. (2012).** Co-immunoprecipitation. *Methods in Cell Biology*, 112, 33–54.
- Stothard, P. (2000).** The sequence manipulation suite: javascript programs for analyzing and formatting protein and DNA sequences. *BioTechniques*, 28(6), 1102–1104.
- Strable, J. and Scanlon, M.J. (2009).** Maize (*Zea mays*): A model organism for basic and applied research in plant biology. *Cold Spring Harbor Protocols*, 2009(10), 132.
- Struk, S., Jacobs, A., Sánchez Martín-Fontecha, E., Gevaert, K., Cubas, P. and Goormachtig, S. (2018).** Exploring the protein-protein interaction landscape in plants. *Plant, Cell & Environment*, 42(2), 387–409.
- Stynen, B., Tournu, H., Tavernier, J. and Van Dijck, P. (2012).** Diversity in genetic *in vivo* methods for protein-protein interaction studies: from the yeast two-hybrid system to the mammalian split-luciferase system. *Microbiology and Molecular Biology Reviews*, 76(2), 331–382.
- Swigonova, Z. (2004).** Close split of sorghum and maize genome progenitors. *Genome Research*, 14(10a), 1916–1923.
- Tagwerker, C., Flick, K., Cui, M., Guerrero, C., Dou, Y., Auer, B., Baldi, P., Huang, L. and Kaiser, P. (2006).** A tandem affinity tag for two-step purification under fully denaturing conditions. *Molecular & Cellular Proteomics*, 5(4), 737–748.
- Taramino, G., Sauer, M., Stauffer, J.L., Multani, D., Niu, X., Sakai, H. and Hochholdinger, F. (2007).** The maize (*Zea mays* L.) RTCS gene encodes a LOB domain protein that is a key regulator of embryonic seminal and post-embryonic shoot-borne root initiation. *The Plant Journal*, 50(4), 649–659.
- Tardif, G., Kane, N.A., Adam, H., Labrie, L., Major, G., Gulick, P., Sarhan, F. and Laliberté, J.-F. (2007).** Interaction network of proteins associated with abiotic stress response and development in wheat. *Plant Molecular Biology*, 63(5), 703–718.

Trigg, S.A., Garza, R.M., MacWilliams, A., Nery, J.R., Bartlett, A., Castanon, R., Goubil, A., Feeney, J., O'Malley, R., Huang, S.C., Zhang, Z.Z., Galli, M. and Ecker, J.R. (2017). CrY2H-seq: a massively multiplexed assay for deep-coverage interactome mapping. *Nature Methods*, 14(8), 819–825.

Tripathi, J.N., Ntui, V.O., Ron, M., Muiruri, S.K., Britt, A. and Tripathi, L. (2019). CRISPR/Cas9 editing of endogenous banana streak virus in the B genome of *Musa spp.* overcomes a major challenge in banana breeding. *Communications Biology*, 2(1).

Tsukagoshi, H., Busch, W. and Benfey, P.N. (2010). Transcriptional regulation of ROS controls transition from proliferation to differentiation in the root. *Cell*, 143(4), 606–616.

Van Leene, J., Eeckhout, D., Cannoot, B., De Winne, N., Persiau, G., Van De Slijke, E., Vercruysse, L., Dedecker, M., Verkest, A., Vandepoele, K., Martens, L., Witters, E., Gevaert, K. and De Jaeger, G. (2014). An improved toolbox to unravel the plant cellular machinery by tandem affinity purification of Arabidopsis protein complexes. *Nature Protocols*, 10(1), 169–187.

Vernoux, T., Brunoud, G., Farcot, E., Morin, V., Van den Daele, H., Legrand, J., Oliva, M., Das, P., Larrieu, A., Wells, D., Guédon, Y., Armitage, L., Picard, F., Guyomarc'h, S., Cellier, C., Parry, G., Koumproglou, R., Doonan, J.H., Estelle, M. and Godin, C. (2011). The auxin signalling network translates dynamic input into robust patterning at the shoot apex. *Molecular Systems Biology*, 7(1), 508.

Vidalain, P.-O., Jacob, Y., Hagemeyer, M.C., Jones, L.M., Neveu, G., Roussarie, J.-P., Rottier, P.J.M., Tangy, F. and de Haan, C.A.M. (2015). A field-proven yeast two-hybrid protocol used to identify coronavirus–host protein–protein interactions. *Coronaviruses*, 213–229.

Vierstra, R. (2003). The ubiquitin/26S proteasome pathway, the complex last chapter in the life of many plant proteins. *Trends in Plant Science*, 8(3), 135–142.

von Behrens, I., Komatsu, M., Zhang, Y., Berendzen, K.W., Niu, X., Sakai, H., Taramino, G. and Hochholdinger, F. (2011). *Rootless with undetectable meristem 1* encodes a monocot-specific AUX/IAA protein that controls embryonic seminal and post-embryonic lateral root initiation in maize. *The Plant Journal*, 66(2), 341–353.

- Waadt, R., Schmidt, L.K., Lohse, M., Hashimoto, K., Bock, R. and Kudla, J. (2008).** Multicolor bimolecular fluorescence complementation reveals simultaneous formation of alternative CBL/CIPK complexes in planta. *The Plant Journal*, 56(3), 505–516.
- Welinder, K.G., Justesen, A.F., Kjaersgård, I.V.H., Jensen, R.B., Rasmussen, S.K., Jespersen, H.M. and Duroux, L. (2002).** Structural diversity and transcription of class III peroxidases from *Arabidopsis thaliana*. *European Journal of Biochemistry*, 269(24), 6063–6081.
- Wiemann S., Weil B., Wellenreuther R., Gassenhuber J., Glassl S., Ansorge W., Böcher M., Blöcker H., Bauersachs S., Blum H., Lauber J., Düsterhöft A., Beyer A., Köhrer K., Strack N., Mewes H.W., Ottenwälder B., Obermaier B., Tampe J., Heubner D., Wambutt R., Korn B., Klein M., Poustka A. (2001).** Toward a catalog of human genes and proteins: sequencing and analysis of 500 novel complete protein coding human cDNAs. *Genome Research*. 11(3), 422-435.
- Woll, K., Borsuk, L.A., Stransky, H., Nettleton, D., Schnable, P.S. and Hochholdinger, F. (2005).** Isolation, characterization, and pericycle-specific transcriptome analyses of the novel maize lateral and seminal root initiation mutant *rum1*. *Plant Physiology*, 139(3), 1255–1267.
- Woodhouse, M.R., Schnable, J.C., Pedersen, B.S., Lyons, E., Lisch, D., Subramaniam, S. and Freeling, M. (2010).** Following tetraploidy in maize, a short deletion mechanism removed genes preferentially from one of the two homeologs. *PLoS Biology*, 8(6), e1000409.
- Xing, S., Wallmeroth, N., Berendzen, K.W. and Grefen, C. (2016).** Techniques for the analysis of protein-protein interactions *in vivo*. *Plant Physiology*, 171(2), 727–758.
- Yang, J.W., Fu, J.X., Li, J., Cheng, X.L., Li, F., Dong, J.F., Liu, Z.L. and Zhuang, C.X. (2013).** A novel co-immunoprecipitation protocol based on protoplast transient gene expression for studying protein–protein interactions in rice. *Plant Molecular Biology Reporter*, 32(1), 153–161.
- Young, E.T., Saario, J., Kacherovsky, N., Chao, A., Sloan, J.S. and Dombek, K.M. (1998).** Characterization of a p53-related activation domain in *Adr1p* that is sufficient for ADR1-dependent gene expression. *Journal of Biological Chemistry*, 273(48), 32080–32087.

- Yu, P., Gutjahr, C., Li, C. and Hochholdinger, F. (2016).** Genetic control of lateral root formation in cereals. *Trends in Plant Science*, 21(11), 951–961.
- Yu, P., He, X., Baer, M., Beirinckx, S., Tian, T., Moya, Y.A.T., Zhang, X., Deichmann, M., Frey, F.P., Bresgen, V., Li, C., Razavi, B.S., Schaaf, G., von Wirén, N., Su, Z., Bucher, M., Tsuda, K., Goormachtig, S., Chen, X. and Hochholdinger, F. (2021).** Plant flavones enrich rhizosphere *Oxalobacteraceae* to improve maize performance under nitrogen deprivation. *Nature Plants*, 7(4), 481–499.
- Yu, P., Hochholdinger, F. and Li, C. (2019).** Plasticity of lateral root branching in maize. *Frontiers in Plant Science*, 10(363).
- Yu, P. (2022),** personal communication
- Zhang, C. and Guy, C.L. (2006).** *In vitro* evidence of Hsc70 functioning as a molecular chaperone during cold stress. *Plant Physiology and Biochemistry*, 44(11-12), 844–850.
- Zhang Y., Marcon C., Tai H., von Behrens I., Ludwig Y., Hey S., Berendzen K.W., Hochholdinger F. (2016).** Conserved and unique features of the homeologous maize Aux/IAA proteins ROOTLESS WITH UNDETECTABLE MERISTEM 1 and RUM1-LIKE 1. *Journal of Experimental Botany* 67(4):1137-47.
- Zhang, Y., Feng, S., Chen, F., Chen, H., Wang, J., McCall, C., Xiong, Y. and Deng, X.W. (2008).** Arabidopsis DDB1-CUL4 ASSOCIATED FACTOR1 forms a nuclear E3 ubiquitin ligase with DDB1 and CUL4 that is involved in multiple plant developmental processes. *The Plant Cell*, 20(6), 1437–1455.
- Zhu, G., Wu, A., Xu, X.-J., Xiao, P.-P., Lu, L., Liu, J., Cao, Y., Chen, L., Wu, J. and Zhao, X.-M. (2015).** PPIM: A protein-protein interaction database for maize. *Plant Physiology*, 170(2), 618–626.
- Zimmermann, R., Sakai, H. and Hochholdinger, F. (2009).** The gibberellic acid stimulated-like gene family in maize and its role in lateral root development. *Plant Physiology*, 152(1), 356–365.

9 SUPPLEMENTAL DATA

Supplemental Table 1 Gene accessions related to *lrt1* in version 3, 4 and 5 of the maize genome annotation. Assignment to the maize subgenomes (SCHNABLE et al., 2011) in brackets.

Gene	RefGen_v3	RefGen_v4	ReffGen_v5
<i>lrt1</i>	GRMZM2G348735	-	-
	GRMZM2G110869 (Subgenome 2)	Zm00001d026691	Zm00001eb434410
<i>lrt1-like</i>	AC212859.3_FG007 (Subgenome 1)	Zm00001d002933	Zm00001eb076460
<i>ddb1-like1</i>	GRMZM2G402002 (Subgenome 1)	Zm00001d039165	Zm00001eb297320
<i>ddb1-like2</i>	GRMZM2G128981, GRMZM2G356142, GRMZM2G430027 (Subgenome 2)	Zm00001d009745	Zm00001eb345240
<i>cullin4</i>	GRMZM2G704093 (Subgenome 1)	Zm00001d034361	Zm00001eb059990
	AC155496.2_FG009 (Subgenome 2)	Zm00001d013116	Zm00001eb213380

Supplemental Table 2 Mutant alleles of *lrt1*.

Allele name	Mutagenesis	Type of mutation	Consequence for LRT1 protein	Mutation site in bp on chr. 10 (AGPv5)
<i>lrt1-1</i>	EMS	G to A transition	Premature stop codon (AA to STOP)	151,511,481
<i>lrt1-2</i>	CRISPR/Cas9	1 bp insertion (A)	Frameshift	151,512,588
<i>lrt1-3</i>	CRISPR/Cas9	531 bp deletion	Frameshift, - 108 AS	151,512,588 – 151,513,119

10 ACKNOWLEDGMENT

First of all, I would like to thank Frank for giving me the opportunity to work on “his” *lrr1* mutant as a PhD student, providing me constant support with advice and helpful discussions, always patient and in his good mood. Also I am very thankful for providing me many traveling and presenting opportunities.

Secondly, I would like to thank Caro for already enthusing me with the *lrr1* project as the supervisor of my master thesis. She always helped me with advise when I had just a quick question again and motivated me with her very own way when an experiment didn't go as expected.

Furthermore, I would like to thank all collaborators, especially Graziana Taramino and Dilbag Multani (DuPont Crop Genetics Research) and the Deutschen Forschungsgemeinschaft for funding this project. Also many thanks to Laurens Pauwels (VIB Center, Ghent, Belgium) for the transformation of the CRISPR/ Cas9 constructs.

Many thanks also to all current and former colleagues of the CFG and CS group who helped me in the lab with practical help, with advice and suggestions, but also who made the time in the lab really enjoyable (officially and unofficially):

Thanks to Jutta, Micha, Annika, Alina, Danning, Mauritz, Alejandra, Marion, Yaping, Xiaming, Zihui, Junwen, Boagang, Ling, Liuyang, Zamiga, Gwen, Stefan, Huanhuan, Anna, Nina, Marine, Sören, Lara, Isa, Anja. Thanks to Alexa, Christa, Selina, Claudia, and Vera for their technical support. Thanks to Britta for helping me with IT questions. Thanks to Christine Jessen, Sonja Skamel and Ellen Kreitz for their incredible helpfulness in administrative matters.

Special thanks also to Peng for many fruitful discussions and advise and for giving me the opportunity to extend the research area to microbes, also in the future.

My special thanks also goes to the current and former “Lab 51” members and friends Verena, Yan, Markus, Linnéa, Bettina and Natascha, who always had to help when something had to go fast and who made the time in the lab really enjoyable.

Special thanks to Helmut, who helped me a lot in the lab and on the field always when his special technical skills were required, but also for being a good friend with whom it is always fun to have coffee and talk shop about agriculture.

Special thanks to Li, Anna-Lena, José, Stefi, Philippe, Felix and David for their advice in methods that were new to me and allowing me planning and analyzing of these experiments.

Thanks to Prof. Gabriel Schaaf for being the second examiner and thanks to Philipp Gaugler from his group, who helped me a lot regarding Y2H.

From the bottom of my heart, I would like to thank my parents for their continuous support, especially my mother for constantly asking and bugging me about the current status of my work and the nice time-outs in between, always with food and drinks.

My special thanks go to my fiancée Mareike, who always and at any time supported me with her motivation, professional and practical help and who always gave me a strong support even if I sometimes came out of the lab grumpy and with lots of questions. I could always recharge the battery together with her, be it on our short trips or together with Almi and Corti.